NASA Contractor Report 178356

Advanced Powder Metallurgy Aluminum Alloys via Rapid Solidification Technology - Phase II

Ranjan Ray and Sunil C. Jha

MARKO MATERIALS, INC.
NORTH BILLERICA, MA 01862

NASA

National Aeronautics and
Space Administration

Langley Research Center
Hampton, Virginia 23665-5225

Table of Contents

PREFACE

This is the final report describing the research activities under Contract No. NAS1-18001 covering the period from April 1, 1985 to March 31, 1987. The program was sponsored by NASA Langley Research Center, Hampton, Virginia. The program's technical monitor was Mr. Dennis Dicus of Langley Research Center.

LIST OF TABLES

LIST OF FIGURES

Advanced Powder Metallurgy Aluminum Alloys via

Rapid Solidification Technology - Phase II

Ranjan Ray and Sunil C. Jha

Marko Materials Inc.

ABSTRACT

The objective of this Phase II NASA-SBIR program was to apply Marko's rapid solidification technology to processing of new high strength aluminum alloys. Four classes of alloys, namely, Al-Li based (class 1) alloy, 2124 type (class 2) alloy, high temperature Al-Fe-Mo (class 3) alloy, and PM X7091 type (class 4) alloy, were produced as melt spun ribbons. The ribbons were pulverized, cold-compacted, hot-degassed and consolidated through single or double stage extrusion. The mechanical properties of all the four classes of alloys were measured at room and elevated temperatures and their microstructures were investigated optically and through electron microscopy. The microstructure of class 1 Al-Li-Mg alloy was predominantly unrecrystallized due to Zr addition. Yield strengths to the order of 50 Ksi were obtained, but tensile elongation in most cases remained below 2%. The class 2 alloys were modified compositions of 2124 aluminum alloy, through the addition of 0.6w% Zr and 1w% Ni. Ni addition gave rise to a fine dispersion of intermetallic particles resisting coarsening during elevated temperature exposure. Class 2 alloy showed good combination of tensile strength and ductility and retained high strength ($\approx$ 40 Ksi) after 1000 hour exposure at 177°C. The class 3 Al-Fe-Mo alloy showed high strength and good ductility both at room and high temperatures. The yield and tensile strength of class 4 alloy exceeded those of the commercial 7075 aluminum alloys.

1 INTRODUCTION

Advanced aluminum alloys with far superior high temperature specific strength and specific stiffness than those from commercial aluminum alloys, are of long-term interest to the aerospace community for potential applications as lightweight materials in aerospace structures. Payoffs will result from weight savings of structural components which in turn, will lead to increased payload, service life, and decreased life-cycle cost.

The principles of rapid solidification technology (RST) are being presently used to produce new aluminum alloys with highly refined, homogenous microstructures[1-7]. The refined microstructures produced by RST aluminum powder metallurgy improve many mechanical properties. Room and elevated temperature strength, toughness, fatigue crack initiation resistance, and resistance to environmentally assisted cracking processes such as stress corrosion cracking have been improved by powder metallurgy. Based on payoff studies, the new RST aluminum alloys appear to have excellent prospects for both aircraft structural parts and gas turbine engine components.

Under a number of industry-government programs at Boeing Aerospace Company, Lockheed Missiles and Space Company,

Lockheed-California Company, ALCOA, Pratt & Whitney Aircrafts, etc., several new aluminum alloys have been developed via rapid solidification processes based on melt atomization techniques.

The objective of the present Phase II NASA-SBIR program is to apply Marko's melt-spinning rapid solidification processing technology to the best aluminum alloys of different categories which have emerged as a result of the aforesaid industry-government research and development programs. The primary thrust of the present program is to examine the feasibility of achieving improved mechanical properties in the existing experimental RST aluminum alloys via utilization of the melt-spinning process which allows rapid solidification of melt at a very high cooling rate of 10^6 °C/second, and compare the properties with those of alloys produced by gas-atomization processes.

The following four classes of alloys were investigated in the present Phase II NASA-SBIR program.

1.1 Class 1 Alloy

The alloy of this class is based on the Al-Li alloy system for stiffness, and high strength applications (i.e. airframe structures). In the Al-Li alloy, the Al_3Li phase precipitates coherently and as a result, slip localization occurs upon plastic deformation leading to concomitant fracture at low macroscopic strains. Alloys of this type have not exhibited

commercially acceptable ductility, fracture toughness, and in some instances, stress corrosion resistance. Numerous investigations have been carried out in the recent past to improve this situation by refining the grain size and also by adding a fine hard dispersoid.

The most promising alloy systems are based on Al-Li-Cu, and Al-Li-Mg. Small amounts of zirconium when added to Al-Li alloys inhibit recrystallization leading to a fine grain structure.

The composition of class 1, Al-Li-Mg alloy is given in Table 1.

1.2 Class 2 Alloy

The alloy of this class is being designed for high strength and damage tolerance with high thermal stability up to 177°C for supersonic aircraft structures. The primary candidate alloy being studied is 2124 containing 0.6w%Zr zirconium and 1w%Ni nickel. Both Zr and Ni is expected to form fine dispersion of highly stable Al_3M compounds upon rapid solidification processing causing stabilization of an ultrafine grain structure and improved high temperature strength by the action of dispersed phase.

1.3 Class 3 Alloy

An Al-8Fe-2Mo alloy belonging to this class was chosen for investigation. This alloy has been developed by Pratt and Whitney Aircraft for potential applications at high temperatures (232-343°C) as gas turbine engine components in substitution of titanium based alloys.

1.4 Class 4 Alloy

Alloys of this class include high strength, corrosion resistant 7XXX aluminum alloys such as 7075 and RST PM X7091. The important microstructural features of 7XXX aluminum alloys include the coherency and distribution of the age-hardening precipitates, the grain size, shape, and distribution, crystallographic texture, and the composition, size, distribution of the intermetallic particles. A reduction in grain size usually promotes homogenous deformation and reduces stress concentration at grain boundaries. This improves the ductility and fatigue crack initiation (FCI) resistance, but sometimes reduces the fatigue crack propagation (FCP) resistance. Large intermetallic particles tend to nucleate voids or cracks and small ones can promote void-sheet formation. Introduction of a smaller volume fraction and/or a finer distribution of these

particles results in an improved fracture toughness, FCI resistance, and fatigue crack propagation (FCP) resistance in the high stress intensity range.

In the present program, a RST X7091 alloy (Bal Al, 6.46 w%Zn, 2.42 w%Mg, 1.49 w%Cu, 0.42 w%Co) was chosen as the candidate alloy.

2 SUMMARY OF WORK PLAN

This two-year program was aimed at achieving specific property goals in four classes of aluminum alloys as described in the previous section. The major thrust of the program was to utilize the rapid solidification processing technique based on melt-spinning with very high uniform cooling rate of 10^6 °C/second to fabricate various aluminum alloys with homogenous structures and improved mechanical properties.

2.1 Principal Project Objectives

Four well-known experimental RST aluminum alloys were investigated by Marko's melt-spinning process combined with standard powder metallurgical consolidation techniques. The consolidated alloys were subjected to specific heat treatments followed by characterization of mechanical and physical properties and microstructures. The properties of the alloys studied in the present program are compared with those of similar alloys (whenever available) fabricated by different RST powder manufacturing processes based on melt atomization. The goal of the program was to determine whether or not the RST process based on melt-spinning is a viable manufacturing method for the fabrication of advanced PM aluminum alloys for future aerospace applications.

2.2 Scope of Work

The work to be performed consists of the following tasks:

Task 1. Preparation and characterization of Al-2.7Li-5.3Mg-0.22Zr made via rapid solidification processing based on melt-spinning.

(a) Preparation of twenty-five pounds of powder.

(b) Canning, cold compaction, hot vacuum degassing, sealing of cans, hot pressing of sealed ca.

(c) Hot extrusion of hot pressed billets.

(d) Heat treatment, characterization of mechanical, physical and microstructural properties.

Task 2. Preparation and characterization of an aluminum alloy (2124 containing 0.6%Zr and 1%Ni) made via rapid solidification processing based on melt-spinning.

(a) Preparation of twenty-five pounds of powder.

(b) Canning, cold compaction, hot vacuum degassing, sealing of cans, hot pressing of sealed cans.

(c) Hot extrusion of hot pressed billets.

(d) Heat treatment, characterization of mechanical, physical and microstructural properties.

Task 3. Preparation and characterization of a PM Al-8Fe-2Mo alloy made via rapid solidification processing based on melt-spinning.

    (a) Preparation of twenty-five pounds of powder.

    (b) Canning, cold compaction, hot vacuum degassing, sealing of cans, hot pressing of sealed cans.

    (c) Hot extrusion of hot pressed billets.

    (d) Heat treatment characterization of mechanical, physical and microstructural properties.

Task 4. Preparation and characterization of an aluminum alloy X-7091.

    (a) Preparation of twenty-five pounds of powder.

    (b) Canning, cold compaction, hot vacuum degassing, sealing of cans, hot pressing of sealed cans.

    (c) Hot extrusion of hot pressed billets.

    (d) Heat treatment, characterization of mechanical, physical and microstructural properties.

3 ALLOY PREPARATION AND PROCESSING

The four alloys listed in Table 1 were prepared by induction melting high purity constituents. Final ingots of each alloy weighed 45 pounds. Approximately ten pounds of ingots of each alloy were consumed to develop the optimum melt-spinning parameters for each alloy. A schematic of the melt spinning process is shown in Figure 1. In the melt-spinning process, the ingot was remelted under argon atmosphere in a refractory crucible with a round orifice at the bottom. The orifice of the crucible was kept closed by a refractory plug. Melt was superheated by 100-200°C and the superheated melt was ejected as a narrow stream by the action of argon overpressure over the melt. The melt stream was allowed to impinge upon a rotating copper-beryllium chill substrate and form a rapidly solidified ribbon. The melt stream was protected from oxidation by an argon blanket surrounding the stream. The rapidly solidified ribbon was collected in air in a container. Utilization of argon gas to prevent oxidation of alloy melt was adequate for class 2,3 and 4 alloys. However oxidation of small amounts of Li in class 1 alloy could not be avoided.

Initial trial runs were made with each of the above four alloys varying the processing parameters such as orifice diameter, argon overpressure for ejection of melt through orifice, length of molten stream from the bottom of the crucible

to the substrate surface, the angle of impingement of the stream with the substrate surface, and the surface speed of the substrate.

Table 2 lists the optimum processing conditions for the various alloys.

After completing the optimization of the melt-spinning parameter, the four alloys were prepared as good quality melt-spun ribbons (about 0.05mm thick and 2.5 to 4mm wide) in thirty pounds quantity each. The ribbons were found to be ductile to 180° bending. The ductile melt-spun ribbons were fragmented into particulates/flakes by a rotary pulverizer. Several passes through the pulverizer were required to get adequate reduction in size of the particulates desirable for subsequent powder metallurgical consolidation processing. About twenty-five pounds of powders of each of the four alloys were prepared.

Pulverization of the melt spun ribbons was achieved in a rotary hammer mill, shown schematically in Figure 2. The hammer mill utilizes hard superalloy hammers and pulverization is achieved by shearing of ribbons between the hammers. Contamination of powders through the wear of hammers is possible. Such contaminants occasionally showed up in the EDS spectrum of the fracture surfaces of alloy samples.

3.1 Powder Microstructure

The microstructure of the as-cast and cold compacted powders was observed optically. The powders were mounted, polished for metallographic observation and were etched with Keller's reagent.

Figures 3-5 show the typical microstructures of powder/particulate of class 1 alloy (Al-2.7Li-5.3Mg-0.22Zr). The microstructure generally shows very fine and uniform grains. The microstructure of the present alloy is quite different from the dendritic microstructures typical of aluminum alloys produced by various melt atomization techniques.

Figures 6-8 represent the microstructures of powders of the class 2 alloy (2124 containing 0.6Zr and 1Ni) and class 3 alloy (Al-8Fe-2Mo). The microstructures are generally comparable to each other and to class 1 alloy consisting of fine and uniform grain structure.

The microstructure of class 4 alloy was found to be somewhat coarser than the other three alloys as shown in Figure 9.

3.2 Consolidation of Powders

Hot extrusion of powders of four aluminum alloys was carried out at Nuclear Metals, Inc., Concord, Massachusetts.

3.3 Cold Compaction

Powders of each alloy were put in 5.5" O.D. x 5.25" ID aluminum cans (6060-T6). Powders were cold compacted at 22,500 psi, hot evacuated at 400°C until the vacuum inside the cans was brought below 1 micron and held under vacuum for 4 hours. The billets (cans) were subsequently sealed off. Two billets were prepared for each alloy. Same outgassing procedures were adopted for all the four classes of aluminum alloys. Optimization of outgassing procedure for each class of alloy was beyond the scope of this work.

3.4 Hot Upset

All eight billets were heated at 400°C for 4 hours and hot upset in 1400 ton extrusion press using a blind die. In the hot upset process, the full ram pressure (1400 ton) was maintained against the billets for 60 seconds inside the press. The temperature of the liner was maintained at 400°C.

3.5 Hot Extrusion

One billet of each alloy was hot extruded following the above upset process. The billets were re-machined to 5.4±.010 inch diameter, heated to and soaked at 400°C for 3 hours and then extruded through a 0.5 inch x 1.5 inch rectangular die. The hot extrusion conditions are given Table 3.

Alloys of classes 1,2 and 4 were successfully hot extruded into rectangular bars with good surface and edge conditions. However the billet of class 3 alloy stalled the extrusion press at a reduction ratio of 31.66:1 at 400°C. The class 3 alloy is a rapidly solidified Al-Fe-Mo alloy which retains its solid solution strength at high temperatures. The stalled billets (5.575 inch dia.) of class 3 alloy were heat-treated at 400°C for 3 hours and extruded into 1.99 inch diameter bar. The hot extrusion conditions in the first stage are given in Table 4.

The 1.99 inch diameter bar was sectioned into four 8 inch long billets which were subsequently heated at 400°C for 2 hours and extruded into rectangular bars (1.625 inch by 0.5 inch) under the hot extrusion conditions reported in Table 5.

The overall reduction ratio suffered by the class 3 alloy under the above two stage extrusion process was 46.7:1. However, the alloy had to be exposed to 400°C for an additional 5 hours.

4 EVALUATION OF RAPIDLY SOLIDIFIED ALLOYS

4.1 Class 1 Alloy:

The composition of class 1 alloys lies in the Al + Al$_2$MgLi phase field of the Al-Mg-Li ternary system. The addition of Zr is mainly to inhibit recrystallization, and provide a finer grain size for obtaining higher strengths. The age hardening response of the class 1 alloys was determined. The goal was to arrive at an aging treatment that would provide 2024-T4 type strength. Samples from extruded bars were solution heat treated at 524°C for one hour to ensure complete dissolution of Al$_2$MgLi precipitates, which form during hot compaction and hot extrusion processing of the alloy powders. The samples were quenched from solution heat treat temperatures into cold water. Alloy 1 samples were aged at temperatures ranging from room temperature to 171°C. The alloy did not show any tendency for natural aging. Figure 10 shows the age hardening response of class 1 alloys at four different temperatures of aging for times up to 100 hours. As is evident from the hardness data in Figure 10, the artificial aging treatment results in appreciable precipitation hardening of the class 1 alloys. Based on this study, the aging treatment to achieve peak hardness for class 1 alloy was identified to be 16 hours at 171°C.

4.1.1 Microstructure of Extruded Class 1 Alloys:

Figures 11-12 show the grain structures of extruded class 1 alloy in the longitudinal and long transverse direction. The microstructure consists of extremely fine grain structure. The microstructure remained predominately unrecrystallized indicating the effectiveness of Zr containing dispersoids in suppressing recrystallization and grain growth. The microstructure was further investigated by transmission electron microscopy (TEM). Samples for TEM studies were mechanically ground into thin sheets to obtain thin 3mm discs and then electropolished in a 30% HNO_3+methanol solution at -20°C. The samples were observed in a 100KV STEM.

Figure 13 shows a dark field TEM image of an extruded class 1 alloy in peak aged condition. The fine second phase particles show the prior flake boundaries. Figure 14 shows the EDAX spectrum obtained from these particles and it is observed that the particles situated at prior particle boundaries are the oxides of magnesium and aluminum. Figure 15 shows the typical sub-grain structure of class 1 alloy. The interior of the grain contains fine Al_3Li precipitates, which are responsible for the strength of the class 1 alloy. The grain boundaries are associated with large, incoherent particles of Al_2LiMg phase. During artificial aging the Al_3Li precipitates, which are metastable with respect to Al_2MgLi precipitates, must dissolve

to supply solute for the continued growth of Al_2LiMg precipitates. This leads to the formation of precipitate free zones (PFZ) near the grain boundary areas, and these PFZs grow with aging time during the artificial aging treatment. Al_2LiMg precipitates also form at other heterogeneous sites such as at the dispersoid (Al_3Zr) – matrix interfaces. The Al_3Zr dispersoids form peritectically during rapid solidification, and hence the distribution of Al_3Zr precipitates within the class 1 alloy microstructures can be highly non-uniform. A high density of Al_3Zr dispersoids at a particular location within the microstructures can give rise to variation in the amount of Al_2LiMg precipitations at various heterogeneous within the microstructure. Figure 16 shows an example of the non-uniform precipitation behavior in a peak aged class 1 alloy. An EDAX spectrum taken from one such region confirms the heterogeneous precipitation of Al_2MgLi on Al_3Zr precipitates and Al-matrix interface.

4.1.2 Tensile Properties of Class 1 Alloys

To obtain the best combination of tensile strength and ductility, samples of extruded class 1 alloy were given a number of different heat treatments. Tables 6 through 11 show the yield strength, ultimate tensile strength, percentage, elongation and percentage reduction in area, of samples of class 1 alloy solution heat treated at 524°C and aged at temperatures

ranging from 71°C to 216°C for aging times extending up to 100 hours. Yield strengths of the order of 50 Ksi were generated by peak aging at 149°F and 171°C, however, the percentage elongation in all cases remained below 2%. Tables 8 and 9 also show the tensile test data for a similar Al-Li-Mg alloy (Al -2.5w%Li -4.8w%Mg -0.10w%Zr) produced by gas atomization process and subsequently consolidated by hot-extrusion (8). From the data shown in Tables 8 and 9, it is apparent that the gas atomized Al-Li-Mg alloys show extremely low ductility, as the class 1 alloys. However, strength levels of the gas atomized alloys is higher than those of class 1 alloy. This difference may arise from several factors. The processing of class 1 alloys was done in air, which may have led to the depletion of Li through oxidation. Moreover, the powder particle morphologies in the two cases were different, and therefore the degassing and consolidation processes for melt spun class 1 alloy flakes may not have been optimum. Optimization of the powder consolidation parameters was outside the scope of this study.

In figures 18 through 21, scanning electron micrographs of the tensile fracture surfaces in peak and over-aged class 1 alloy samples are shown. It is observed that fracture initiates by void nucleation at large constituent particles, and that the fracture propagates intergranularly throughout the microstructure in both peak and over aged samples. The fracture facets in

both the peak and overaged samples are dimpled indicating the presence of intergranular particles, and the copious intergranular precipitation appears to be the major cause for the poor ductility of Al-Li based alloys.

In an effort to explore the effect of changing solution heat treatment temperature on the resulting tensile properties of artificially aged class 1 alloys, the samples of class 1 alloy were solution heat treated at 468°C and 482°C for one hour and cold water quenched. Theses samples were then artificially aged, and subsequently tested for room temperature tensile properties. Table 12 shows the tensile properties of class 1 alloy samples solution heat treated at different temperatures. It appears that regardless of different solution heat treatment and artificial aging practice, the percentage elongation remains below 2.0%.

Further fractographic work was undertaken to investigate the fracture modes in samples of class 1 alloy, which were artificially aged to underaged, peak and overaged conditions. The following specific heat treatments were given to four samples of class 1 alloy, and subsequently, the samples were tested in tension until failure.

Sample (1):Solution heat treated at 524°C/1 hour, cold water quenched, aged at 70°C/1 hour.

Sample (2):Solution heat treated at 524°C/1 hour, cold water quenched, aged at 185°C/16 hours.

Sample (3):Solution heat treated at 524°C/1 hour, cold water quenched, aged at 70°C/24 hours.

Sample (4):Solution treated at 524°C/1 hour, cold water quenched, aged at 171°C/100 hours.

SEM fractographs of the above samples fractured in tension, and results of EDS analysis are shown in Figures 22 through 30. The only inclusions, which were clearly seen, were associated with the fracture initiation sites of samples 1,3 and 4. Table 13 summarizes the results of EDS. analysis of the inclusions. The inclusion at the fracture origin of sample 1 showed a high level of titanium and minor amount of associated aluminum. The inclusion at the fracture origin of sample 3 contained substantial amounts of aluminum, cobalt, chromium and tungsten. The inclusion at the fracture origin of sample #4 contained a major level of aluminum and minor levels of titanium and iron.

There are two major factors affecting the ductility of Al-Li based class 1 alloy. Upon continued aging of class 1 alloy samples, the Al_3Li precipitates, which are responsible for the strengthening of Al-Li alloys coarsen. The Al_3Li precipitates are $L1_2$ ordered and coherent with the Al-matrix, with a very small misfit strain. Due to the structural similarities between

the Al_3Li precipitates and Al matrix, the precipitate and the matrix have common slip planes. Passage of a dislocation through Al_3Li precipitates shears the precipitate and decreases the precipitate strength, by decreasing its effective size. Therefore, due to softening of the slip planes, slip becomes planar and localized. As a result of planar slip, the dislocations pile up at the grain boundary generating high stresses, which leads to failure at the grain boundary region. The other factor is the copious precipitation of equilibrium Al_2MgLi precipitate at the grain boundary regions, and the attendant PFZ growth, which renders the grain boundary regions weak, and the grain boundaries become the preferred path for crack propagation.

Therefore, it appears that the low ductility of Al-Li based alloys is inherently due to their precipitation behavior. Further aging treatments were performed on the sample of class 1 alloy. The samples were solution heat treated at 499°C for one hour, cold water quenched and then isochronally aged for 24 hours at temperatures ranging from 149°C to 216°C. The aged samples were tested for tensile properties and the results are shown in Table 14. It is observed that the ductility may be improved by sacrificing strength by overaging treatment at 216°C.

The low density Al-Li based class 1 alloy studied under the present NASA-Langley Phase II program failed to exhibit adequate tensile ductility for damage tolerant applications. The major physical metallurgical aspects of Al-Li alloy development are well understood, and several studies are available in the literature, which address the poor ductility and fracture behavior of Al-Li alloys.

Further alloy development strategies by modifying the alloy composition should be explored. Attempts should be made to make innovative alloying additions and introduction of dispersoids, which would disperse the planar slip inherent to Al-Li alloys. Attempts should also be made to alter the nature of grain boundary precipitates.

4.2 Class 2 Alloys

The composition of class 2 alloy is based on 2124 alloy with the addition of 0.6% Zr and 1.0% Ni. Zr addition was made primarily to provide a fine grained unrecrystallized structure, and Ni additions were made to introduce a fine dispersion of intermetallic compounds of Al and Ni, which are stable and resist coarsening at elevated temperatures. This strategy was undertaken to design a high strength, damage tolerant alloy exhibiting good thermal stability up to 177°C.

The class 2 alloy samples were extruded, and after extrusion, were subjected to solution heat treatment and natural and artificial aging treatments. The hardness of as-extruded class 2 alloy was R_B 67. The alloy samples were solution heat treated at 488°C for 1 hour and then cold water quenched. The hardness of solution treated samples was R_B 62. Subsequently the alloy was aged at 185°C for 12 hours (T6 Temper) to a hardness value of R_B 78. The T4 temper corresponded to natural aging for 96 hours after solution heat treatment. The tensile properties of the alloy under various heat treatment conditions (T4 and T6) were determined at room and elevated temperatures up to 177°C. Test specimens were taken from the longitudinal and long-transverse directions of the extruded bars. The mechanical property data are listed in Table 15 and 16. Tables 15 and 16 also show the tensile data for 2124 alloys in T4 and T6

conditions, produced via a gas atomization process (9). These alloys did not contain any additions of Zr and Ni. The room temperature yield and ultimate tensile strengths of class 2 and gas atomized 2124 alloys are of similar magnitude, however the ductility of class 2 alloys is lower. The dispersoids of Zr and Ni do not show any considerable strength improvement of class 2 alloys. However, the elevated temperature tensile properties of the class 2 alloy in T4 aged condition measured in longitudinal direction showed good improvement when compared with the commercial ingot metallurgy 2124 alloy (Table 17). High temperature tensile data for PM 2124 alloys, under similar microstructural and heat treatment conditions as those for class 2 alloys, are not available in the open literature.

4.2.1 Thermal Stability of Class 2 Alloy:

The specimens from the extruded bar was solution treated at 488°C/1 hour followed by water quenching to room temperature. Subsequently the alloy was naturally aged at room temperature for 4 days (T4 condition). The aged samples were isothermally exposed at 121°C, 149°C, 177°C and 204°C for 1000 hours and then tested for tensile properties at room and elevated temperatures. The data are plotted in Figure 31 a-d. In the same Figure, the data of tensile properties of the alloy prior to 1000 hours thermal exposure at high temperatures are plotted. From the data shown in Figure 31, the tensile properties of class 2 alloy

did not seem to deteriorate appreciably after 1000 hours exposure at temperature up to 149°C, indicating good stability of the microstructures. The alloy suffered considerable loss of strength after exposure at 177°C and 204°C.

4.2.2 Microstructures

Optical photomicrographs of class 2 alloy in as-extruded condition and in T4 aged condition are shown in Figures 32 and 33. The material in as-extruded condition exhibited an extremely fine grained unrecrystallized microstructure. Individual grains-subgrains were barely discernible at the range of magnifications obtainable by optical microscopy. The alloy in T4 condition also shows an extremely fine grained microstructure.

A sample of class 2 alloy heat treated in T-4 condition was subjected to microstructural analysis by the TEM technique. Figures 34-36 show typical areas in this sample which exhibits a grain size of 2 to 10 microns. The size distribution of the second phase particles (labeled A,B,C in Figure 34) ranges between a few hundred Angstroms to one-half micron. The dislocation density is low. A few grains have a very mottled appearance which seems to be associated with a high density of spherical strain centers. STEM analysis of this sample shows

that the larger precipitates (A) contain Cu and Ni; the smallest precipitates (C) contain Cu and Zr; and the mid-size precipitates (B) are rich in Cu, Mn, and Zr.

4.2.3 High Cycle Fatigue Properties

High cycle axial tension/tension fatigue test was carried out with test specimens prepared with loading axis parallel to the longitudinal and transverse directions of the extruded bar of the class 2 alloy. Figure 37 shows the sketch of the high cycle fatigue test specimen ($K_t=1$). The test conditions and the results are given in Table 18. The specimens were fully heat treated to T4 condition prior to HCF testing. The S-N curves based on the high cycle fatigue data are shown in Figure 38.

4.2.4 SEM Fractography of High Cycle Fatigue Specimens

SEM fractographic investigation of a typical fatigue fracture surface of one specimen (which failed at 86,000 cycles and 39.5 Ksi stress) is reported herein.

SEM photomicrographs of the fracture surface of the fatigue specimen are exhibited in Figures 39-42. The fracture initiation site showed a large silicon-rich inclusion. Another large inclusion, a particle about 230 µm in diameter, was rich in molybdenum and nickel; Si, Al, Mg were subminor elements. No features resembling fatigue beach marks were seen.

SEM photomicrographs of the fracture surface of the fatigue specimen (L-T orientation) of class 2 alloy are exhibited in Figures 43 and 44. The specimen failed during HCF test at 122 x 10^3 cycles and 29 Ksi stress. There are ridges oriented in the general direction of crack propagation. Flat featureless plateaus characterize the ridges. The origin of fracture was not identified in the photomicrograph. However, an aluminum rich inclusion was observed as identified by EDS (Figure 45). There was no evidence of fatigue markings.

4.2.5 Fatigue Crack Growth (FCG) Rate

Fatigue crack growth rate was measured with compact tension samples of class 2 alloy in T-4 heat treated condition. Figure 46 shows the sketch of the specimen and the Tables 19, 20 and 21 show the various test conditions and test data. The data shown are plotted in Figure 47 as a function of stress intensity factor. Data for ingot metallurgy (IM) 2124 plates (containing no Zr) are also shown in Figure 47. These data were obtained from a study by Rao and Ritchie (10), where the tests were carried out on compact tension specimens machined along the T-L orientation, tested in air with R=0.1, at 50 Hz. The IM-2124 plates were in peak-aged (T351) condition. The fatigue crack growth characteristics of ingot metallurgy 2124 alloy appears comparable to those of class 2 alloy, although it is difficult to make any sensible comparison between the two sets of data

since they were acquired at different experimental conditions. The fatigue crack growth resistance characteristics of fine grained PM aluminum alloy are generally poor at low stress intensity factor compared to ingot metallurgy (IM) alloys. However the present class 2 alloy shows reasonably good combination of high fatigue strength and fatigue crack growth resistance compared to IM 2219 alloy (16)(Figure 48). In Figure 49 the S-N curve data for class 2 alloy is compared with the data band for ingot metallurgy 2219-T851 alloy (16). The fatigue life behavior of the class 2 alloy appears to be far superior than that of the corresponding ingot metallurgy alloys.

4.2.6 Fracture Toughness

Fracture toughness tests were carried out with pre-cracked test specimens of class 2 alloy in T-4 condition. Specimens in L-T and T-L orientations were prepared according to the sketch (Figure 50). The results are shown in Table 22. Chellman (11) has reported the fracture toughness of PM 2124 alloys, produced by the consolidation of gas atomized powders. Although no valid K_{Ic} values are available, the K_Q values have been reported to be as high as 44.3 $Ksi\sqrt{in}$ for PM 2124 plates. No valid comparison of the data for class 2 alloys and PM 2124 studied by Chellman (11) can be made, since the solution heat treatment temperature and the aging temperatures used in the two studies are different.

4.3 <u>Class</u> <u>3</u> <u>Alloy</u>

Class 3 alloy is an Al-8Fe-2Mo alloy, which has been designed for structural applications at elevated temperatures. Table 23 shows the tensile test data on smooth and notched specimens of class 3 alloy in as extruded condition (orientation). The tensile tests were performed at room temperatures elevated temperature tests were carried out after exposing the specimens at the test temperature for 30 minutes. The tensile properties were measured along the longitudinal direction (parallel to the extrusion direction). For comparison, tensile properties of powder metallurgy Al-8Fe-2Mo alloys investigated by Zindel et al. (12) is also included in Table 23. The tensile strength of class 3 alloys is lower, primarily due to the prolonged high temperature exposure (total of 8 hours at 400°C) during the two stage hot - extrusion process. There may also be some difference in the actual chemistries of the two alloys.

Table 23 also shows the notched tensile strengths of class 3 alloy at different testing temperatures. The ratio of notched tensile strength to the yield strength gives a rough estimate of the fracture toughness(6). At all the three temperatures of measurement, the ratio of notched tensile strength to the yield strength of class 3 alloy is above 1.4, which indicates that these alloys possess good fracture toughness.

4.3.1 Microstructural Details

Figures 51-53 show the microstructure of class 3 alloy in as-extruded condition. The optical micrograph in Figure 51 shows the fine grained structure as a result of rapid solidification. The photomicrographs also show isolated oxide stringers shown in Figure 49 pointed out by arrow along the extrusion direction. The fine details of the microstructure were obtained through transmission electron microscopy. Figures 53 through 56 are typical fields of view of the class 3 alloy samples, which show a grain size of 2-5μm and the second phase particle size ranges from 100 A to 1.0μm. These particles are mostly Al_6Fe precipitates. STEM analysis shows that larger particles (shown as A in Figure 54) are an Al-Fe phase with some amount of Mo in solution. The smaller particles (labeled B in Figure 54) also possess small amounts of Mo. Therefore Mo is partitioned between solid solution and the dispersoid phase; and contributes to solid solution strengthening. However, during processing, such as hot extrusion, or exposure to elevated temperatures, Mo tends to precipitate out along with Fe, as very fine precipitates (labeled A in Figure 55) within the matrix. The large primary particles and smaller intermetallic precipitates and their distributions are shown in the STEM micrographs of Figures 57 and 58.

As reported in Table 23, class 3 alloy showed good ductility. The fracture surfaces of the tensile samples tested at room temperature, were observed in SEM. Figure 59 a-d show the fracture surfaces of tensile samples of as-extrudedclass 3 alloy. There is little evidence of de-cohesion or delamination between powder particles. The majority of the fracture surface is dimpled suggesting that cracks in the tensile specimens mostly propagated by coalescence of voids nucleated at the prior powder particle boundaries.

4.3.2 Thermal Stability

Al-Fe-Mo alloys are being designed for structural applications at temperatures ranging from 232°C to 343°C. Tensile properties at elevated temperatures are shown in Table 23, and it is clear that the alloy retains substantial amount of its strength at 343°C. Further tensile tests were performed after annealing the alloys at 371°C and 400°C for 500 hours, Table 24 shows the tensile data of specimens annealed at high temperature. After 500 hours at 400°C, the class 3 alloy retained 75% of its initial yield and tensile strength. The excellent thermal stability of these alloys is also supported by the micrographs in Figures 60 and 61. The microstructure of class 3 alloy shows excellent resistance to coarsening during exposure to high temperature.

4.3.3 Creep Behavior of Class 3 Alloy

Since class 3 alloys are being designed for elevated temperature structural applications, their creep behavior has been characterized. Stress rupture tests were performed at 3 different temperatures, ranging from 232°C to 343°C, and the tests were performed under different loads at each temperature. Table 25 shows the stress rupture data for class 3 alloy at different temperatures and loads. Figure 62 shows stress rupture data plotted on a semi-log plot, where the time to rupture has been plotted against the stress for different temperatures. These data plot linearly and can be fit to the Sherby-Dorn or Larsen and Miller framework of creep phenomena. Figures 63 and 64 show the creep curves of class 3 alloys samples at 232°C and 343°C. Steady state creep is attained at both the temperatures. To elucidate the exact mechanism of creep, extensive mechanical testing and microstructural examination will be required.

4.4 Class 4 Alloy

This is an experimental alloy designated as X7091 (Bal Al,6.46Zn,2.42Mg,1.49Cu, and 0.42Co). The extruded bar of the alloy was solution heat treated at 488°C for one hour and subsequently cold water quenched. Natural aging was performed by holding the sample at room temperature for 96 hours. The peak aging treatment consisted of exposure at 121°C for 24 hours; and heat treatment at 145°C for 14 hours led to overaging.

Table 26 lists the properties of class 4 alloy in peak and over aged condition. In the same table, the tensile properties of commercial high strength 7075-T6 aluminum alloy are listed. The strength values of RST X7091 in peak aged condition exceeded the 7075-T6 values.

4.4.1 Microstructure

Figure 65 shows the optical micrographs of class 4 alloy in the as-extruded condition. The microstructure is very fine, consisting of a random dispersion of second phase particles. Figure 66 shows a higher magnification photomicrograph of class 4 alloy in as-extruded condition. A closer examination of the micrograph shows a fine grain size and a uniform dispersion of the second phase particles. Figure 67 contains the photomicrographs of a peak age samples of class 4 alloy, and one observes

that most of the primary phases have dissolved, with the exception of the dispersoids. A fine grain structure of class 4 alloy can be seen more clearly after solution heat treating and aging.

4.4.2 Fractographic Studies

Tensile fracture surfaces of solution heat treated and aged alloys were examined by the SEM technique. The alloy in the peak aged temper failed in the 45 degree shear mode, which is characteristic of ductile materials. Scanning electron micrographs obtained from the 45 degree shear faces of the class 4 alloy in the peak aged condition revealed that the fracture was predominantly transgranular (Figure 68). Dimples associated with ductile failure were evident on the fracture surface at high magnification (Figure 69).

4.4.3 Effect of Different Heat-Treatments

Samples of class 4 alloy were subjected to different heat treatments and their treatments and their tensile properties were compared. T7E69 treatment consisted of solution heat treatment at 488°C for 1 hour; cold water quench; natural aging at room temperature for 96 hours; age at 121°C for 24 hours and subsequently age at 163°C for 4 hours. Whereas in T7E70 temper, after natural aging for 96 hours, the alloy is aged at 163°C for

20 hours. In T7E70 treatment, the alloy sample is aged for longer time at 163°C. Room temperature tensile properties of class 4 alloy were measured and are shown in Table 27. Figures 68 and 69 show the true stress-true strain plots of the specimens tested in tension. Table 27 also shows the tensile data for X7091-T7E69 extrusions produced by Alcoa's gas atomization process (13). The tensile strength of alloys produced at Alcoa is higher. The difference in strengths between Alcoa's X7091 alloy and class 4 alloy mainly arises due to the differences in processing and consolidation parameters.

4.4.4 Fatigue of Class 4 Alloy

The class 4 alloy samples were given the T6 aging treatment before fatigue testing. The T6 aging treatment consists of the following heat treatment cycles:

(1) Solution heat treatment at 488°C for 1 hour

(2) Cold water quench

(3) Age at room temperature for 96 hours

(4) Age at 121°C for 24 hours (peak age)

High cycle fatigue test specimens were prepared from the heat treated bars of class 4 alloy. The specimens axis was

chosen to lie parallel to the longitudinal direction of the bar. Table 28 shows test conditions and results of high cycle fatigue tests.

The fracture surface of the specimens which failed after fatigue at 26Ksi and 265,000 cycles were examined in the scanning electron microscope. Figures 72-74 show the SEM fractographs of the fatigue fracture surfaces of the class 4 alloy. The fatigue of fine grained material does not always reveal beach marks typical of fatigue failure. No evidence of large inclusions was seen in the fracture surface. Figure 74 shows some additional fractographs showing the morphology of the fracture propagation area.

Additional high cycle fatigue tests were performed on class 4 samples aged to T7E70 condition. Tests were carried out on six longitudinal and two transverse smooth bar specimens. Table 29 contains the test conditions and the results of high cycle axial tension fatigue tests. The S-N curves based on the HCF data are shown in Figure 75. It is apparent from the data that the fatigue strength of the samples of class 4 alloy tested in the transverse orientation is considerably lower than the fatigue strength in longitudinal orientation.

In figure 76 the S-N curves are plotted for class 4 alloy heat treated to T6 and T7E70 aging treatment. T6 treatment gives rise to higher strengths, but lower fatigue strengths.

This is a common observation that improvement of property through microstructural manipulations or thermomechanical treatments is achieved at the expense of another property.

Additional fractography was carried out on class 4 alloy - T7E70 specimens which failed during the high cycle fatigue tests. The following three samples were investigated:

Specimen 1: Longitudinal specimen which failed at 38 Ksi/97,000 cycle.

Specimen 2: Longitudinal specimen which failed at 45 Ksi/92,000 cycle.

Specimen 3: Transverse specimen which failed at 20 Ksi/325,000 cycle.

The origin of fracture of Specimen 1 showed material inside an elongated void (Figure 77). The material had more magnesium than a typical fracture region (Figures 78 and 79). The fracture mode is intergranular and shows dimple formation.

The fracture surface of Specimen 2 had an origin site which showed high level of silicon (Figures 80 and 81) as compared to the general fracture propagation region away from the origin (Figure 82).

The fracture surface of Specimen 3 (transverse) showed a "woody" structure devoid of fatigue markings (Figure 83). The fracture origin was uncertain, but subtle markings suggested that the fracture might have originated at the location near void (Figure 84). The general fracture surface containing ridges in the direction of crack propagation is shown in Figure 85.

High cycle fatigue tests were also performed on class 4 alloy samples aged to T7E69 condition. The tests were performed for two different stress concentration factors, namely K_t = 2.7 and K_t = 4.0. The relevant test data and conditions are given in Table 30. Figure 86 shows the data of Table 30 in the form of S-N curves. It is apparent from the curves in Figure 86 that varying the stress concentration factor from 2.7 to 4.0 does not change the fatigue life appreciably. In figure 87, the high cycle fatigue data on class 4 alloy in T7E69 conditions is compared with the fatigue data of Langenbeck (13) on X7091-T7E69 alloy acquired under same test conditions. The fatigue strength of X7091-T7E69 alloy is higher than that of class 4 alloy aged to the same temper.

4.4.5 Fatigue Crack Growth Behavior

Fatigue crack growth characteristics of high strength powder metallurgy aluminum alloy such as X7091 are of great interest

due to damage tolerant design requirements. One concern of the fine grain powder metallurgy alloys is the faster fatigue crack growth rates in the linear regions of the curve in comparison to conventional ingot metallurgy alloys.

Fatigue crack growth rate was measured with compact tension samples of class 4 alloy in T7E70 condition. Tables 31, 32, and 33 show the various test conditions and fatigue crack growth data. The data are plotted in Figure 88 as a function of stress intensity factor. The fatigue crack growth rate of the present alloy in L-T orientation is less than that in the longitudinal orientation. All the curves, however, appear to converge at 1 x 10^{-6} inches/cycle. The fatigue crack growth rate of the class 4 alloy (T7E70) is similar to PM X7091-T7E69 studied by various other investigators (13-15). However, fatigue crack growth data for IM or PM X7091 alloys in the T7E70 temper is not available in the open literature.

4.4.6 Fracture Toughness

Fracture toughness tests were carried out with pre-cracked test specimens of class 4 alloy in T7E70 conditions. Specimens in L-T and T-L orientations were prepared according to the sketch shown in Figure 48. The results are given in Table 34. No fracture toughness data for X7091 alloys under similar experimental conditions are available in the open literature.

5 SUMMARY

Four different types of aluminum alloys were prepared by Marko's rapid solidification process. The class 1 alloy was based on Al-Li system; class 2 alloy was based on commercial 2124 composition with the addition of 0.6% Zr and 1% Ni; class 3 alloy was based on Al-Fe-Mo system, which has been identified as candidate alloys for structural applications at elevated temperatures (approx. 316°C); and class 4 alloy was based on high strength Al-Zn-Mg alloys with small additions of Co. The rapidly solidified alloy ribbons were pulverized, canned, and cold compacted at 22.5 Ksi, hot evacuated at 400°C to vacuum level below 1 μm and held isothermally for four hours. The cans were vacuum sealed and hot upset using a blind die and at full ram pressure 1400 ton.

Powders of alloys 1, 2 and 4 were successfully hot extruded at a reduction ratio of 31.66:1 at 400°C. The class 3 alloy billet stalled at above was double extruded to a total reduction of 46.7:1 at 400°C.

Microstructure and mechanical properties of alloys of each class were evaluated. The goals for class 1 alloy development was to produce alloys based on Al-Li system, which gave 2024-T4 type strength levels, but low density and higher modulus. Zr additions were made to class 1 alloy to maintain the unrecrystallized structure during solution heat treatment. The

alloys were successfully extruded, and were given different combinations of heat treatments to optimize strength and ductilities. Yield strength to the level of 50 Ksi were achieved, but tensile elongation in most cases remained below 2%. The fracture surfaces after tensile testing appeared intergranular for most of the aged samples. The poor ductility of Al-Li has been shown to be due to slip planarity promoted by Al_3Li precipitates and a very high density of intergranular coarse precipitates, which form during the artificial aging treatment. It appears that to alleviate the low ductility problem of class 1 Al-Li-Mg alloys, one must try further alloying additions of Cu and Zr to obtain (i) more precipitates in the matrix that would disperse slip, and (ii) avoid the precipitation of intergranular AlLi phase by changing the phase equilibrium.

Goal for class 2 alloy development based on 2124 commercial Al alloy with the addition of Zr and Ni was to develop damage tolerant alloy showing good thermal stability up to 177°C. Small additions of Zr and Ni were made to obtain fine and stable dispersoids in the alloy microstructure through rapid solidification processing. Zr also inhibits recrystallization and helps maintain a fine grain structure after solution heat treatment. The dispersoids based on the intermetallic compounds of Al and transition metal elements (e.g. Ni) resist coarsening at elevated temperatures. The rapidly solidified class 2 alloy

showed higher strength than the IM 2024 alloys, with high levels of ductility. The RS class 2 alloy maintained good tensile strength (approx. 53 Ksi) after 1000 hour exposure at 149°C. Rapidly solidified class 2 alloy showed better high cycle fatigue strength and fatigue crack growth resistance, when compared to the same properties of ingot metallurgy 2219-T851 alloy. The fatigue crack propagation behavior of class 2 alloys was comparable to that of IM 2124 alloys.

Class 3 alloy is based on the Al-Fe-Mo alloy system, which can be produced only via rapid solidification route, which helps in the incorporation of a large amount of Fe and Mo in the solid solution phase. Upon exposure to high temperatures, a number of solid state precipitation processes occur, which lead to additional strengthening. A fine level of dispersion of intermetallic phases also exists in the as rapidly solidified ribbons. The class 3 alloy powders were consolidated through a two stage hot extrusion process. The as-extruded alloys showed a good combination of room and elevated temperature tensile strength and ductilities. The class 3 alloy retained sufficient strength (approx. 20 Ksi) at 343°C. Stress rupture tests were also performed at several temperatures and different stress levels. The rupture life at 288°C and under a load of 17 Ksi was 191.7 hours. The stress rupture data can be fitted to the

framework of Sherby-Dorn or Larsen-Miller creep phenomenon. More work will be required to understand the actual mechanism governing creep of class 3 alloys.

The class 4 alloy is based on high strength Al-Zn-Mg alloys with small additions of Co as the dispersoid forming element. The composition of the class 4 alloy is very similar to that of PM X7091 alloy. The yield and tensile strengths of rapidly solidified class 4 alloy exceeded those of the commercial high strength 7075-T6 aluminum alloys. The microstructure of class 4 alloy in the heat-treated condition consisted of a fine grain size and a uniform dispersion of the fine, micron size intermetallic particles. Different heat treatment schedules were tried to optimize the strength and ductility of class 4 alloy. The treatment T7E69 and T7E70 resulted in similar levels of strength and ductility. The strength obtained after T7E69 or T7E70 is lower than that obtained after the T6 temper.

High cycle fatigue tests were carried out for class 4 alloy aged to T6, T7E69 and T7E70 conditions. Higher fatigue strengths are obtained in the T7E69 and T7E70 conditions, at the cost of tensile strengths. High cycle fatigue tests were performed on class 4 alloy - T7E69 sample at stress concentration factors (K_t) of 2.7 and 4.0. Varying the stress concentration factor K_t from 2.7 to 4.0 did not alter the

fatigue life appreciably. The high cycle fatigue characteristics of class 4 alloy agrees well with the published data on high cycle fatigue of PM X7091 alloys.

The fatigue crack growth rate in class 4 alloy T7E70 samples is faster in longitudinal orientation, when compared with that in the L-T orientation. The fatigue crack growth rate data of class 4 alloy is similar to the reported data on PM X7091 alloys by other investigators, although no direct comparisons are available.

In conclusion, wherever the properties of melt-spun aluminum alloys prepared in this study could be compared with the mechanical properties of equivalent gas-atomized alloys, the melt-spun alloys showed equivalent or inferior properties. This was due to the presence of inclusion and contaminants, probably introduced during the pulverization step. Moreover, since the consolidation parameters were not optimized, the inadequate consolidation procedure translated into inferior mechanical properties. Large scale production of melt-spun Al-Li based alloys will require considerable process modifications to alleviate the problem of excessive loss of lithium from the molten metal.

6 REFERENCES

(1) Mehrabian, Robert, B.H. Kear, and M. Cohen, eds.: _Rapid Solidification Processing: Principles and Technologies II._ Claitor's Publishing Division, 1980.

(2) Jones, H.: Observations on a Structural Transition in Aluminum Alloys Hardened by Rapid solidification. _Materials Science and Engineering,_ Vol. 5, no. 1, Nov. 1969, pp. 1-18.

(3) Jones, H.: Developments in Aluminum Alloys by Solidification at Higher Cooling Rates. _Aluminum,_ Vol. 54, No. 4 Apr. 1978, pp. 274-281.

(4) Sanders, R.E.,Jr. and G.J. Hildeman: Elevated Temperature Aluminum Alloy Development, Final Technical Report, September. 1977-May 1981. AFWAL-TR-81-4076, 1981.

(5) Adam C.M.: Structure/Property Relationships and Applications of Rapidly Solidified Aluminum Alloys. Rapidly Solidified Amorphous and Crystalline Alloys, B.H. Kear, B.C. Giessen, and M. Cohen, eds., North-Holland, 1982, pp. 411-422.

(6) Paris, H.G., F.R. Billman, W.S. Cebulak, and J.J. Petit: The Influence of Particulate Morphology and the Thermal History in Consolidation and Metalworking on Mechanical Properties of Al-Fe-Ni-Co and Al-Mn-Si alloys. _Rapid Solidification Processing: Principles and Technologies II,_ Robert Mehrabian, B.H. Kear, and M. Cohen, Eds., Claitor's Publishing Division, 1980, pp. 331-341.

(7) Grant, N.J.: A Review of Various Atomization Processes. _Rapid Solidification Processing: Principles and Technologies,_ R. Mehrabian, B.H. Kear, and M. Cohen, Eds., Claitor's Publishing Division, 1978, pp. 230-245.

(8) G. Chanani, G.H. Narayanan and I.J. Telesman, in, _High Strength Powder Metallurgy Aluminum Alloys,_ Eds., M.J. Koczak and G.J. Hildeman, Vol.1, Conf. Proc. TMS-AIME, 1982, pp. 341-368.

(9) B. Sarkar and W.B. Lisagor, _Rapidly Solidified Powder Aluminum Alloys,_ ASTM STP 890, M.E. Fine and E. A. Starke, Jr., eds., ASTM, Philadelphia, 1986, pp. 333-353.

(10) K.T. Venkateswara Rao and R.O. Ritchie, "Effect of Prolonged High-Temperature Exposure on the Fatigue and Fracture Behavior of Aluminum-Lithium Alloy 2090", March 1987, submitted to Materials Science and Engineering.

(11) D.J. Chellman, "Development of Powder Metallurgy 2XXX Series Al Alloys for High Temperature Aircraft Structural Applications", NASA Contractor Report 172408, November 1984.

(12) J.W. Zindel, P. Kurath and H.L. Fraser, High Strength Powder Metallurgy Aluminum Alloys II, Conf. Proc., TMS-AIME, eds. G.J. Hildeman and M.J. Koczak, 1986, pp. 213-222.

(13) Langenbeck S.L.: Investigation of the Fatigue and Crack Propagation Properties of X7091-T7E69 Extrusion; High Strength Powder Metallurgy Aluminum Alloys, Eds., M.J. Koczak and G.J. Hilderman, Vol.1, Conf. Proc. TMS-AIME, 1982, pp. 87-105.

(14) S. Hirose and M.E. Fine, "Fatigue Crack Initiation and Microcrack Propagation in X7091 Type Aluminum P/M Alloys", in High-Strength Powder Metallurgy Aluminum Alloys" Conf. Proc., TMS-AIME, eds. M.J. Koczak and G.J. Hildeman, 1982, pp.19-40.

(15) Y.W. Kim and L.R. Bidwell, "Effects of Microstructure and Aging Treatment on the Fatigue Crack Growth Behavior of High Strength P/M Aluminum Alloy X7091", High-Strength Powder Metallurgy Aluminum Alloys , Conf. Proc., TMS-AIME, eds. M.J. Koczak and G.J. Hildeman, 1982, pp.107-124.

(16) Technical Report Number AFML-TR-78-40

TABLE 1

ALLOY TYPE	COMPOSITION (WEIGHT PERCENT)
CLASS 1 (AL-LI)	AL-2.7LI-5.3MG-0.22ZR
CLASS 2 (2124+NIZR)	AL-4.4CU-0.6MO-L.5MG-0.6ZR-1NI
CLASS 3 (AL-FE-MO)	AL-8FE-2MO
CLASS 4 (X-7091)	AL-6.4ZN-2.42MG-1.49CU-0.4CO

Alloy	Melt Spinning Temperature (°C)	Orifice diameter (mm)	Argon pressure (psi)	Length of Stream (mm)	Impingement angle (degrees)	Surface speed (m/sec)
Class 1	760-788	1.5-2.0	10-12	6-10	45-60	2200
Class 2	721-799	1.5-2.0	10-12	6-10	60	2200
Class 3	1011-1038	1.5-2.0	10-12	6-8	45-60	2200
Class 4	760-788	1.5-2.0	10-12	10-15	60	2200

Table 2: Optimum Melt-Spinning Parameters.

Table 3: Hot Extrusion of Four Powder Metallurgy Aluminum Alloys

Alloy	Ram Speed (in/min)	Upset Force (Tons)	Running Force (Tons)	Remarks
Class 1	5	718	578	Extruded as continuous bar with good surface and edge condition
Class 2	5	858	718	Extruded as continuous bar with good surface and edge condition
Class 3	5	1400	Stalled	The Billet Stalled the Press
Class 4	5	718	630	Extruded as continuous bar with good surface and edge condition

Table 4:   First Stage Hot Extrusion of 5.575 Inch Diameter Billet of Class 3 Alloy

Ram Speed (in/min)	Upset Force (Tons)	Running Force (Tons)	Remarks
5	980	875	Extruded as continuous bar with good surface and edge conditions.

Table 5:   Second Stage Hot Extrusion of Class 3 Alloy

Billet Number	Ram Speed (in/min)	Upset Force (Tons)	Running Force (Tons)	Remarks
1	25	120	110	Extruded as
2	25	125	120	Continuous bar
3	25	110	100	With Good Surface
4	25	110	100	and Edge Conditions

Table 6: Room Temperature Tensile Properties (Longitudinal Orientation) of Class 1 Alloy Solution Treated at 524°C and aged at 71 and 127°C.

Aging Treatment	0.2%Y.S. (Ksi)	UTS (Ksi)	%Elong.	%RA
71°C/24 Hrs.	*	*	*	*
127°C/24 Hrs.	49.7	49.7	1.2	0.8
127°C/72 Hrs.	*	*	*	*

* Specimen failed before reaching yield.

Table 7: Room Temperature Tensile Properties of Class 1 Alloy Solution Treated at 524°C and Aged at 149°C.

Aging Time (Hrs.)	Specimen Direction	0.2% Y.S. (Ksi)	U.T.S. (Ksi)	%Elong	%RA	Young's Modulus (10^3Ksi)
1	L	52.5	54.0	2.0	2.3	11.1
1	L	53.4	53.4	2.0	2.0	10.3
1	L-T	55.5	56.3	2.0	2.5	10.9
24	L	62.2	62.6	2.0	1.4	11.7
24	L-T	58.5	59.0	2.0	1.9	11.5

Table 8: Room Temperature Tensile Properties of Class 1 Alloy Solution Treated (SHT) at 524°C and aged at 171°C Tested in Longitudinal Orientation. Data for a similar alloy (8) produced by gas atomization, SHT at 525°C and aged at 170°C is also included.

Aging Time (Hrs.)	0.2% Y.S. (Ksi)	U.T.S. (Ksi)	%Elong	%RA	Young's Modulus (10^3Ksi)
1	–	–	–	–	11.6
1	–	–	–	–	11.1
12	62.0	62.6	2.0	2.2	12.0
12	–	–	–	–	10.7
100	44.0	46.7	1.5	1.1	11.4
100	–	–	–	–	11.7
0.25*	49.0	69.0	7.0		
0.50*	55.0	74.0	6.5		

(–) Specimen failed before reaching yield.
(*) Data From Reference 8.

Table 9: Room Temperature Tensile Properties of Class 1 Alloys Solution Treated (SHT) at 524°C and Aged at 185°C, Tested in Longitudinal Orientation. Data for a similar alloy (8) produced by gas atomization, SHT at 525°C and aged at 170°C is also included.

Aging Time (Hrs.)	0.2% Y.S. (Ksi)	U.T.S. (Ksi)	%Elong	%RA
4	–	–	–	–
8	40.9	46.4	1.8	1.5
16	–	–	–	–
24	40.9	40.9	1.4	0.9
3*	63.0	74.0	3.0	
8*	61.0	76.0	3.0	

(–) Specimen failed before reaching yield.
(*) From Reference (8).

Table 10 Room Temperature Tensile Properties (Longitudinal Orientation) of Class 1 Alloy Solution Treated at 524°C and Aged at 200°C.

Aging Time at 200°C (Hrs.)	0.2%Y.S. (Ksi)	UTS (Ksi)	%Elong.	%RA
4	46.0	47.5	1.8	1.5
8	44.6	48.2	1.8	1.2
16	44.8	49.7	2.0	2.0
24	41.6	41.6	1.8	1.4

Table 11: Room Temperature Tensile Properties (Longitudinal Direction) of Class 1 Alloy Solution Treated at 524°C and Aged at 215°C.

Aging Time at 215°C (Hours)	0.2% Y.S. (Ksi)	UTS (Ksi)	%Elong.	%RA
4	42.2	47.0	1.8	1.7
8	42.0	47.0	2.0	2.2
16	45.1	48.3	1.7	1.6
24	42.3	44.1	1.5	0.8

Table 12:   Room Temperature Tensile Properties of Class 1 Alloy (Longitudinal Orientation) Solution Treated at Different Temperatures and Aged.

Solution Treatment Temperature (°C)	Aging Treatment (°C/Hours)	0.2% Y.S. (Ksi)	UTS (Ksi)	%Elong.	%RA
468	166/24	42.8	43.1	2.0	2.3
468	182/15	37.1	40.9	2.0	2.1
482	166/24	47.9	50.0	1.4	2.2
482	182/15	42.7	43.7	1.2	1.4

TABLE 13

ENERGY DISPERSIVE X-RAY SPECTROGRAPHY OF TENSILE FRACTURES

OF CLASS 1 ALLOY

SAMPLE NO.	LOCATION	ELEMENTS DETECTED		
		MAJOR	MINOR	SUBMINOR
1	CRACK ORIGIN SITE	Ti	Al	------
2	CRACK ORIGIN SITE	Al	-----	------
3	CRACK ORIGIN SITE	Al, Co, Cr, W	-----	Fe
4	CRACK ORIGIN SITE	Al	Fe, Ti	Cu

Table 14: Room Temperature Tensile Properties (Longitudinal Orientation) of Class 1 Alloy Solution Treated at 499°C and Aged at Different Temperatures.

Aging Treatment (°C/Hours)	Test No.	0.2% Y.S. (Ksi)	U.T.S. (Ksi)	%Elong.	%RA
149/24	1	–	53.7	1.9	2.4
149/24	2	55.8	58.2	2.7	4.1
166/24	1	50.7	54.3	1.9	3.3
166/24	2	–	–	–	–
182/24	1	58.8	60.4	2.6	3.6
182/24	2	60.0	61.4	2.7	4.1
199/24	1	39.0	39.0	1.2	2.2
199/24	2	44.0	46.0	1.3	3.1
216/24	1	41.1	47.7	4.0	4.4
216/24	2	43.3	47.9	4.3	3.3

Table 15:   Room and Elevated Temperature Tensile Properties of Class 2 Alloy
            Following Solution Treatment and Natural Aging for 96 Hours (T4). Data
            for Gas Atomized 2124 Alloys in Similar Conditions are Also Included (9).

Specimen Direction	Test Temp. (°C)	Test No.	0.2% Y.S. (Ksi)	U.T.S. (Ksi)	%Elong.	%RA	Young's Modulus (10^3 Ksi)
L	Room	1	60.1	72.0	7.0	6.7	11.6
L	Room	2	59.6	67.2	5.8	5.5	11.8
L–T	Room	1	53.0	53.9	1.6	3.1	11.6
L*	Room		53.6	78.4	19.2		
L	121	1	60.6	72.2	11.4	12.3	–
L	121	2	60.6	71.3	9.9	10.1	–
L–T	121	1	52.0	54.7	2.6	4.6	–
L	177	1	52.0	60.0	14.0	13.9	–
L	177	2	51.3	59.2	11.0	12.3	–
L–T	177	1	47.0	47.9	3.6	3.8	–

* From Reference (9).

Table 16: Room and Tensile Properties of Class 2 Alloy Solution Treated and Aged at 185°C for 12 Hours (T6). Data for Gas Atomized 2124 Alloys in Similar Conditions are Also Included (9).

Specimen Direction	Test Temp. (°C)	Test No.	0.2% Y.S. (Ksi)	U.T.S. (Ksi)	%Elong.	%RA	Young's Modulus (10^3 Ksi)
L	Room	1	52.0	61.6	11.0	18.2	11.1
L	Room	2	52.2	61.4	8.5	10.5	11.3
L–T	Room	1	51.6	53.4	2.1	3.1	11.7
L*	Room		51.1	75.5	19.6		
L	121	1	47.0	54.5	11.7	13.7	–
L	121	2	46.8	54.3	12.0	15.9	–
L–T	121	1	46.3	48.2	3.4	4.0	–
L	177	1	38.9	41.5	25.2	36.3	–
L	177	2	36.8	41.2	27.2	42.2	–
L–T	177	1	37.7	39.8	4.8	6.8	–

* From Reference (9).

Table 17: Elevated Temperature Tensile Properties of Class 2 Alloy and Commercial 2124 Alloy in T4 Temper.

Alloy	Test Temp. (°C)	0.2%Y.S. (Ksi)	U.T.S. (Ksi)	%Elong.	%RA
Class 2	121	60.6	71.8	10.7	11.2
2124	121	41.7	60.6	13.5	19.5
Class 2	177	51.7	59.5	11.9	14.8
2124	177	37.2	55.5	17.0	22.5

TABLE 18

CONDITIONS AND RESULTS OF FATIGUE TESTS

ON CLASS 2 ALLOY IN LONG TRANSVERSE AND LONGITUDINAL DIRECTION

TEST MODE: HIGH CYCLE FATIGUE, AXIAL TENSION/TENSION
TEST ENVIRONMENT: ROOM TEMPERATURE LABORATORY AIR
TEST LOADING: A CONSTANT AMPLITUDE SINUSOIDAL WAVEFORM OF
                   30 HZ FREQUENCY
TEST STRESS RATIO: R=MIN./MAX=0.1
SPECIMEN: SMOOTH BAR

SPECIMEN ORIENTATION	TEST NUMBER	MAXIMUM STRESS (KSI)	CYCLES $(\times 10^3)$	RESULTS (1)
TRANSVERSE (L-T)	1	30	78	GSF
	2	28	122	GSF
	3	25	10,000	RO
LONGITUDINAL	1	40	117	GSF
	2	39.5	86	GSF
	3	39	158	GSF
	4	38.5	71	GSF
	5	38	3,825	GSF
	6	37.5	10,279	RO
	7	37	203	GSF
	8	36.5	10,105	RO
	9	36	10,097	RO
	10	34	10,150	RO

(1) GSF = GAGE SECTION FAILURE
      RO = RUN OUT

TABLE 19
COMPACT TENSION CRACK GROWTH DATA

SAMPLE: CLASS 2 ALLOY (T-4 CONDITION)
ORIENTATION: L-T
TEST TEMPERATURE = ROOM TEMPERATURE
RELATIVE HUMIDITY = 55-60%
TEST ENVIRONMENT = LABORATORY AIR
FREQUENCY = 29Hz
R = 0.1

TOT CYCLES NT (10^3)	CRACK LGTH A (IN)	LOAD RNG (LBS)	STR INT RNG KSI $\sqrt{IN}$	CRACK GROWTH RATE IN/CYC
0	0.317	343	8.05	....
10	0.325	343	8.12	7.5×10^{-7}
20	0.335	343	8.31	1×10^{-6}
30	0.349	343	8.57	1.45×10^{-6}
37	0.362	343	8.88	1.79×10^{-6}
42	0.371	343	9.13	1.8×10^{-6}
46	0.383	343	9.38	3×10^{-6}
49	0.388	343	9.59	1.67×10^{-6}
52	0.394	343	9.72	1.83×10^{-6}
55	0.404	343	9.93	3.5×10^{-6}
58	0.413	343	10.18	2.83×10^{-6}
61	0.426	343	10.48	4.33×10^{-6}
63	0.436	343	10.81	5×10^{-6}
65	0.442	343	11.06	3×10^{-6}
67	0.458	343	11.4	8×10^{-6}
68	0.465	343	11.79	7.5×10^{-6}
69	0.478	343	12.13	1.25×10^{-5}
69.8	0.489	343	12.56	1.37×10^{-5}
70.6	0.498	343	12.96	1.19×10^{-5}
71.4	0.515	343	13.5	2.12×10^{-5}
72.2	0.529	343	14.18	1.75×10^{-5}
72.6	0.54	343	14.78	2.87×10^{-5}
72.9	0.552	343	15.37	3.83×10^{-5}
73.2	0.558	343	15.84	2×10^{-5}
73.5	0.568	343	16.29	3.33×10^{-5}
73.8	0.59	343	17.27	7.33×10^{-5}
74	0.608	343	18.64	9×10^{-5}
74.1	0.627	343	20.08	1.9×10^{-4}
74.2	0.663	343	22.6	3.6×10^{-4}

TABLE 20
COMPACT TENSION CRACK GROWTH DATA

SAMPLE: CLASS 2 ALLOY (T-4 CONDITION)
ORIENTATION: T-L
RELATIVE HUMIDITY = 60%
TEST TEMPERATURE = ROOM TEMPERATURE
TEST ENVIRONMENT = LABORATORY AIR
FREQUENCY = 29 Hz
R = 0.1

TOT CYCLES NT (10^3)	CRACK LGTH A (IN)	LOAD RNG (LBS)	STR INT RNG KSI $\sqrt{IN}$	CRACK GROWTH RATE IN/CYC
0	0.353	429	11.02	....
2	0.37	429	11.27	8.5 x 10^{-6}
3	0.38	429	11.66	9.5 x 10^{-6}
3.8	0.401	429	12.14	2.69 x 10^{-5}
4.1	0.407	429	12.59	2 x 10^{-5}
4.4	0.412	429	12.77	1.5 x 10^{-5}
4.6	0.417	429	12.93	2.5 x 10^{-5}
4.8	0.431	429	13.27	7 x 10^{-5}
4.9	0.435	429	13.61	4.5 x 10^{-5}

TABLE 21
COMPACT TENSION CRACK GROWTH DATA

SAMPLE: CLASS 2 ALLOY (T-4 CONDITION)
ORIENTATION: T-L
RELATIVE HUMIDITY = 63%
TEST ENVIRONMENT = LABORATORY AIR
TEMPERATURE = ROOM TEMPERATURE
R = 0.1
FREQUENCY = 29Hz

TOT CYCLES NT (10^3)	CRACK LGTH A (IN)	LOAD RNG (LBS)	STR INT RNG KSI $\sqrt{IN}$	CRACK GROWTH RATE IN/CYC
0	0.324	214	5.08	············
10	0.328	214	5.11	4.5×10^{-7}
30	0.338	214	5.21	5.25×10^{-7}
48	0.347	214	5.33	4.44×10^{-7}
66	0.361	214	5.49	8.06×10^{-7}
81	0.375	214	5.69	9.33×10^{-7}
91	0.387	214	5.89	1.2×10^{-6}
99	0.396	214	6.05	1.12×10^{-6}
107	0.408	214	6.22	1.5×10^{-6}
114	0.422	214	6.44	2×10^{-6}
120	0.431	214	6.64	1.42×10^{-6}
125	0.443	214	6.83	2.4×10^{-6}
129	0.454	214	7.06	2.88×10^{-6}
132	0.465	214	7.28	3.5×10^{-6}
134	0.474	214	7.49	4.5×10^{-6}
136	0.483	214	7.69	4.5×10^{-6}
137	0.489	214	7.87	6.5×10^{-6}
138	0.496	214	8.03	7×10^{-6}
139	0.505	214	8.23	9×10^{-6}
139.9	0.515	214	8.48	1.11×10^{-5}
140.7	0.528	214	8.8	1.62×10^{-5}
141.3	0.542	214	9.2	2.42×10^{-5}
141.5	0.547	214	9.51	2.5×10^{-5}
141.9	0.555	214	9.72	1.88×10^{-5}
142.1	0.562	214	9.97	3.75×10^{-5}
142.3	0.576	214	10.35	6.75×10^{-5}
142.4	0.591	214	10.9	1.45×10^{-4}

TABLE 22

FRACTURE TOUGHNESS DATA OF CLASS 2 ALLOY (T-4)

TEST SPECIFICATION: ASTM E399-83

TEST ENVIRONMENT: Room Temperature, Ambient Air

70% RELATIVE HUMIDITY

ELASTIC MODULUS = 10×10^6 PSI

ORIENTATION	TEST NO.	K_Q KSI (IN.)$^{\frac{1}{2}}$ (MPA$\sqrt{M}$)	K_{IC} KSI (IN.)$^{\frac{1}{2}}$ (MPA$\sqrt{M}$)
L - T	1	20.8 (22.9)	--
T - L	1	----	15.7 (17.3)
T - L	2	16.1 (17.7)	--

Table 23: Room and Elevated Temperature Tensile Properties (in Longitudinal Orientation) of As-extruded Class 3 Alloy (Al-8Fe-2Mo).

Test Temperature (°C)	Specimen Condition	0.2%Y.S. (Ksi)	U.T.S. (Ksi)	%Elong.	%RA
23	Smooth	46.6	59.2	9.4	12.4
23	Smooth	47.1	59.5	8.1	8.7
20*	Smooth	58.6	67.0		4.0
23	Notched	–	71.3	–	–
232	Smooth	33.1	37.1	14.0	19.1
232	Smooth	33.6	37.8	12.5	20.3
232	Notched	–	47.5	–	–
315*	Smooth	34.7	40.5		32.5
343	Smooth	18.5	22.2	14.8	28.0
343	Smooth	19.1	22.4	13.2	18.2
343	Notched	–	33.0	–	–

* From Reference (12).

TABLE 24

ROOM TEMPERATURE TENSILE PROPERTIES OF CLASS 3 ALLOY

CONDITION	0.2% OFFSET YIELD STRENGTH (PSI)	UTS (PSI)	% ELONG	% RA
AS EXTRUDED	47,100	59,500	9.4	12.4
EXTRUDED + ANNEALED AT 371°C/500 HRS	38,500	50,700	4.7	5.1
EXTRUDED + ANNEALED AT 399°C/500 HRS	36,100	47,600	5.0	4.6

TABLE 25

STRESS RUPTURE DATA ON CLASS 3 ALLOYS

TEST TEMP	STRESS KSI	STRESS MPₐ	RUPTURE LIFE (HRS)	% ELONG	% RA
232°C (505K)	20	137.9*			
	25	172.4*			
	26.5	182.7	133.8	7.3	8.8
	28.5	196.5	8.8	6.9	10.3
	30.0	206	9.75	8.3	12.3
287°C (560K)	17	117.2	191.7	8.5	9.7
	20	137.9	33.1	9.5	12.0
	23	158.6	4.7	8.0	9.1
	26	179.2	0.2	12.3	15.8
343°C (616K)	11	75.8	71.2	14.0	14.5
	13	89.6	12.5	11.3	13.0
	15	103.4	6.4	15.2	17.0
	18	124.1	0.5	13.6	13.8

* NO FAILURE AND TEST WAS TERMINATED

TABLE 26

TENSILE PROPERTIES OF CLASS 4 ALLOY (RST X7091) AND COMMERCIAL 7075-T6

ALLOY	HEAT TREATMENT	SPECIMEN DIRECTION	SPECIMEN NUMBER	0.2% OFFSET YIELD STRENGTH (PSI)	ULTIMATE TENSILE STRENGTH (PSI)	% ELONG	% RA
RST-X7091	PEAK AGED TEMPER	LONGITUDINAL	1	79,600	86,100	9.6	9.7
			2	79,500	84,400	7.0	8.2
RST-X7091	OVERAGED TEMPER	LONGITUDINAL	1	68,600	75,700	9.3	6.4
			2	68,700	73,300	5.1	4.8
7075	T-6	LONGITUDINAL		72,000	81,000	---	---

Table 27: Room Temperature Tensile Properties of Class 4 Alloy (Longitudinal Orientation) in T7E69 and T7E70 Conditions.

Heat Treatment	0.2%Y.S. (Ksi)	U.T.S. (Ksi)	%Elong.	%R.A.
T7E69	69.3	76.8	9.9	15.7
T7E69	69.2	75.5	7.7	9.3
T7E69*	79.0	87.0	12	
T7E70	67.7	75.5	9.4	8.0
T7E70	68.3	76.2	9.5	12.0

* Data From Reference (13).

TABLE 28

CONDITIONS AND RESULTS OF FATIGUE

TESTS ON CLASS 4 ALLOY AGED TO TC CONDITION IN

LONGITUDINAL DIRECTION

TEST MODE: HIGH CYCLE FATIGUE, AXIAL TENSION/TENSION
TEST ENVIRONMENT: ROOM TEMPERATURE LABORATORY AIR
TEST LOADING: A CONSTANT FORCE, SINUSOIDAL WAVEFORM
                OF 30 H_z FREQUENCY
TEST STRESS RATIO : R = MIN./MAX = 0.1

TEST NUMBER	MAXIMUM STRESS (KSI)	CYCLES ($X10^3$)	RESULTS (1)
1	37	441	GSF
2	35	186	GSF
3	30	302	GSF
4	26	265	GSF
5	25.5	10175	RO
6	25	10185	RO
7	24	12246	RO
8	22	10183	RO
9	20	10141	RO

(1) GSF: GAGE SECTION FAILURE

RO: RUN OUT

TABLE 29

CONDITIONS AND RESULTS OF FATIGUE TESTS ON CLASS 4 ALLOY (T7E70)

TEST MODE: HIGH CYCLE FATIGUE AXIAL TENSION/TENSION
TEST ENVIRONMENT: ROOM TEMPERATURE LABORATORY AIR
TEST LOADING: A CONSTANT AMPLITUDE SINUSOIDAL WAVE FORM OF 30Hz
               FREQUENCY
TEST STRESS RATIO: 0.1
0.2% YIELD STRENGTH = 67,7000 PSI
ULITMATE TENSILE STRENGTH = 75,500 PSI

SPECIMEN ORIENTATION	TEST NUMBER	MAXIMUM STRESS (KSI)	CYCLES (X10^3)	RESULTS (1)
LONGITUDINAL	1 (2)	45	92	GSF
"	2	40	40	GSF
"	3	38	97	GSF
"	4	37	10,040	RO
"	5	36	68	GSF
"	6	35	10,043	RO
"	7	30	4,816	TF
TRANSVERSE	1	25	103	GSF
"	2	20	325	GSF

NOTES: (1) GSF = GAGE SECTION FAILURE
           TF = THREAD FAILURE
           RO = RUN OUT

       (2) THIS TEST WAS CONDUCTED WITH A SPECIMEN WHICH HAD RUN OUT AT A LOWER STRESS LEVEL

       (3) AFTER THE THREAD FAILURE OF THE SPECIMEN 7, ALL SPECIMENS WERE SHOT PEENED ON THE THREADS AND RADIUS EXCEPT FOR THE CENTER 3/8 INCH OF GAGE SECTION

Table 30: Axial Tension/Tension High Cycle Fatigue Data on Class 4 Alloy in T7E69 Temper.

Test Environment   Room Temperature, Laboratory Air
Test Loading   Constant Amplitude Sinusoidal, 30 Hz
Test Stress Ratio $R = 0.1$
Specimen Orientation   Longitudinal

Specimen Number	K_T	Max. Stress (Ksi)	Cycles (x10³)	Results
1	2.7	30.0	13	GSF
3	2.7	20.0	91	GSF
6	2.7	14.0	206	GSF
9	2.7	12.0	567	GSF
11	2.7	10.0	6,349	GSF
5	2.7	8.0	10,024	RO
2	4.0	30.0	9	GSF
4	4.0	15.0	155	GSF
8	4.0	14.0	284	GSF
10	4.0	13.0	469	GSF
12	4.0	12.5	484	GSF
7	4.0	12.0	12,045	RO

GSF: Gage Section Failure
RO: Run Out

TABLE 31: COMPACT TENSION CRACK GROWTH DATA

SAMPLE: CLASS 4 ALLOY (T7E70)
ORIENTATION: L-T: ROOM TEMPERATURE: AIR
RELATIVE HUMIDITY = 55%

TOT CYCLES NT (10^3)	CRACK LGTH A (IN)	LOAD RNG (LBS)	STR INT RNG KSI√IN	CRACK GROWTH RATE IN/CYC
0	0.306	220	5.02	....
8	0.318	220	5.09	1.44×10^{-6}
15	0.323	220	5.2	7.14×10^{-7}
22	0.333	220	5.3	1.43×10^{-6}
28	0.34	220	5.42	1.25×10^{-6}
33	0.348	220	5.52	1.4×10^{-6}
41	0.358	220	5.65	1.31×10^{-6}
45	0.363	220	5.76	1.25×10^{-6}
49	0.368	220	5.84	1.25×10^{-6}
53	0.375	220	5.93	1.75×10^{-6}
57	0.381	220	6.03	1.38×10^{-6}
61	0.389	220	6.14	2.13×10^{-6}
65	0.396	220	6.26	1.63×10^{-6}
69	0.402	220	6.37	1.63×10^{-6}
73	0.411	220	6.5	2.25×10^{-6}
76.5	0.418	220	6.64	1.86×10^{-6}
80	0.426	220	6.77	2.29×10^{-6}
83.5	0.435	220	6.93	2.57×10^{-6}
87	0.444	220	7.1	2.57×10^{-6}
90.5	0.454	220	7.29	2.86×10^{-6}
93.5	0.462	220	7.48	2.67×10^{-6}
96.5	0.47	220	7.66	2.83×10^{-6}
99.5	0.482	220	7.89	4×10^{-6}
102.3	0.493	220	8.17	3.93×10^{-6}
104.9	0.502	220	8.42	3.46×10^{-6}
107.4	0.513	220	8.68	4.4×10^{-6}
109.9	0.528	220	9.04	5.8×10^{-6}
112.1	0.54	220	9.44	5.45×10^{-6}
114.2	0.554	220	9.87	6.9×10^{-6}
116.1	0.567	220	10.36	6.84×10^{-6}
117.8	0.581	220	10.86	7.94×10^{-6}
119.3	0.594	220	11.44	9.33×10^{-6}
120.5	0.611	220	12.12	1.33×10^{-5}
121.3	0.618	220	12.72	1×10^{-5}
122.1	0.631	220	13.27	1.56×10^{-5}
122.7	0.643	220	13.99	2×10^{-5}
123.1	0.649	220	14.56	1.5×10^{-5}
123.5	0.659	220	15.08	2.38×10^{-5}
123.9	0.667	220	15.75	2.25×10^{-5}
124.3	0.683	220	16.69	3.75×10^{-5}
124.7	0.688	220	17.59	1.5×10^{-5}
125.0	0.714	220	19.1	8.5×10^{-5}
125.2	0.729	220	21.38	7.5×10^{-5}
125.4	0.746	220	23.51	8.5×10^{-5}
125.6	0.756	220	25.59	5.0×10^{-5}

TABLE 32
COMPACT TENSION CRACK GROWTH DATA

SAMPLE: CLASS 4 ALLOY (T7E70)
ORIENTATION: T-L
ROOM TEMPERATURE: AIR
RELATIVE HUMIDITY = 64%
R = 0.1
FREQUENCY = 29 H_2

TOT CYCLES NT $(10^{**}3)$	CRACK LGTH A (IN)	LOAD RNG (LBS)	STR INT RNG KSI$\sqrt{}$IN	CRACK GROWTH RATE IN/CYC
0	0.311	220	5.08	∗∗∗∗∗∗∗∗∗∗∗
20	0.321	220	5.14	4.5 x 10^{-7}
40	0.341	220	5.34	1.03x 10^{-6}
50	0.355	220	5.58	1.4 x 10^{-6}
55	0.365	220	5.75	1.9 x 10^{-6}
59	0.374	220	5.89	2.25x 10^{-6}
62	0.376	220	5.98	8.33x 10^{-6}
65	0.385	220	6.07	3.17x 10^{-6}
68	0.391	220	6.19	1.67x 10^{-6}
71	0.399	220	6.3	2.67x 10^{-6}
74	0.407	220	6.43	2.67x 10^{-6}
77	0.413	220	6.56	2.17x 10^{-6}
80	0.422	220	6.7	3 x 10^{-6}
83	0.436	220	6.91	4.67x 10^{-6}
86	0.463	220	7.31	8.83x 10^{-6}
87	0.469	220	7.65	6 x 10^{-6}
88	0.483	220	7.89	1.45x 10^{-5}

TABLE 33
COMPACT TENSION CRACK GROWTH DATA

SAMPLE: CLASS 4 ALLOY (T7E70)
ORIENTATION: T-L
ROOM TEMPERATURE: AIR
R = 0.1; RELATIVE HUMIDITY = 63%
FREQUENCY = 29Hz

TOT CYCLES NT (10**3)	CRACK LGTH A (IN)	LOAD RNG (LBS)	STR INT RNG KSI√IN	CRACK GROWTH RATE IN/CYC
0	0.307	216	4.92	....
8	0.313	216	4.95	6.88×10^{-7}
16	0.318	216	5.02	6.25×10^{-7}
24	0.324	216	5.09	7.5×10^{-7}
32	0.33	216	5.18	8.13×10^{-7}
40	0.338	216	5.27	8.75×10^{-7}
48	0.345	216	5.36	9.38×10^{-6}
56	0.354	216	5.48	1.12×10^{-6}
63	0.363	216	5.61	1.36×10^{-6}
68	0.371	216	5.74	1.5×10^{-6}
73	0.38	216	5.86	1.8×10^{-6}
77	0.388	216	5.99	1.88×10^{-6}
80	0.395	216	6.1	2.33×10^{-6}
83	0.406	216	6.25	3.67×10^{-6}
85	0.413	216	6.4	3.75×10^{-6}
87	0.419	216	6.53	3.25×10^{-6}
89	0.428	216	6.66	4.25×10^{-6}
91	0.437	216	6.82	4.25×10^{-6}
93	0.446	216	6.99	4.75×10^{-6}
95	0.465	216	7.27	9.25×10^{-5}
95.8	0.476	216	7.58	1.37×10^{-5}
96.3	0.49	216	7.87	2.8×10^{-5}
96.5	0.495	216	8.1	2.5×10^{-5}
96.7	0.501	216	8.24	3.25×10^{-5}
96.9	0.511	216	8.45	5×10^{-5}
97	0.517	216	8.67	6×10^{-5}
97.1	0.524	216	8.85	7×10^{-5}
97.2	0.529	216	9.02	5×10^{-5}
97.3	0.542	216	9.3	1.35×10^{-4}

TABLE 34

FRACTURE TOUGHNESS DATA OF CLASS 4 ALLOY (T7E70)

TEST SPECIFICATION: ASTM E399-83

TEST ENVIRONMENT: Room Temperature, Ambient Air

                     70% RELATIVE HUMIDITY

CRACK PLANE	K_Q KSI $(INCH)^{\frac{1}{2}}$
L-T	24.4
T-L	10.2
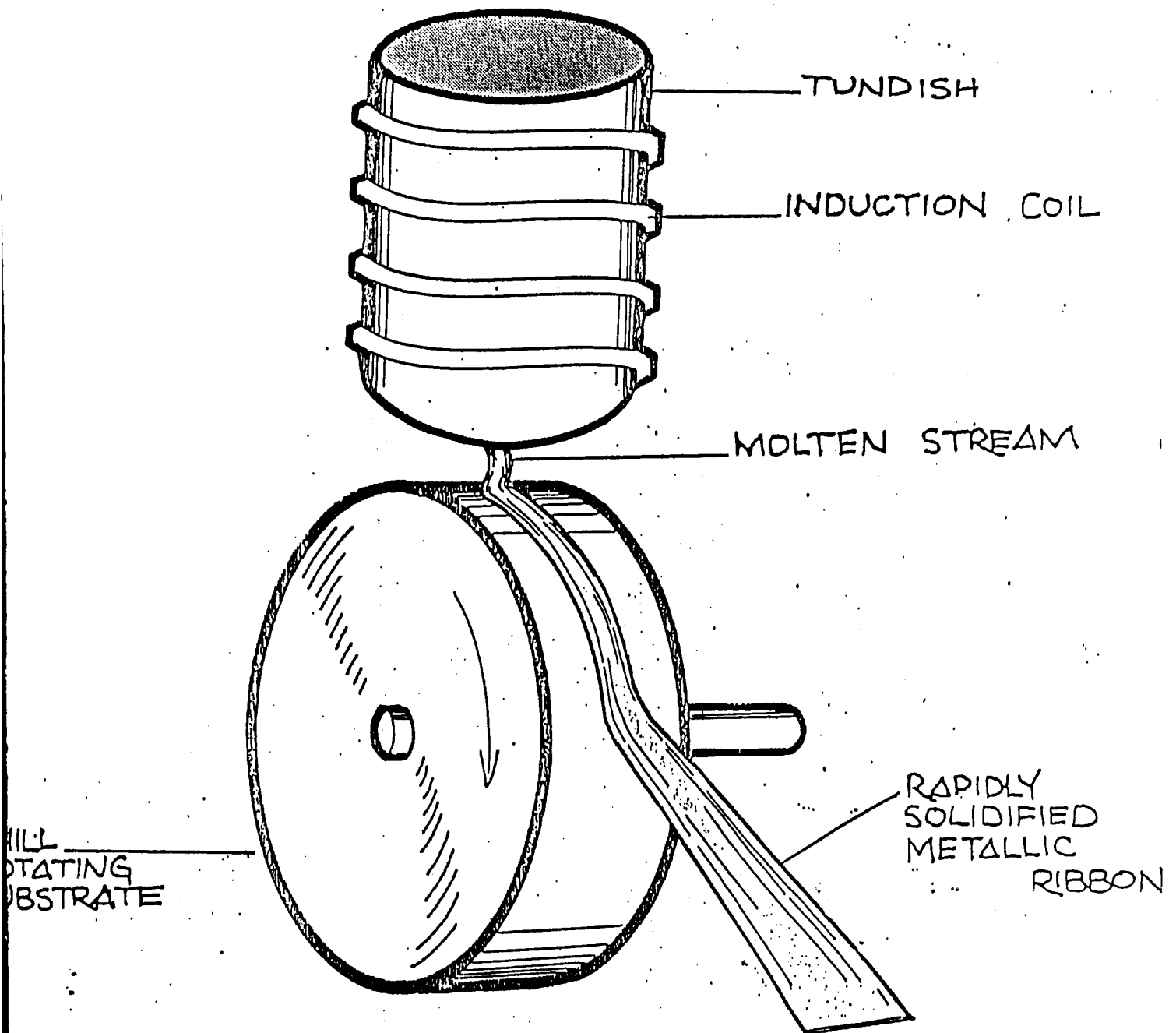
Figure 1   Schematic of Melt Spinning Equipment
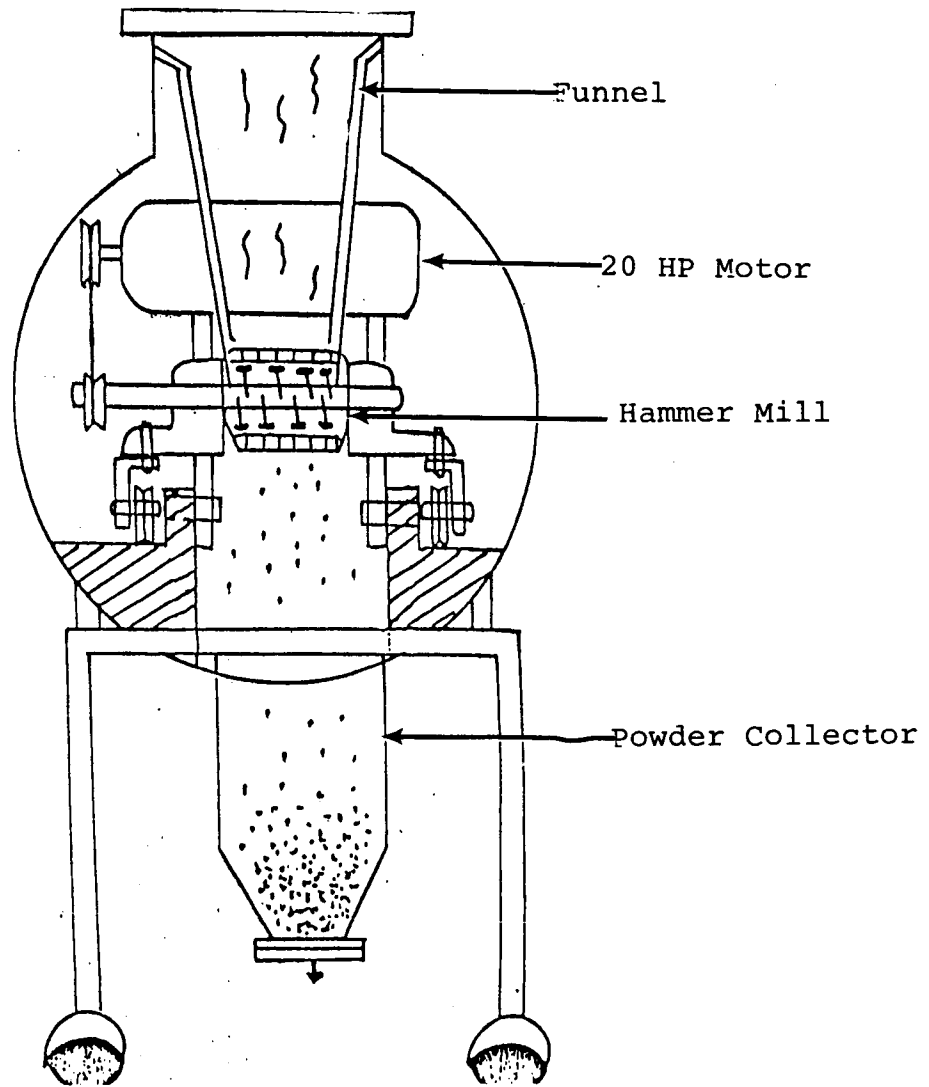
Figure 2   Schematic of Pulverization equipment
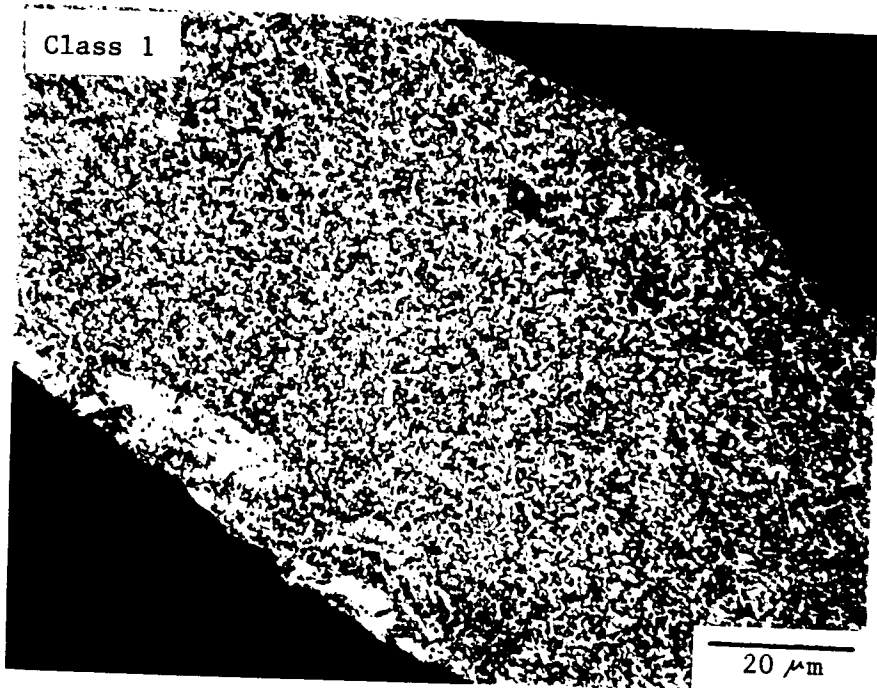
Figure 3   Optical Photomicrograph of Particulates of
            Class 1 Alloy
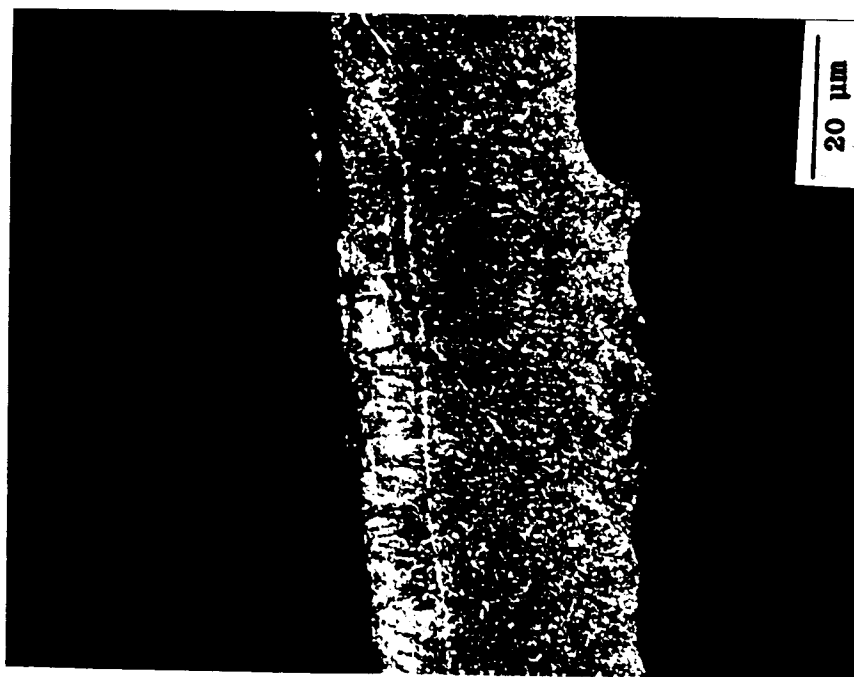
Figure 4   Optical Photograph of Particulates of Class
1 Alloy
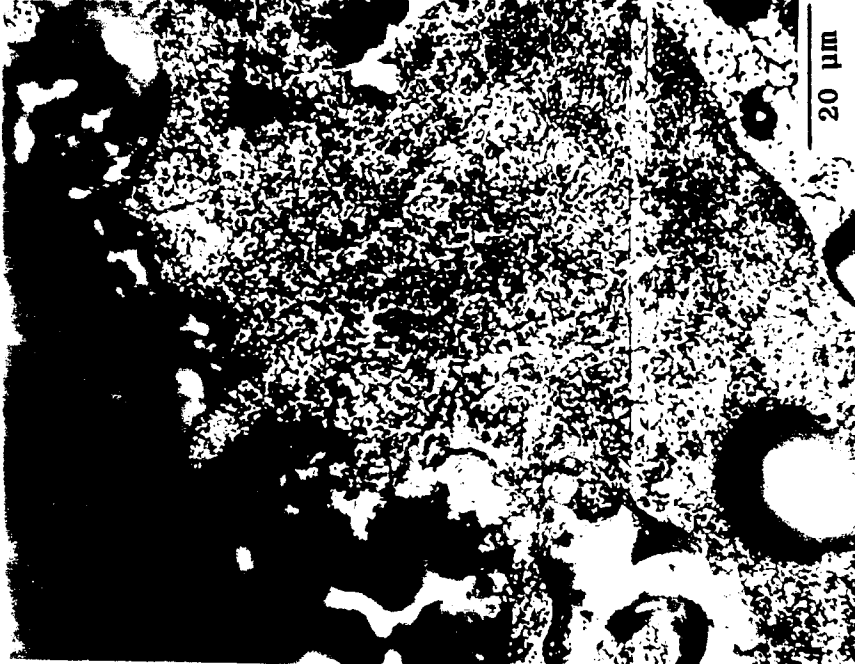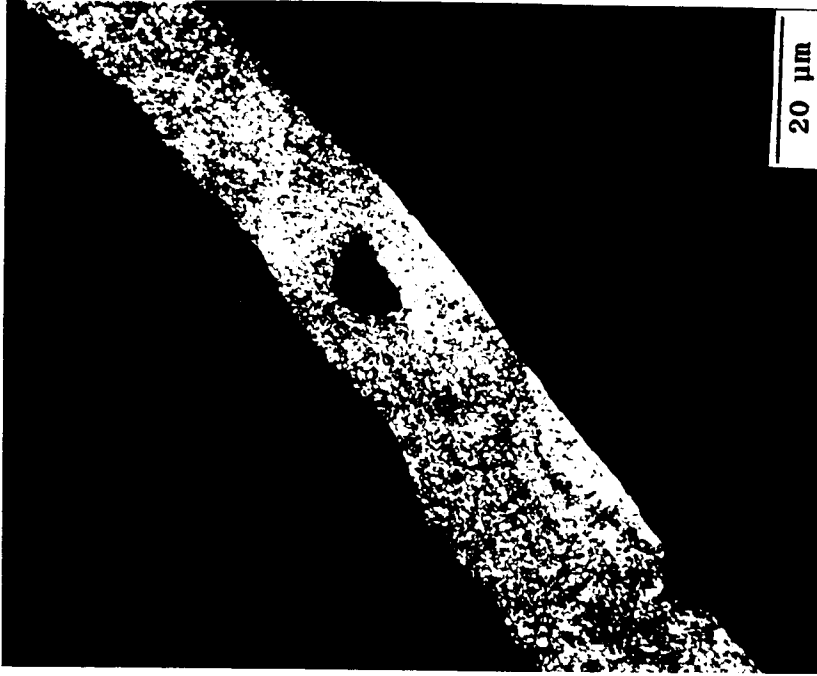
Figure 5 Optical Photomicrograph of Particulates of
Class 1 Alloy
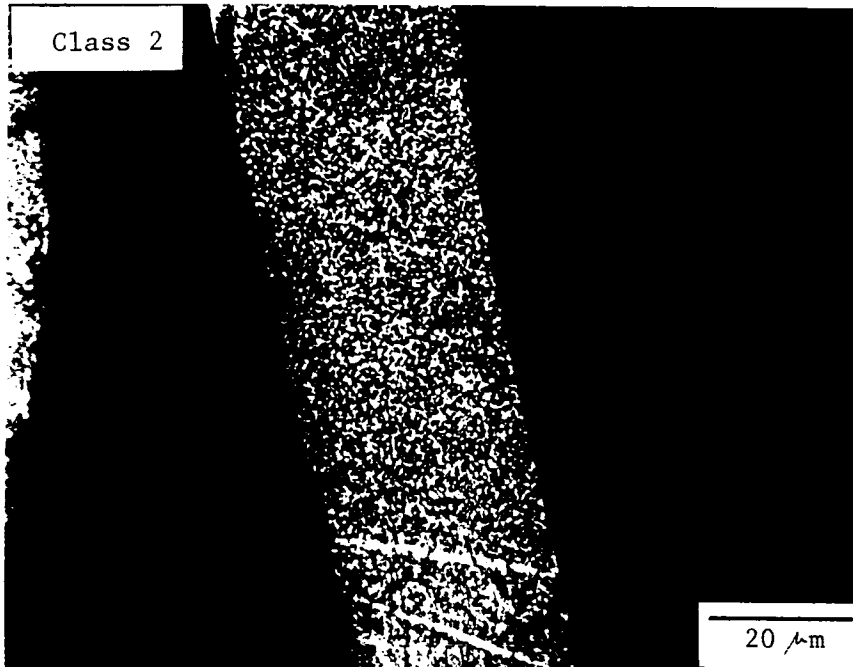
Figure 6   Optical Photomicrographs of Particulates of
Class 2 Alloy

C - 2

ORIGINAL PAGE IS
OF POOR QUALITY
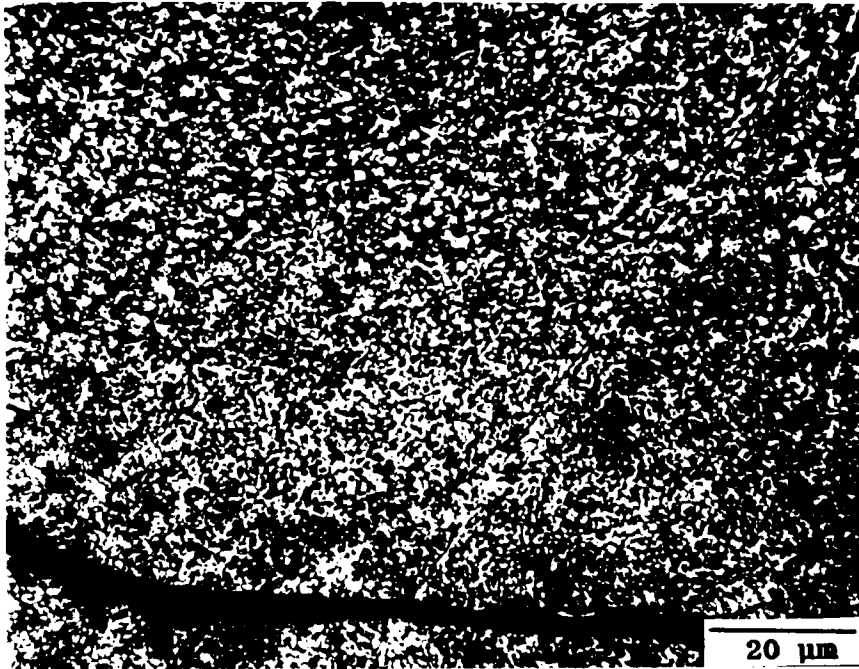
Figure 7   Optical Photomicrograph of Particulates of
           Class 2 Alloy
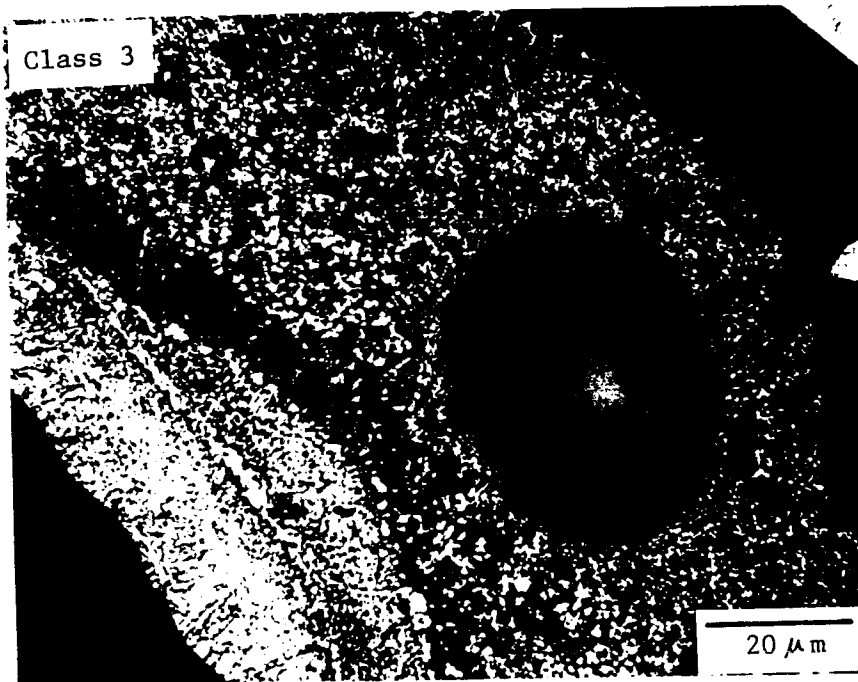
FIGURE 8: OPTICAL PHOTOMICROGRAPH OF PARTICULATES OF
CLASS 3 ALLOY.
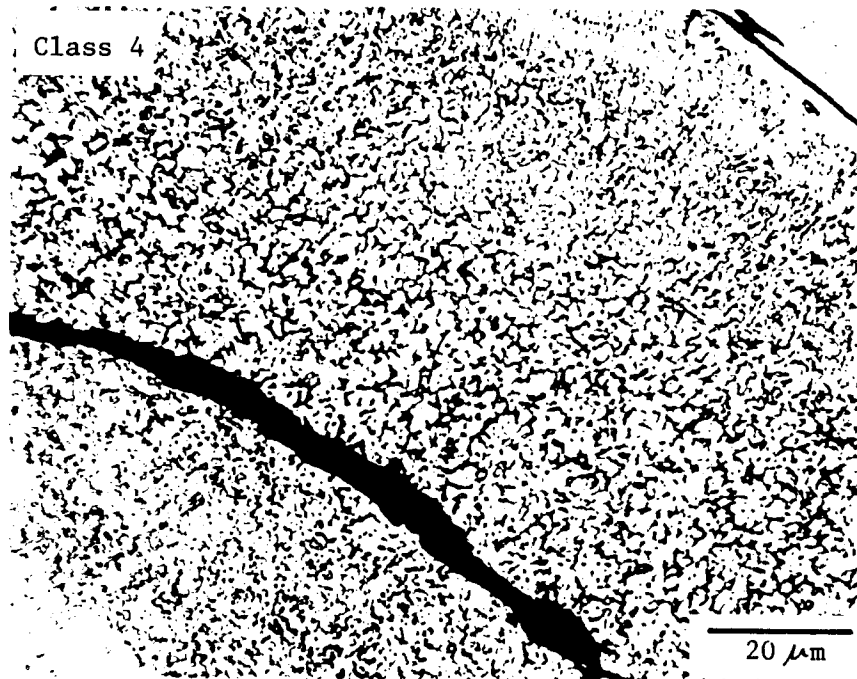
Figure 9   Optical Photomicrograph of Particulates of
Class 4 Alloy
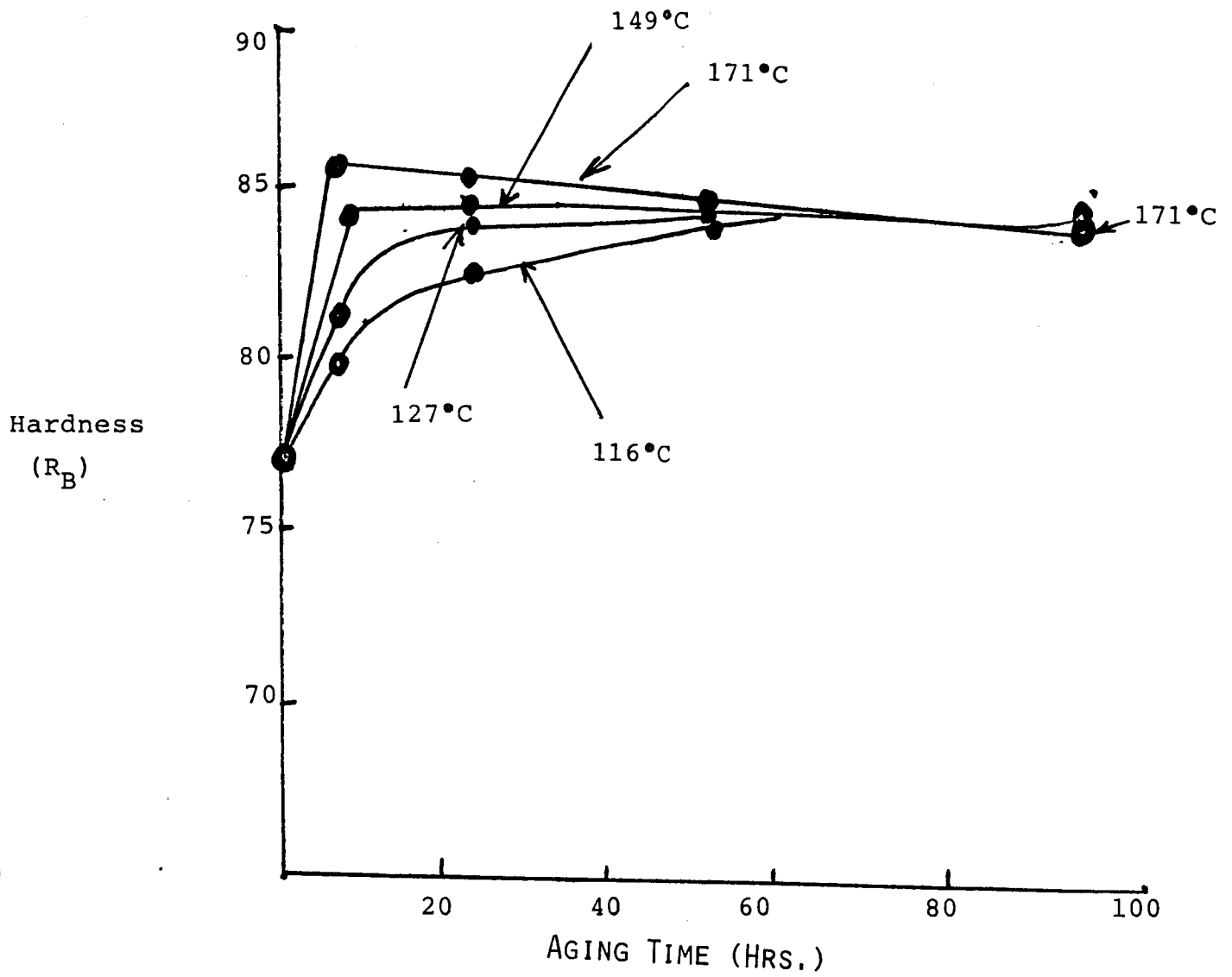
FIGURE 10: ISOTHERMAL AGING CHARACTERISTICS OF CLASS 1 ALLOY
(AL-LI-MG-ZR)
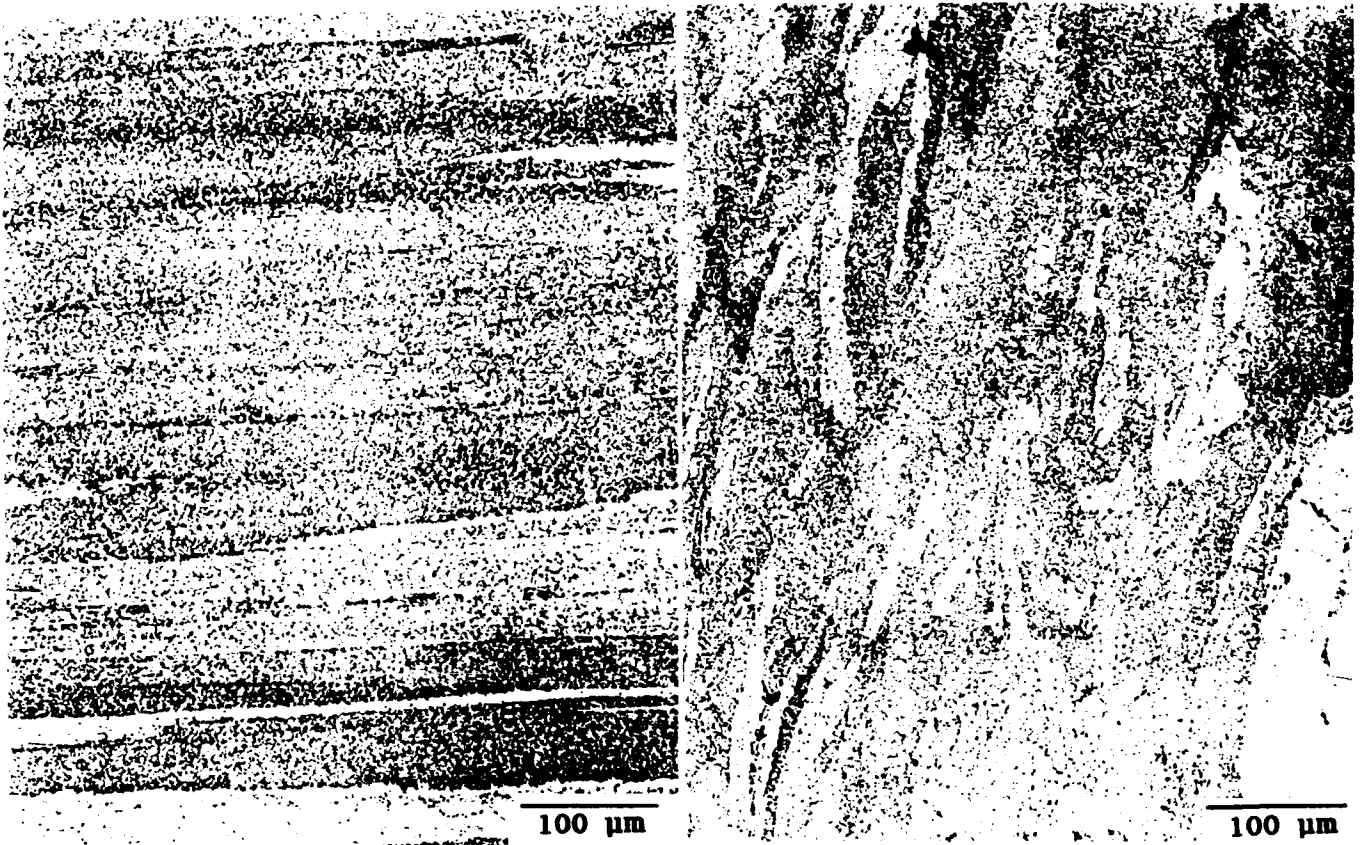
180X
LONGITUDINAL

180X
LONG TRANSVERSE

Figure 11 Optical Photomicrograph of As-extruded
Class 1 Alloy
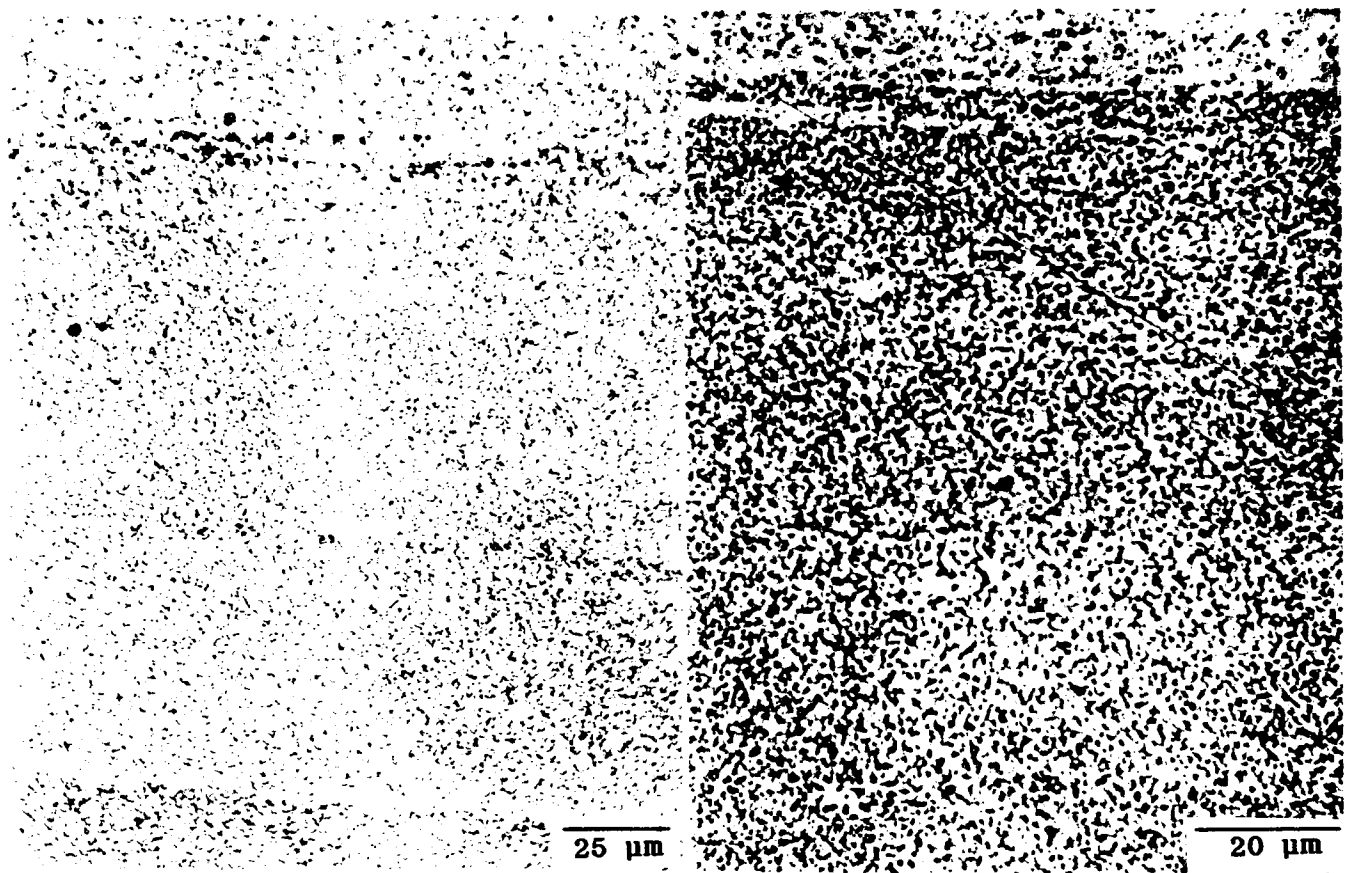
545X
LONGITUDINAL

960X
LONGITUDINAL

FIGURE 12 Optical Photomicrograph of As-extruded
Class 1 Alloy
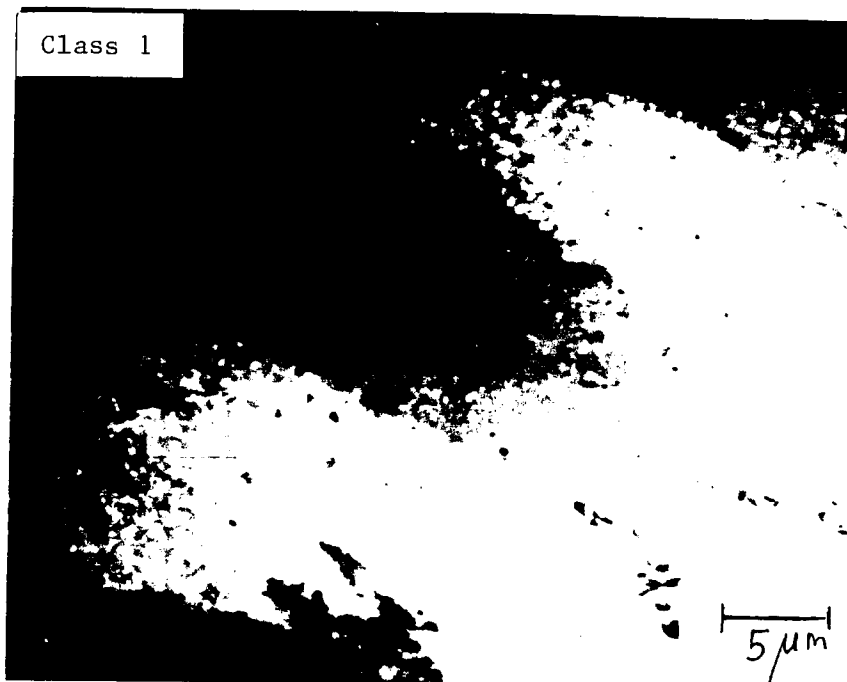
FIGURE 13 Dark field TEM Micrograph of Extruded Class
1 Alloy in Peak Aged Condition

X-RAY
Live: 60s Preset: 60s Remaining: 0s
Real: 75s   20% Dead

O

Mg

Al

.000   1.280   keV →   2.560 >
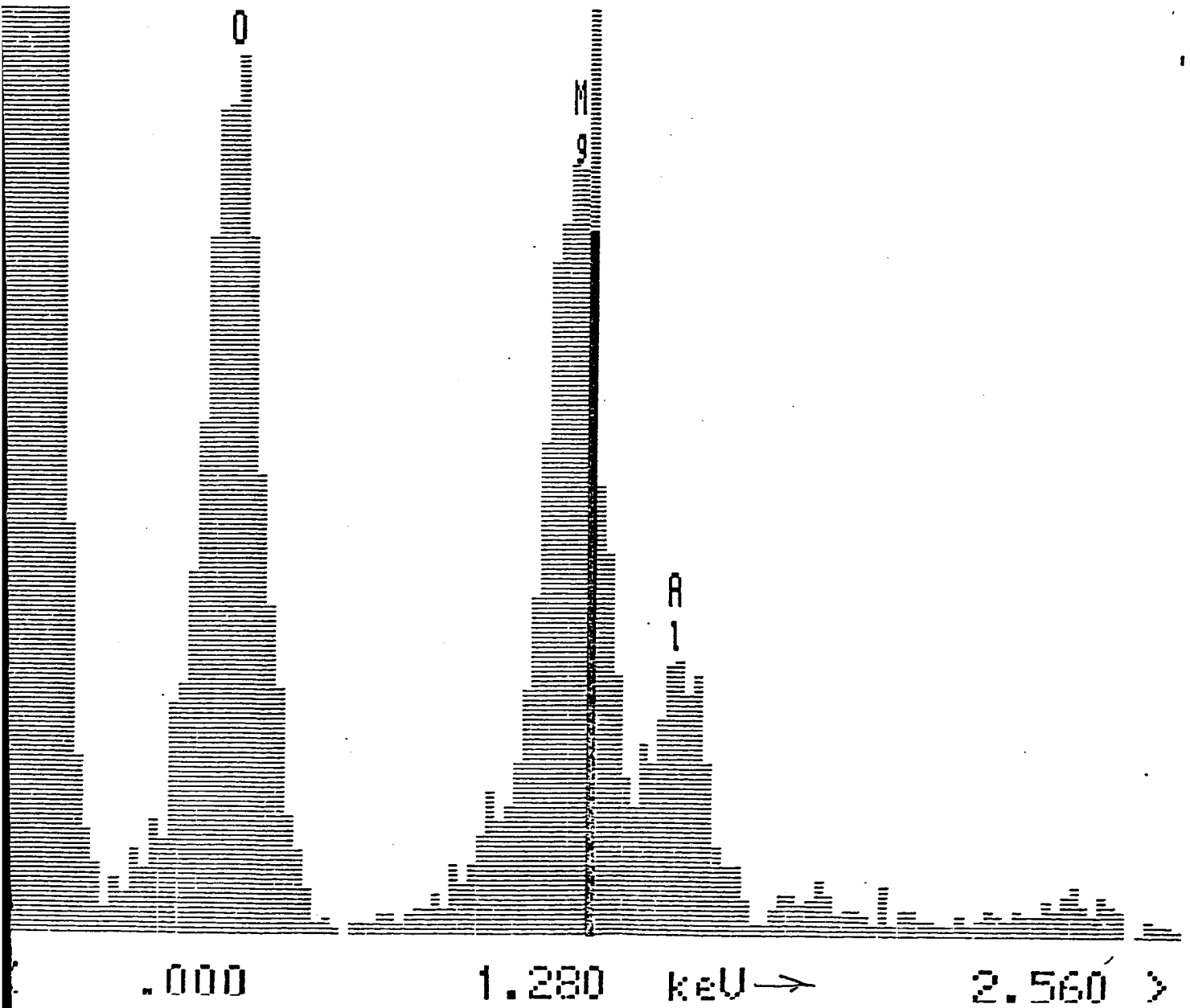
FIGURE 14:   EDAX SPECTRUM FROM PARTICLES OBSERVED IN
             FIGURE 13.
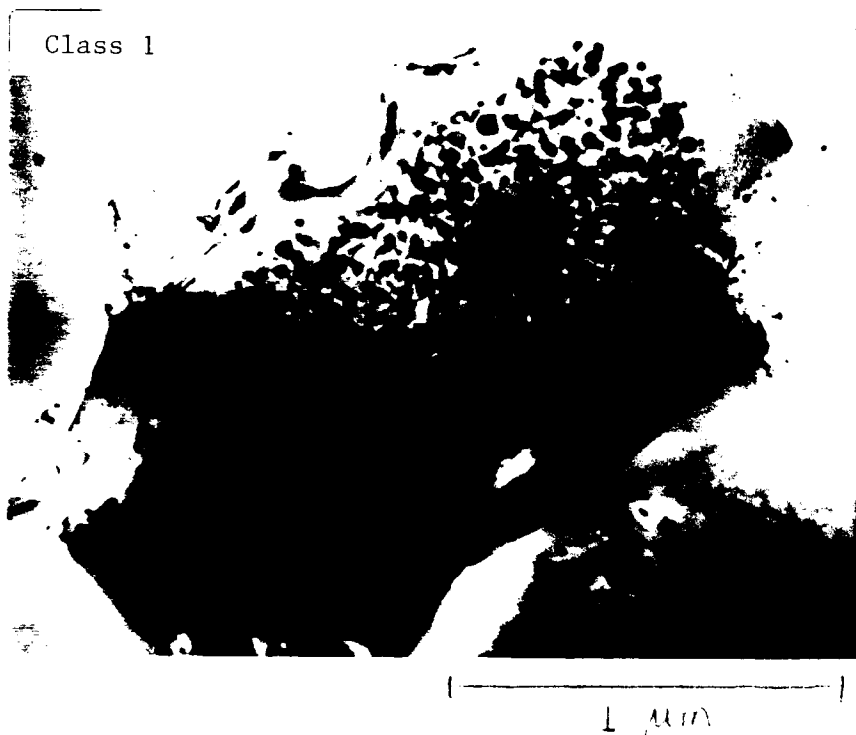
FIGURE 15: TYPICAL SUB-GRAIN MORPHOLOGY OF CLASS 1 ALLOY
PEAK-AGED CONDITION

—
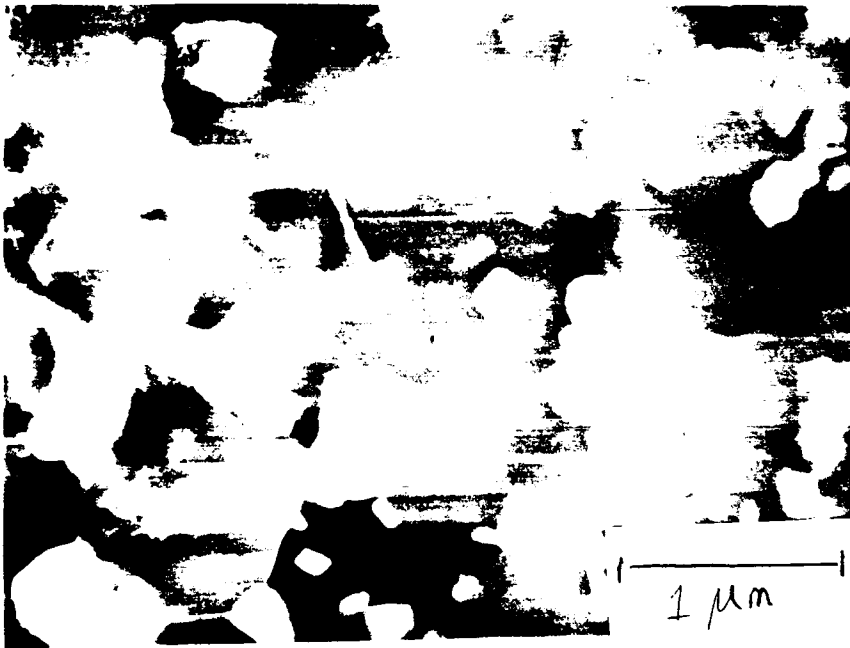
FIGURE 16 Dark field Image Showing an Unusually Large
Density of Coarse Precipitates in Class 1
Alloy
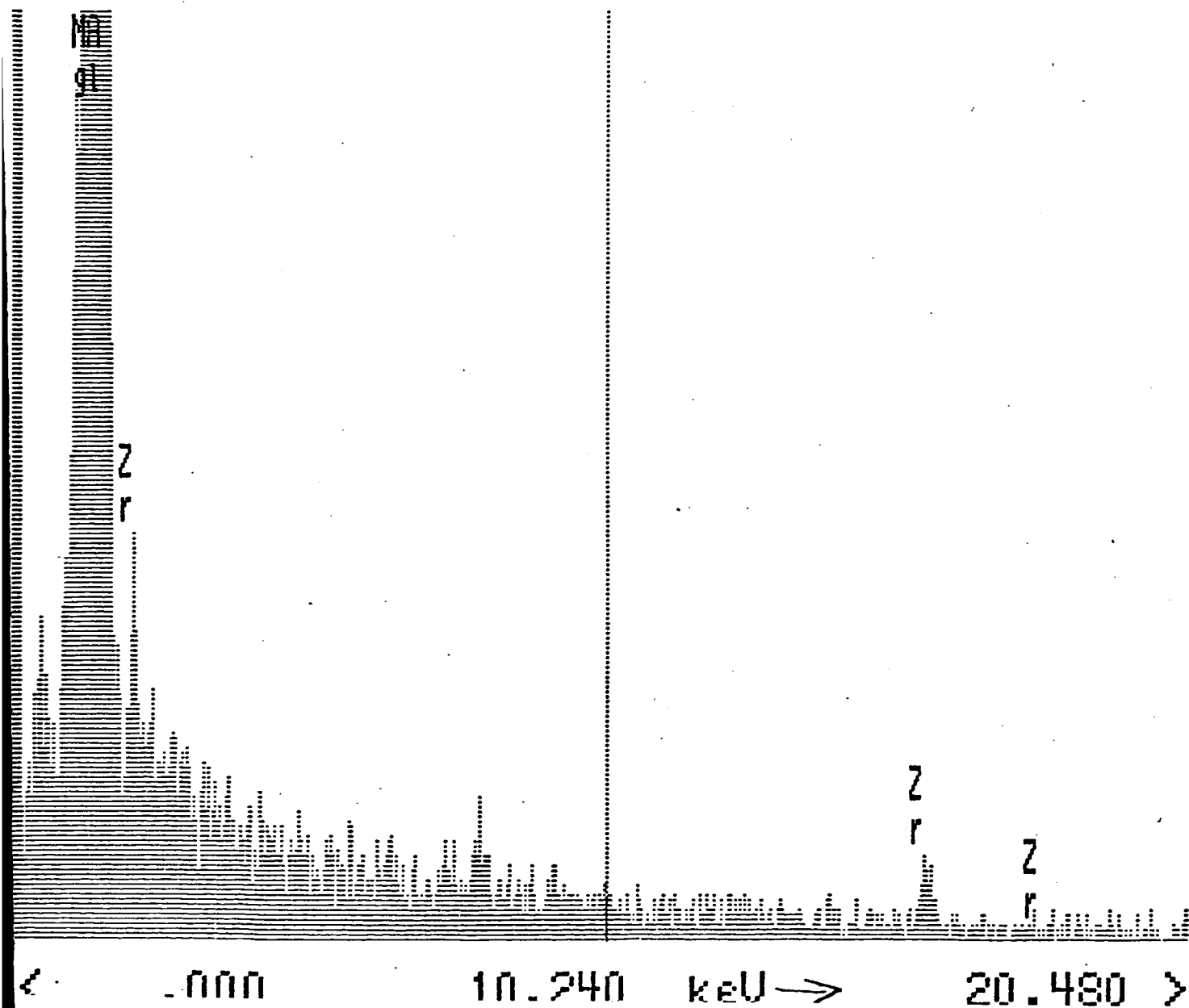
FIGURE 17 EDAX Spectrum from Coarse Particles in Figure 16.

500 μm

Class 1 Peak Aged

50 μm
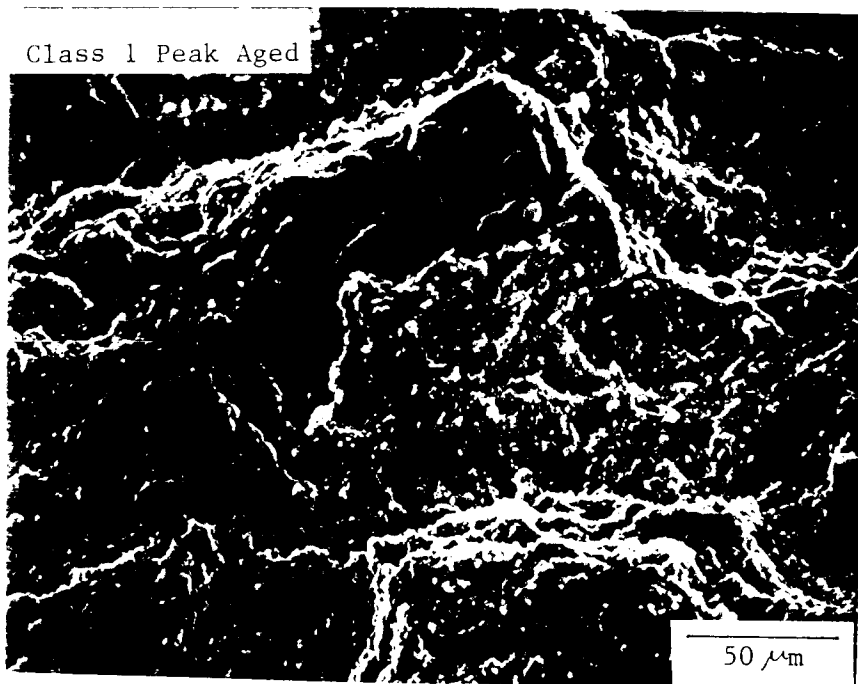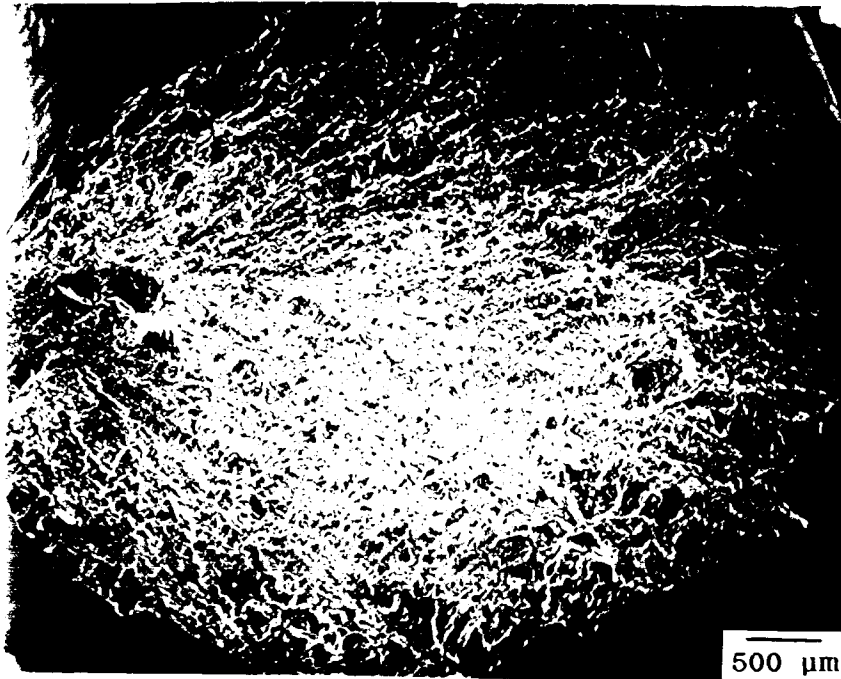
FIGURE 18 Scanning Electron Micrographs Showing
Tensile Fracture Mode for Class 1 Alloy in
the Peak Aged Condition
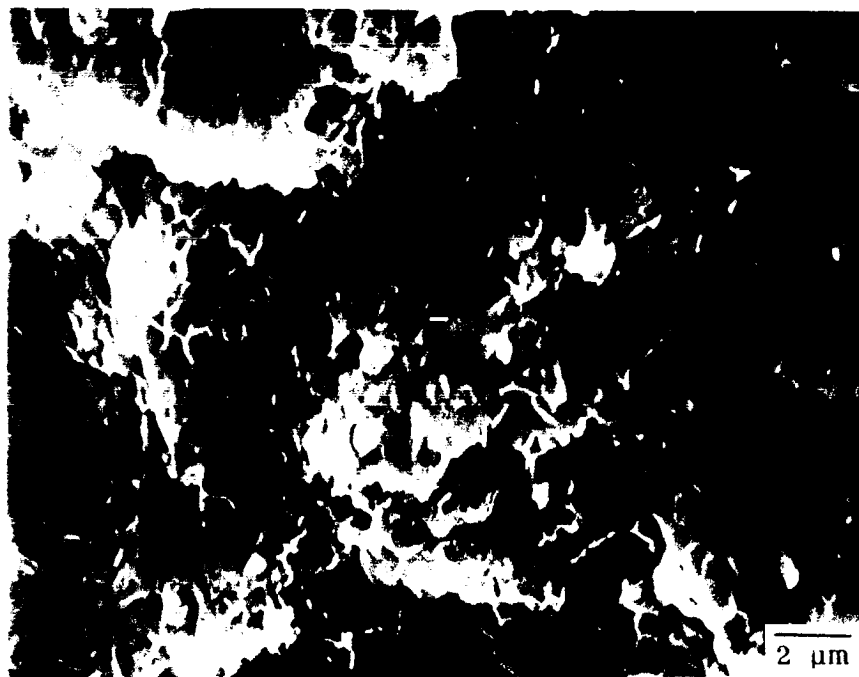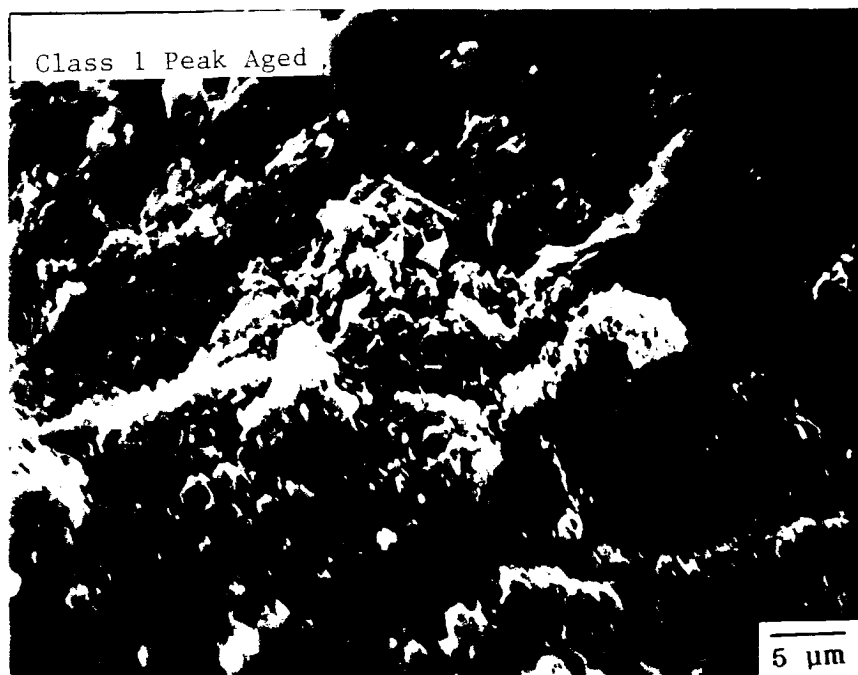
FIGURE 19 Scanning Electron Micrographs for Class 1
Alloy Showing Intergranular Fracture in
Areas Away from the Inclusion and Dimples
on Fracture Facets

500 μm

Class 1 Over Aged

50 μm
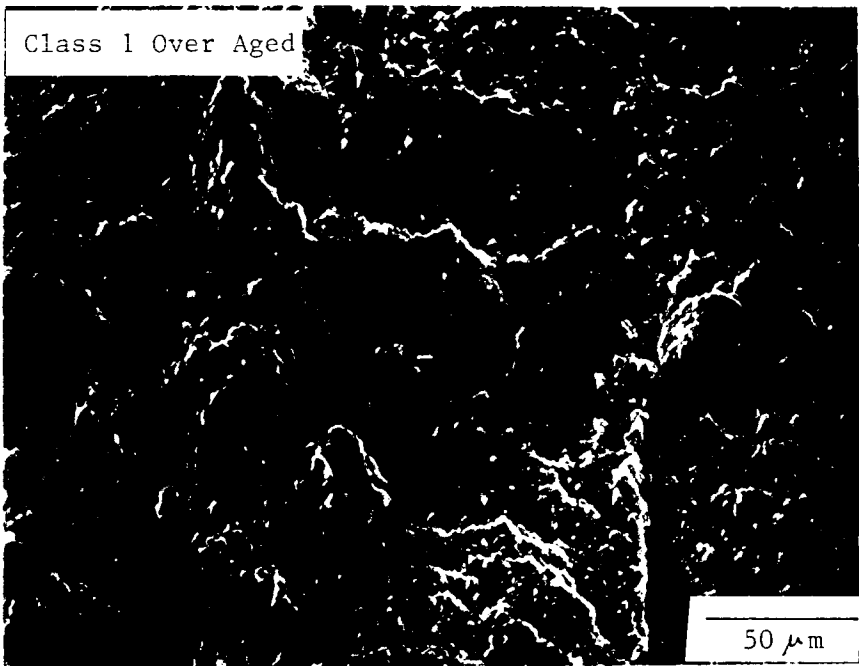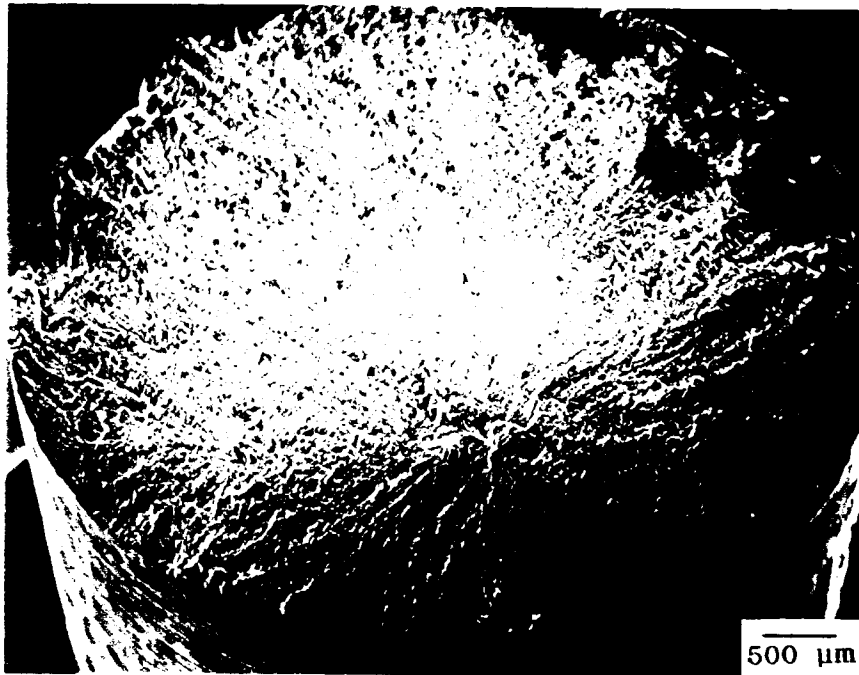
FIGURE 20 Scanning Electron Micrograph Showing Tensile Fracture Mode for Class 1 Alloy in the Over-aged Condition

Class 1 Over Aged

5 µm

2 µm
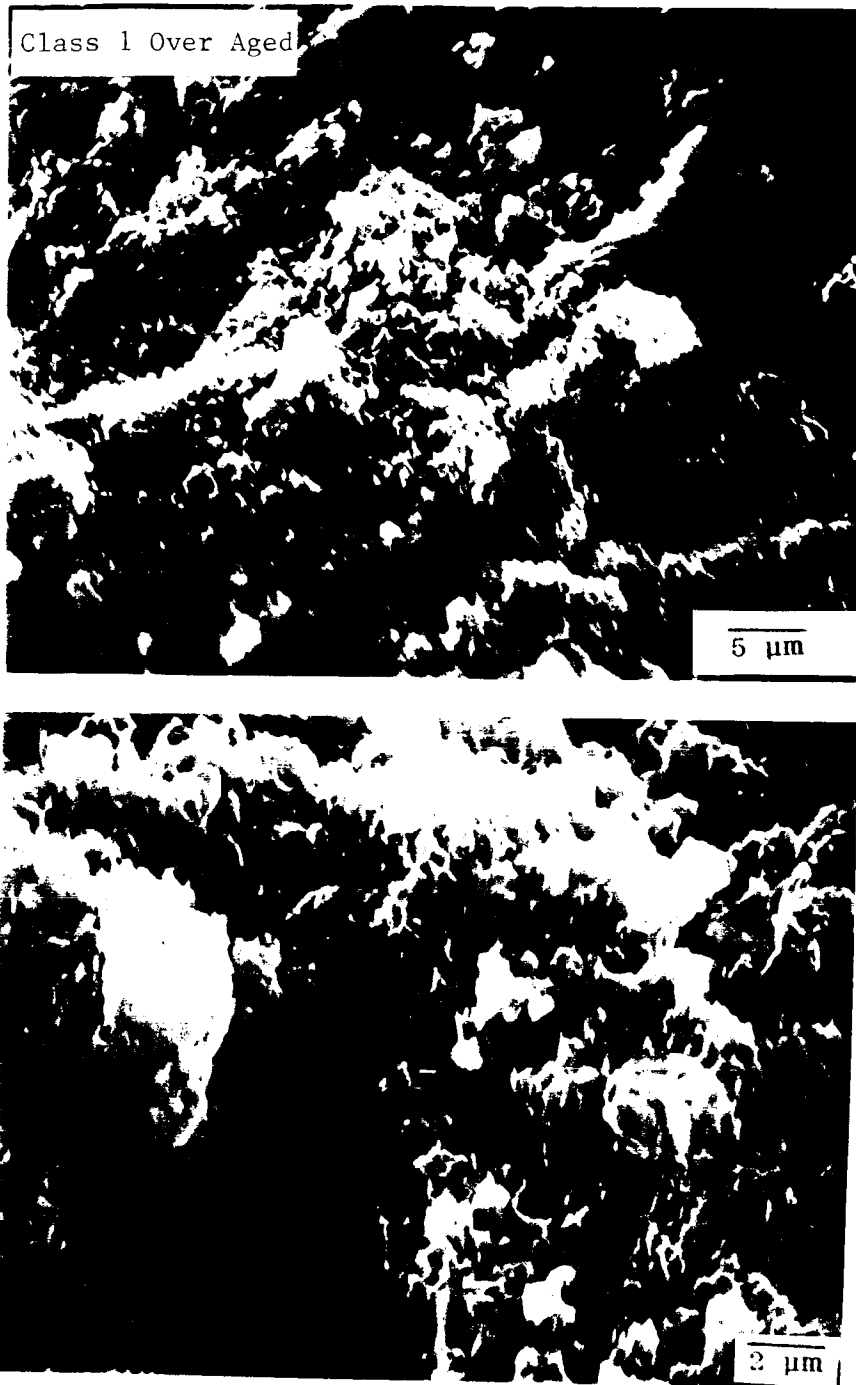
FIGURE 21 Scanning Electron Micrographs for Class 1
Alloy in the Over-aged Condition Showing
Intergranular Fracture in Areas Away from
the Inclusions and Dimples on Fracture
Facets

100.0 u H
01-1 20.0 21 128 626

2000 µm

(A) S. E. M. 10X

500 µm

(B) S. E. M. 30X
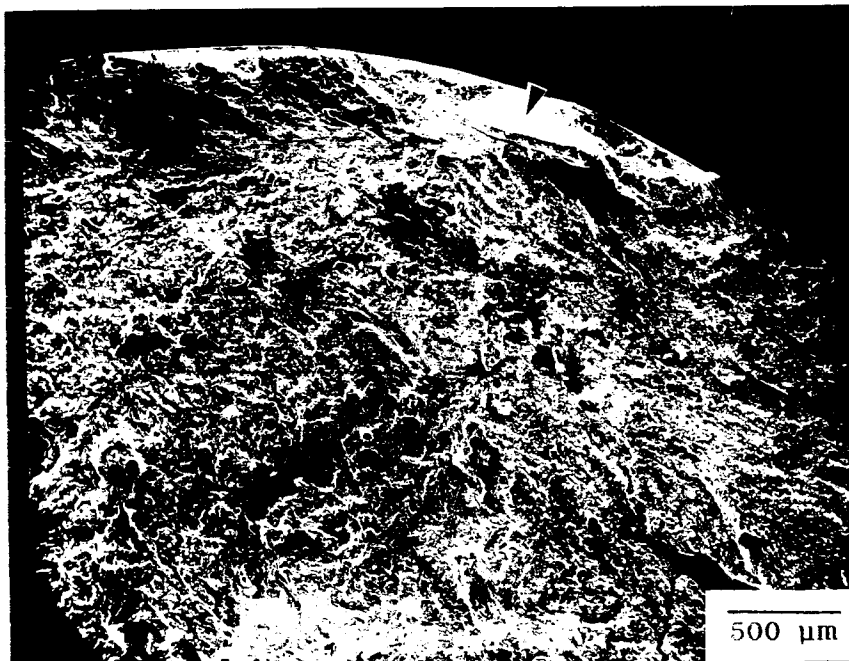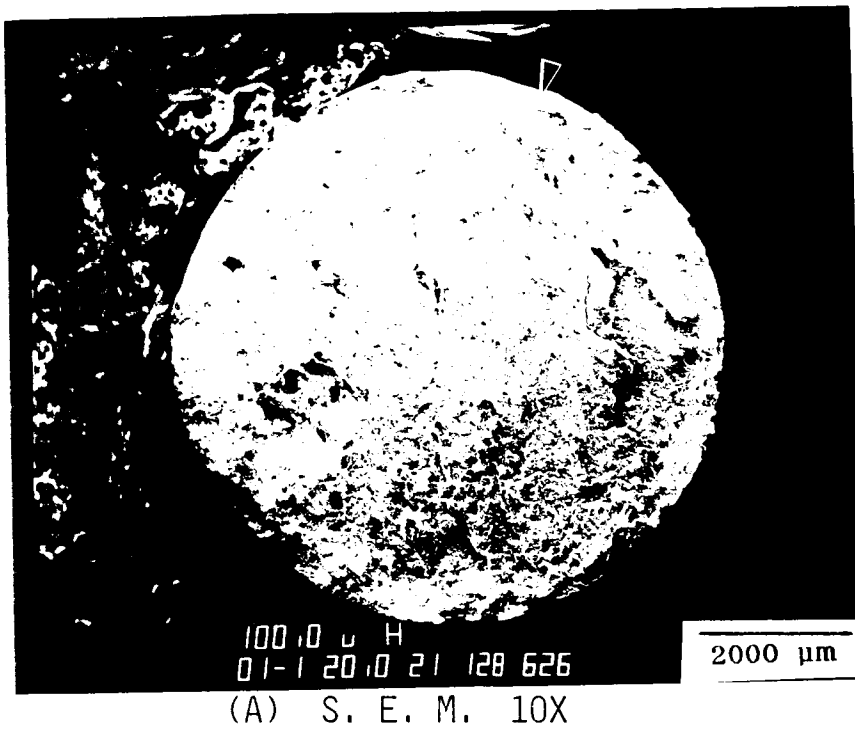
FIGURE 22: SCANNING ELECTRON MICROGRAPH SHOWING TENSILE FRACTURE MODE OF CLASS 1 ALLOY AGED AT 70°C FOR 1 HOUR.

100 µm
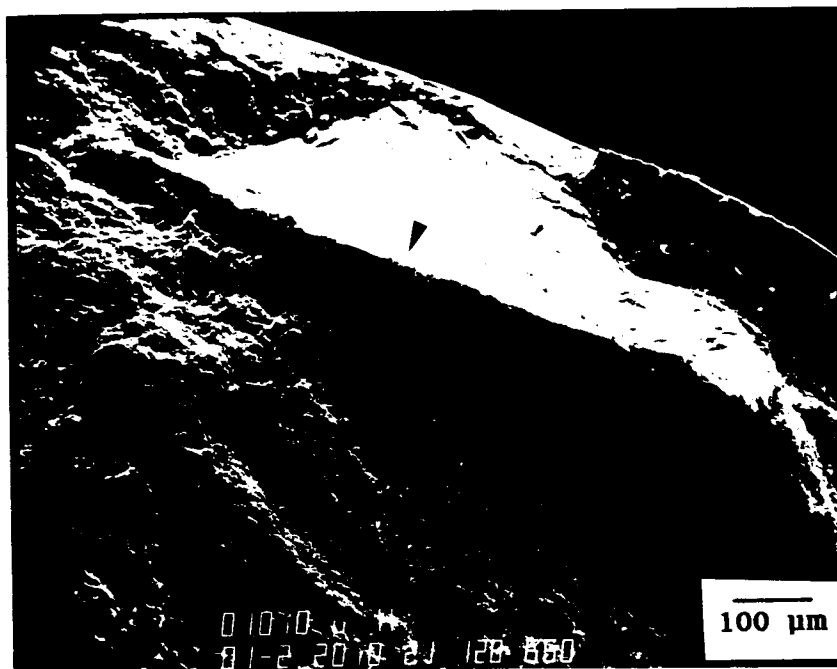
(A) S. E. M. 100X

FIGURE 23 Scanning Electron Micrograph of Specimen in
Figure 22 at Higher Magnification
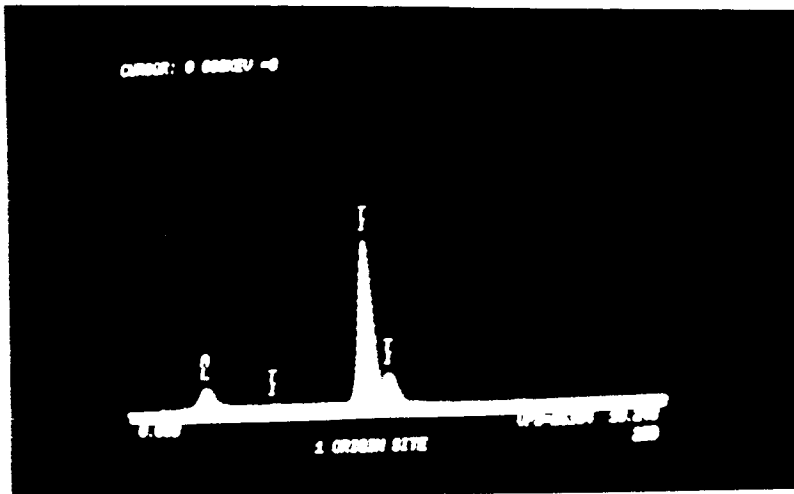
(A) EDXA - ORIGIN SITE
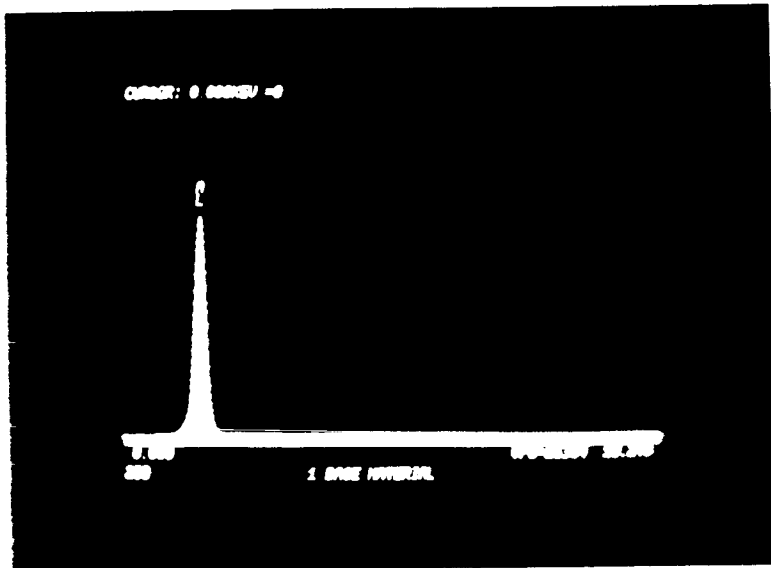
(B) EDXA - BASE MATERIAL

FIGURE 24 EDXA Spectrums of Specimen in Figure 22
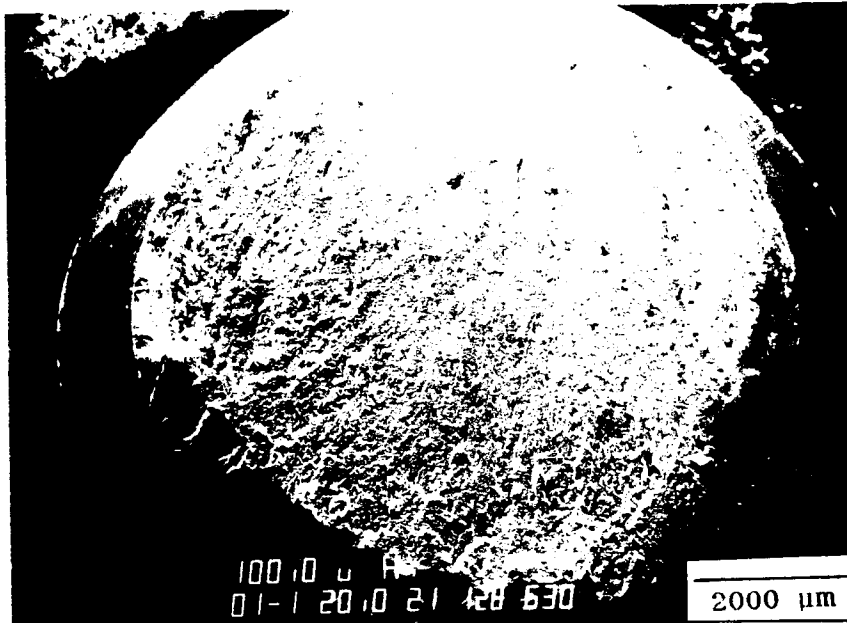
(A) S. E. M. 10X
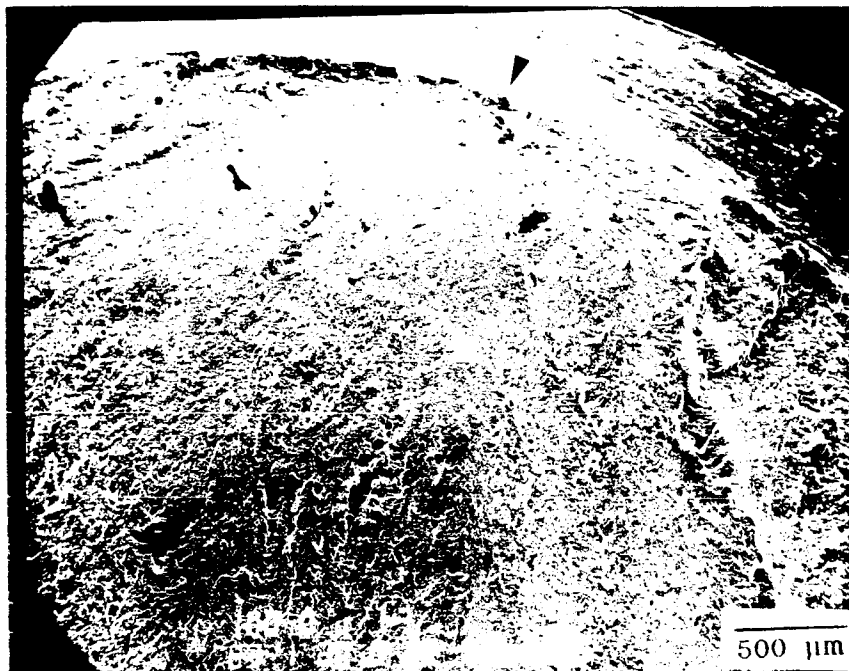
(B) S. E. M. 30X

FIGURE 25 Scanning Electron Micrographs Showing Tensile Fracture Mode of Class 1 Alloy Aged at 185 C for 16 hours
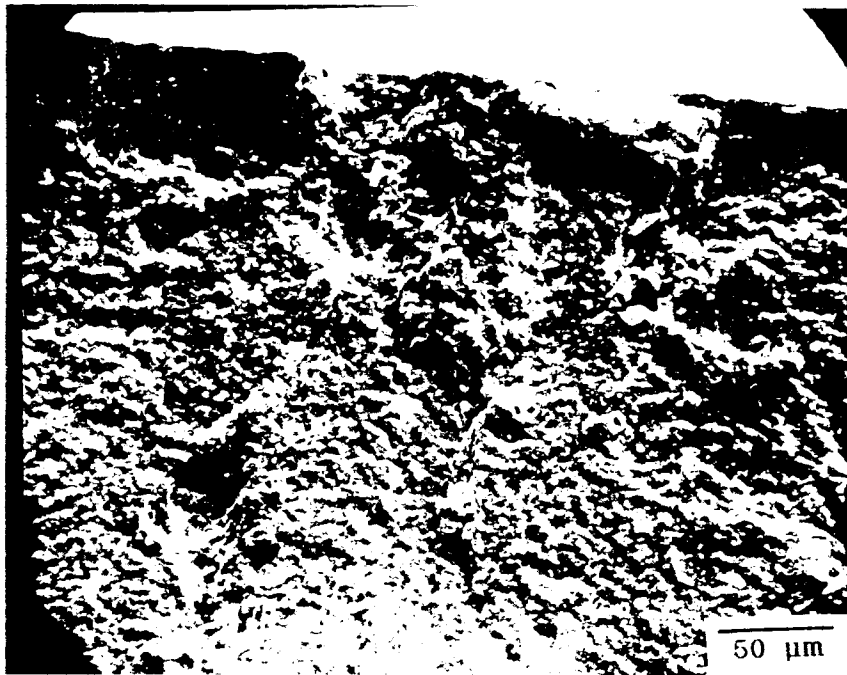
(A) S.E.M. 300X
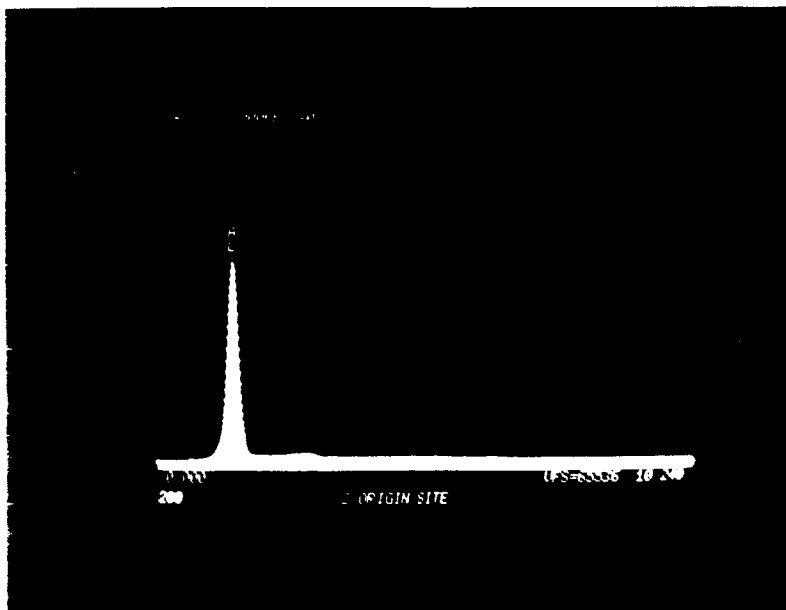
(B) E.D.X.A. 500 X

FIGURE 26 (A) Scanning Electron Micrograph of Speci-
men in Figure 25 at Higher Magnification
(B) EDXA Spectrum of the Origin Site
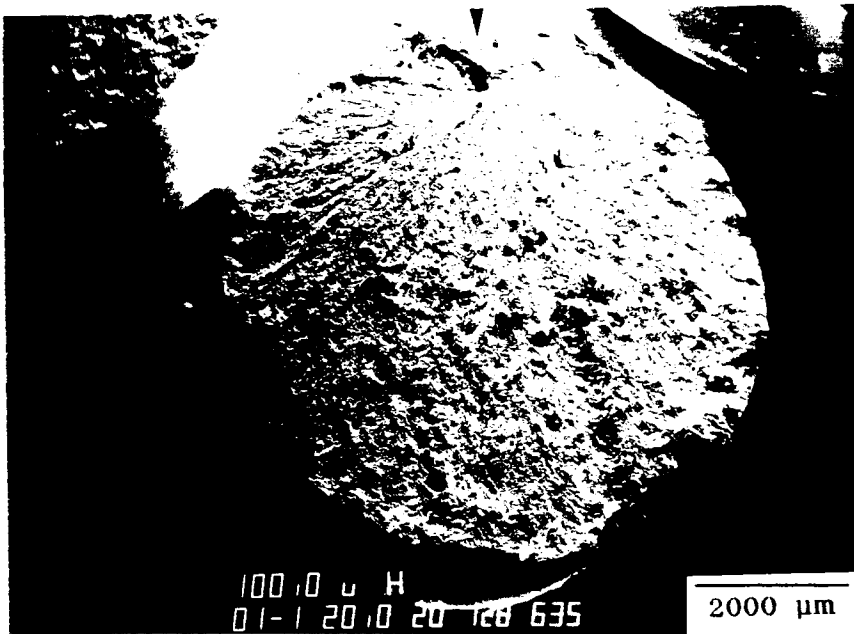
(A) S. E. M. 10X
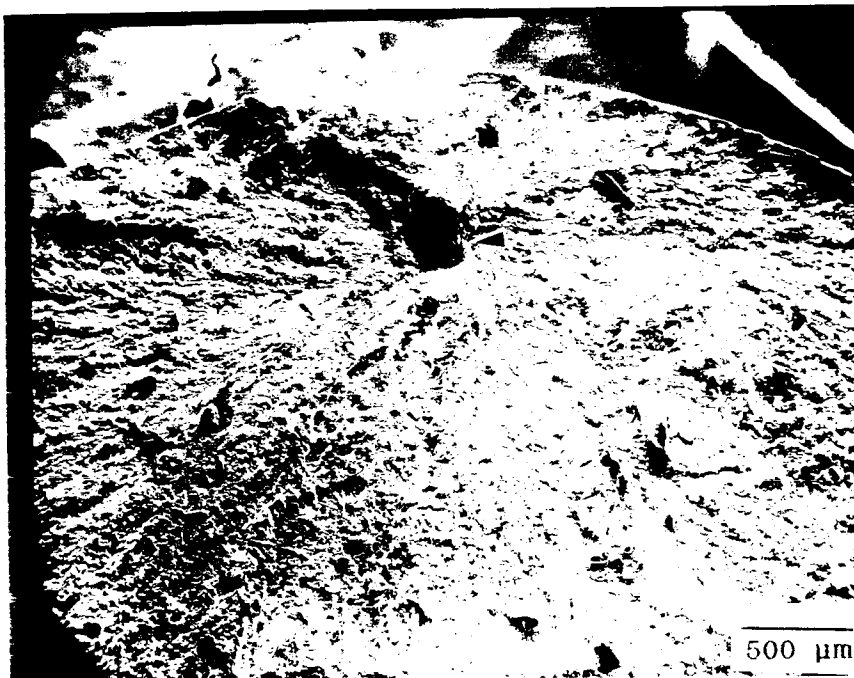
(B) S. E. M. 30X

FIGURE 27 Scanning Electron Micrograph Showing Tensile Fracture Mode of Class 1 Alloy Aged at 70 C for 24 hours

(A) S. E. M. 500X
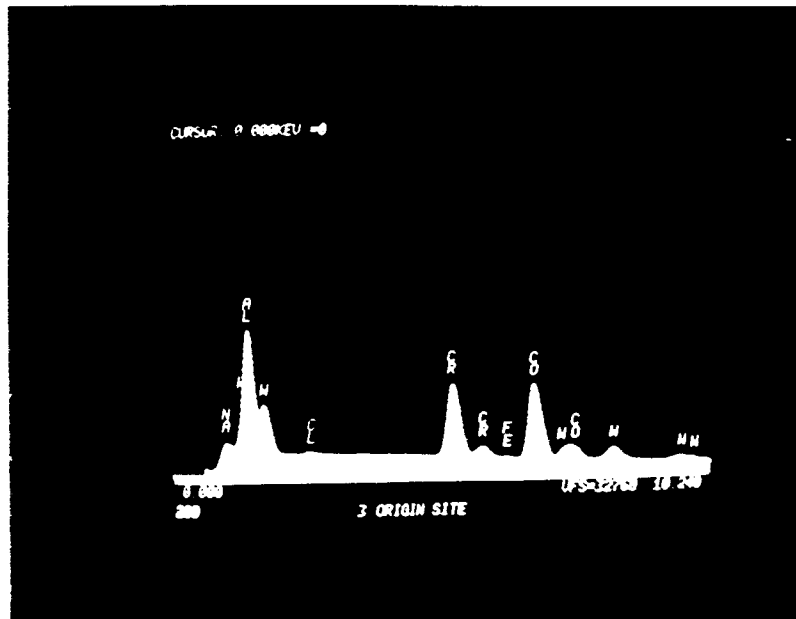
(B) E. D. X. A. 500X

FIGURE 28 (A) Scanning Electron Micrograph of Speci-
men in Figure 27 at Higher Magnification
(B) EDXA Spectrum of the Origin Site

(A) S.E.M. 1CX
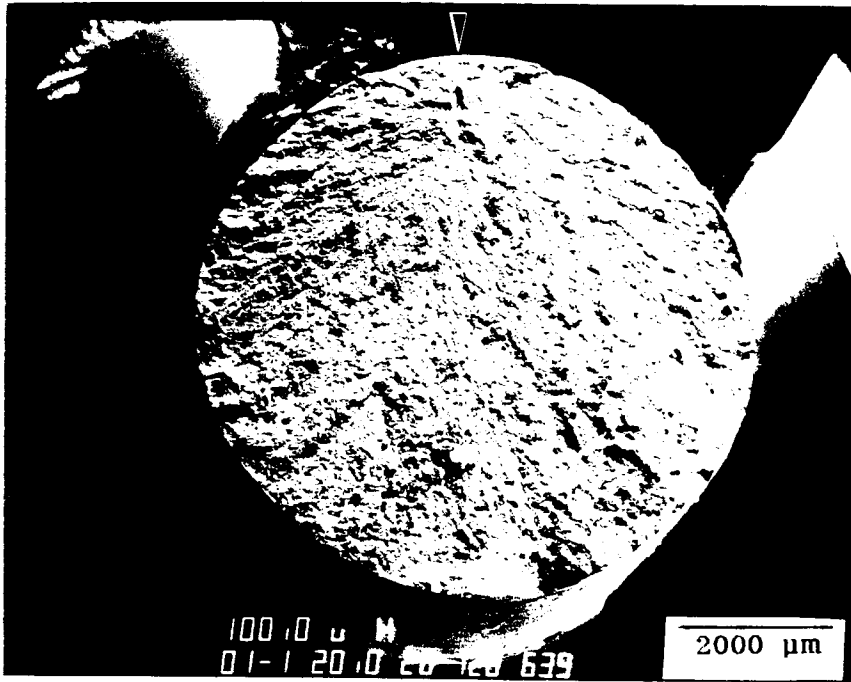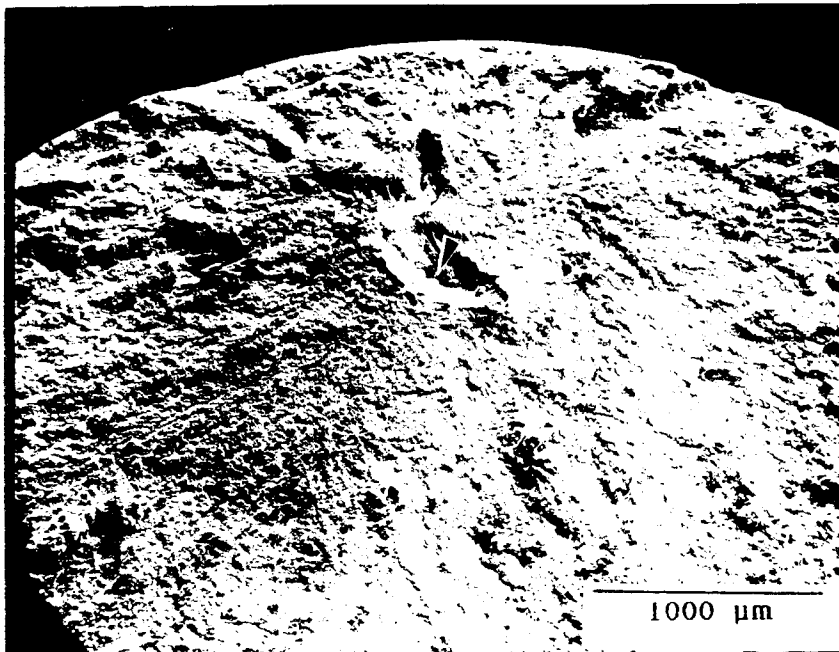
(B) S.E.M. 30X

FIGURE 29 Scanning   Electron   Micrographs   Showing
Tensile Fracture Mode of Class 1 Alloy Aged
at 171 C for 100 hours
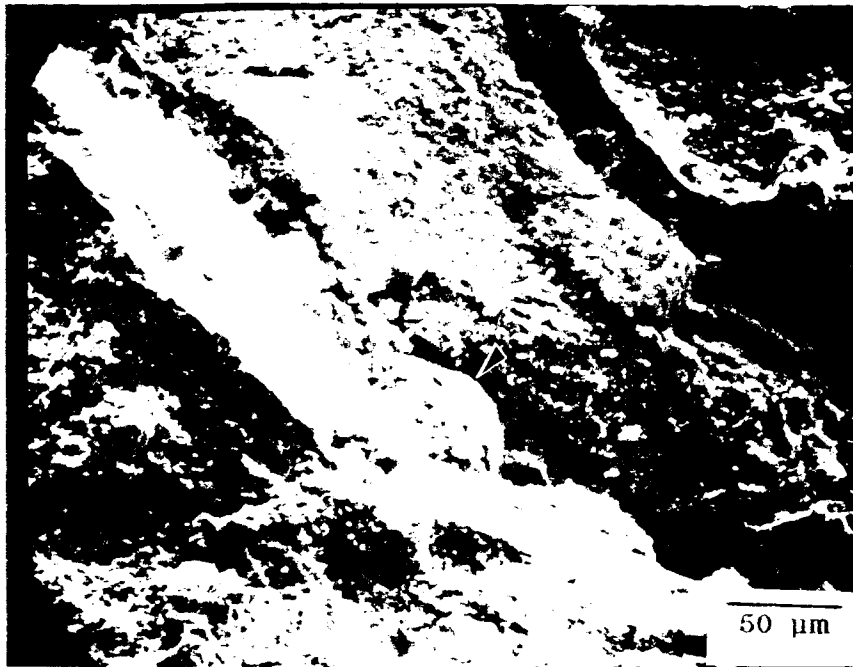
(A) S. E. M. 300X
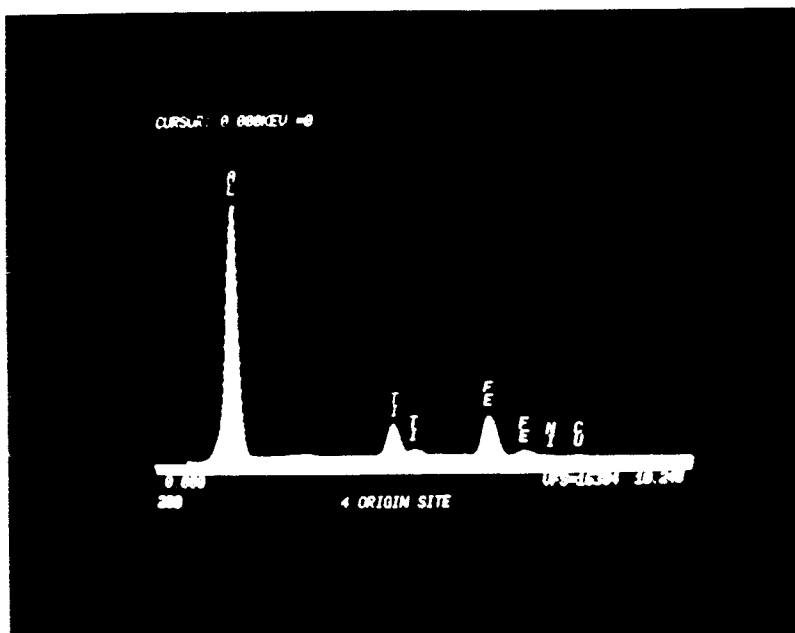
(B) E. D. X. A. 2000X

FIGURE 30 (A) Scanning Electron Micrograph of Specimen in Figure 29 at Higher Magnification
(B) EDXA Spectrum of the Origin Site
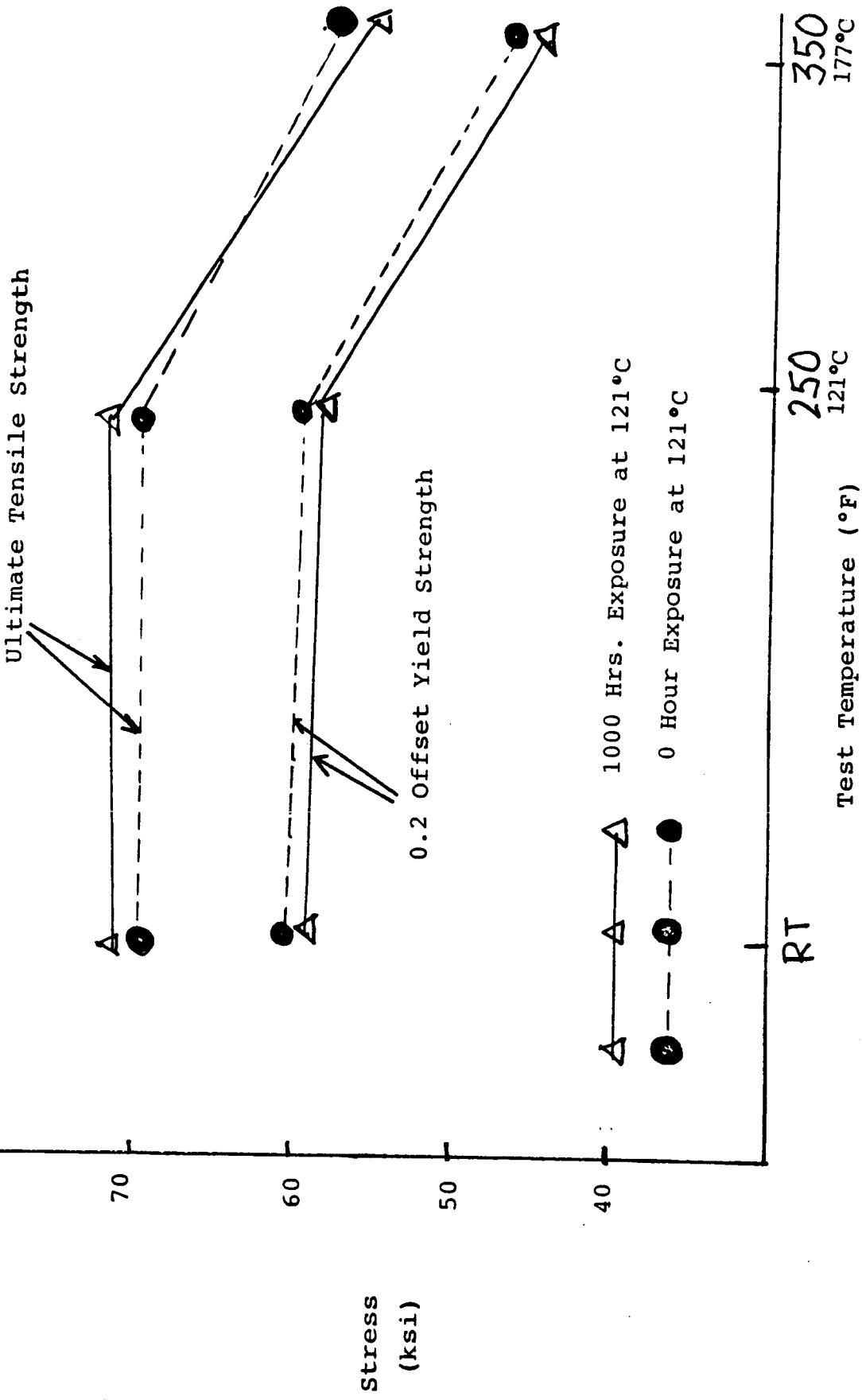
FIGURE 31A   Effect of Long Term Thermal Exposure on Tensile and Yield Strength Values of Class 2 Alloy at Room and Elevated Temperatures
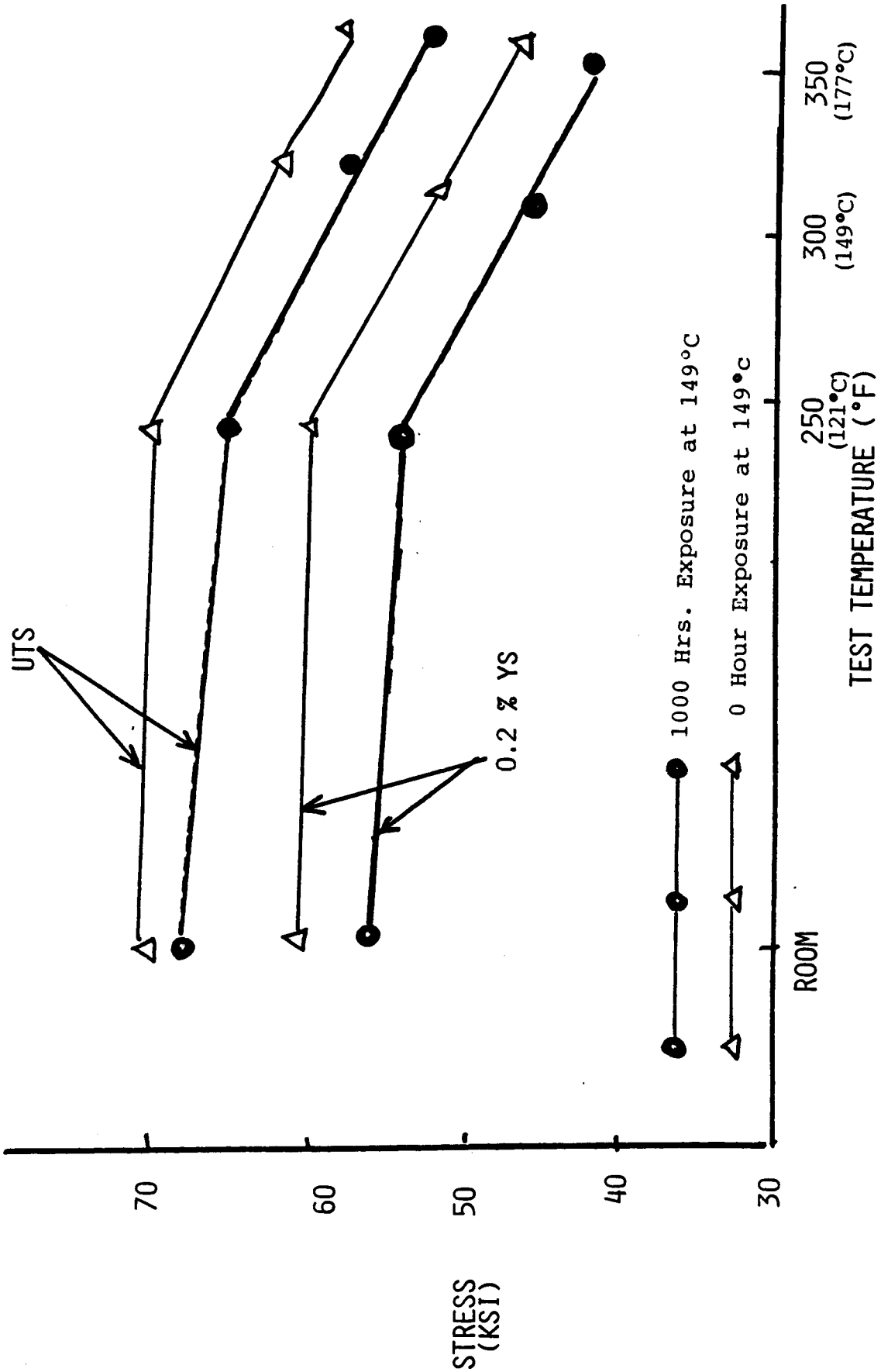
FIGURE 31B — Effect of Long Term Thermal Exposure at 149 C of Tensile and Yield Strength Values of Class 2 Alloy at Room and Elevated Temperatures
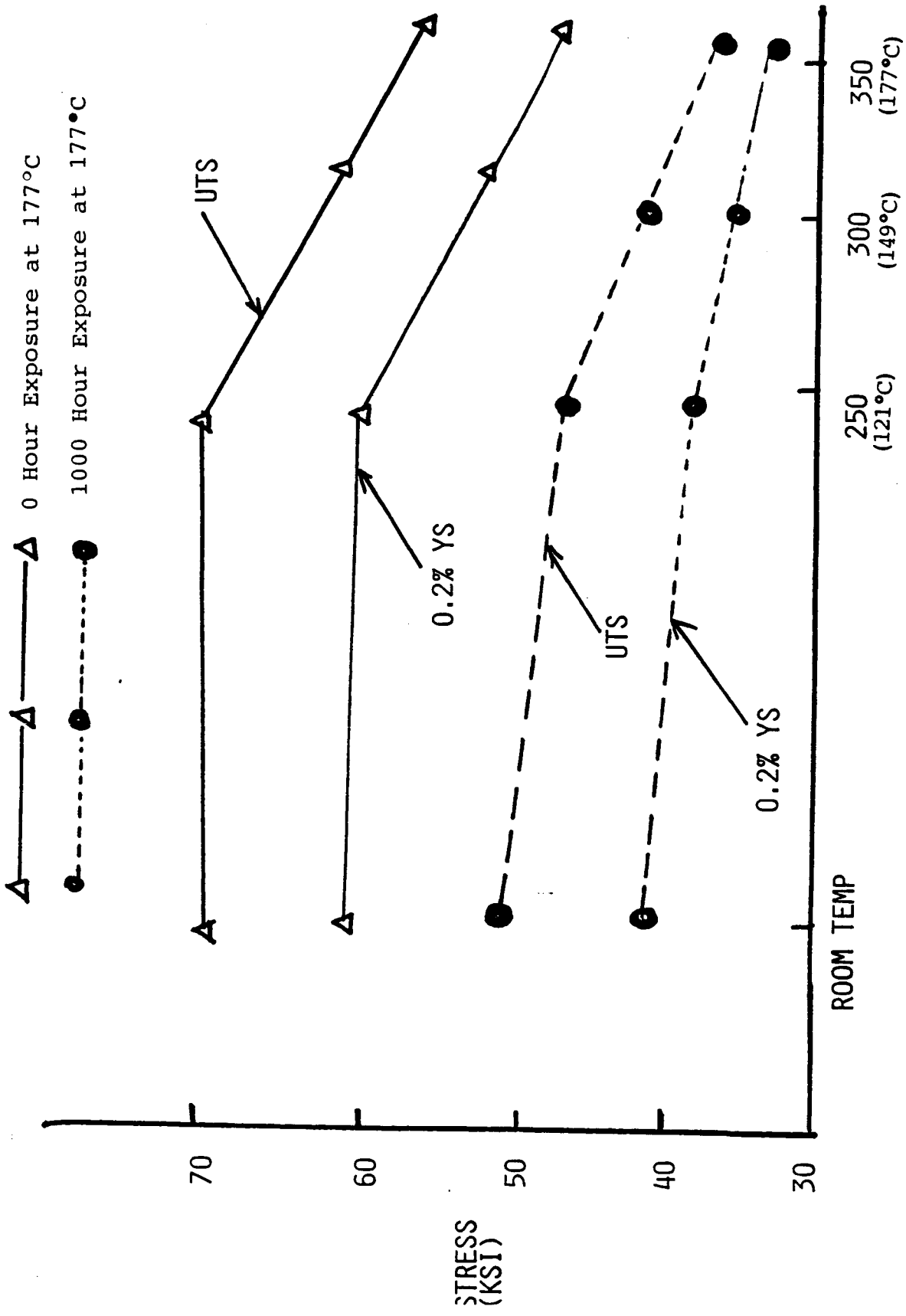
FIGURE   Effect of Long Term Thermal Exposure at 177
31C   C on Tensile and Yield Strength Values of
          Class 2 Alloy at Room and Elevated
          Temperatures

112
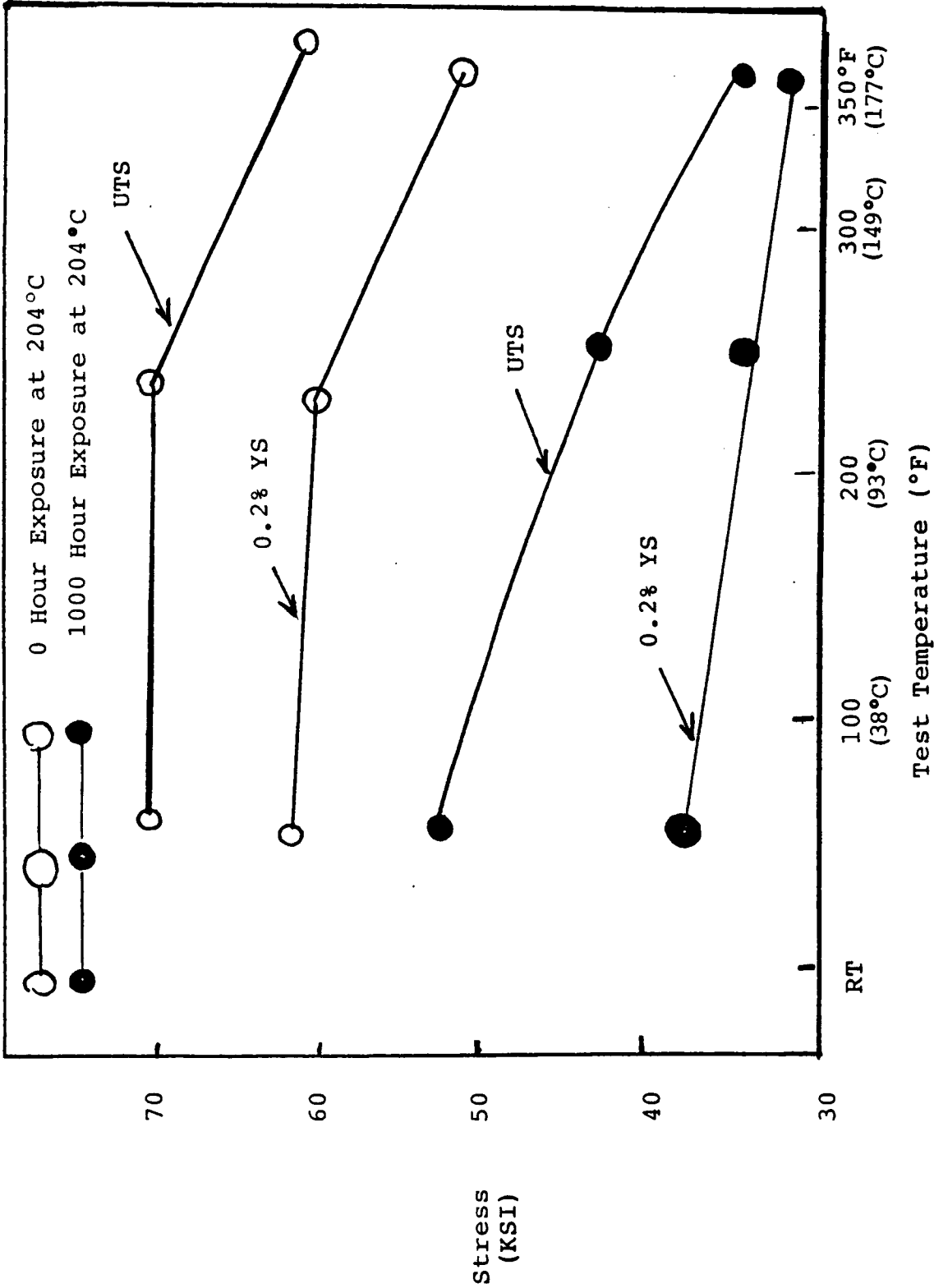
FIGURE 31D

Effect of Long Term Thermal Exposure on Tensile and Yield Strength Values of Class 2 Alloy at Room and Elevated Temperatures

180X   180X

AS-EXTRUDED   HEAT TREATED (T4)
(LONGITUDINAL)   (LONGITUDINAL)
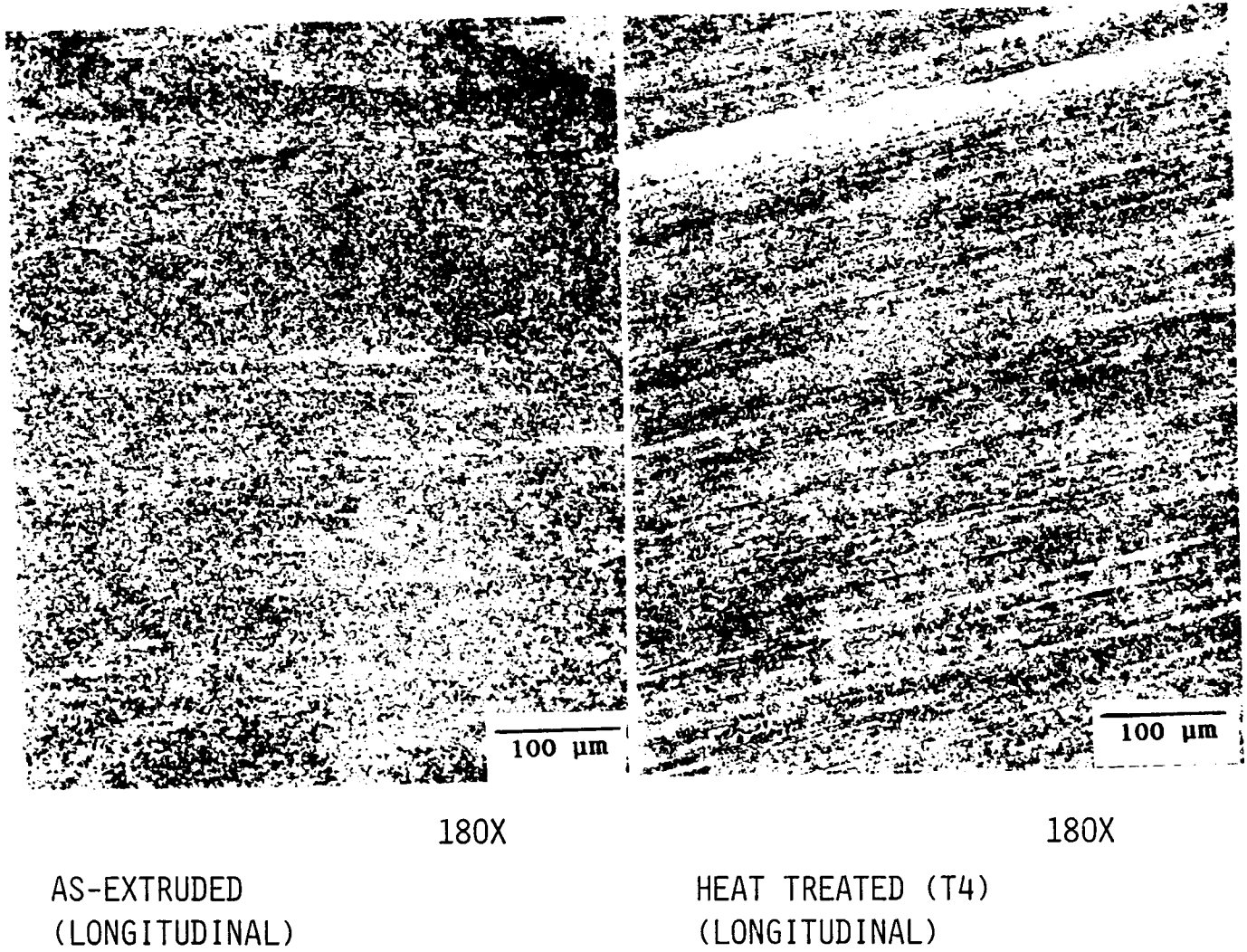
FIGURE 32 Optical Photomicrographs of Class 2 Alloy
           in As-extruded and in Heat Treated (T4)
           Conditions
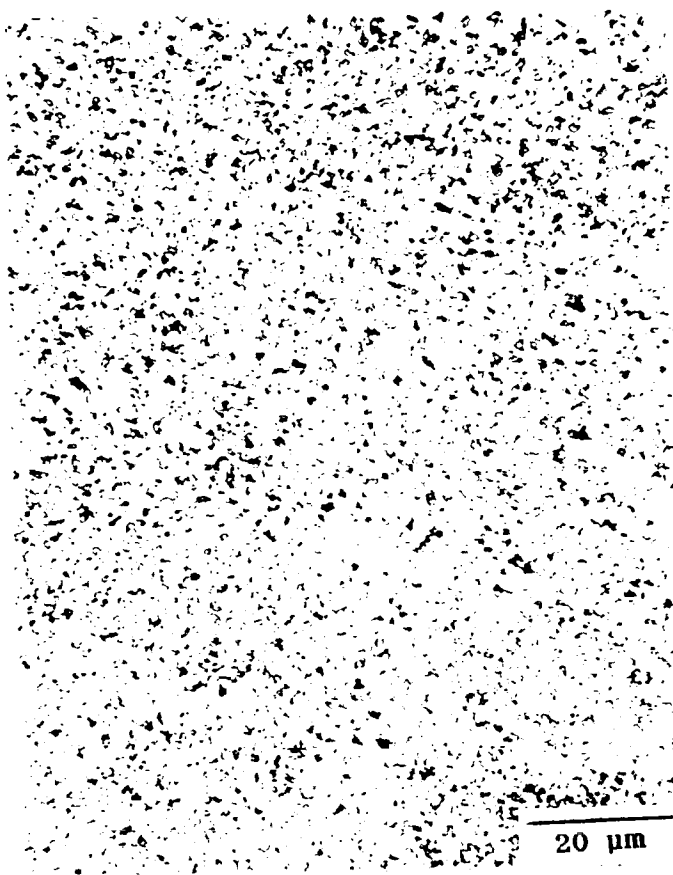
960X   960X

AS-EXTRUDED   HEAT TREATED (T4)
(LONGITUDINAL)   (LONGITUDINAL)

FIGURE 33   Optical Photomicrographs at High Magnifica-
tion of Class 2 Alloy in As-extruded and in
Heat Treated (T4) Conditions

FIGURE 34 Transmission Electron Micrograph of a Typical Area of Class 2 Alloy in T4 Condition

FIGURE 35 Transmission Electron Micrograph of Another
Area of Class 2 Alloy in T4 Condition

0.25 μm

FIGURE 36 Transmission Electron Micrograph of Another
Area of Class 2 Alloy in T4 Condition
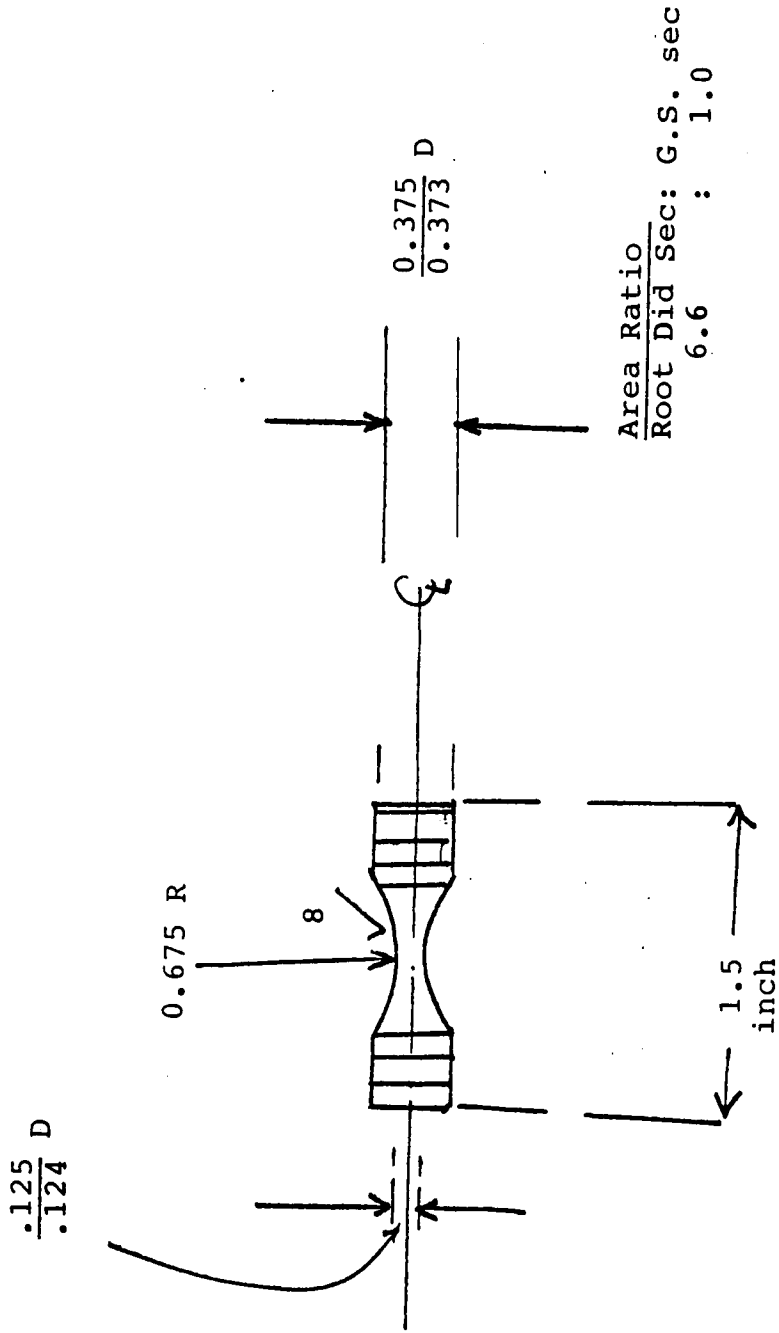
FIGURE 37 Fatigue Test Specimen
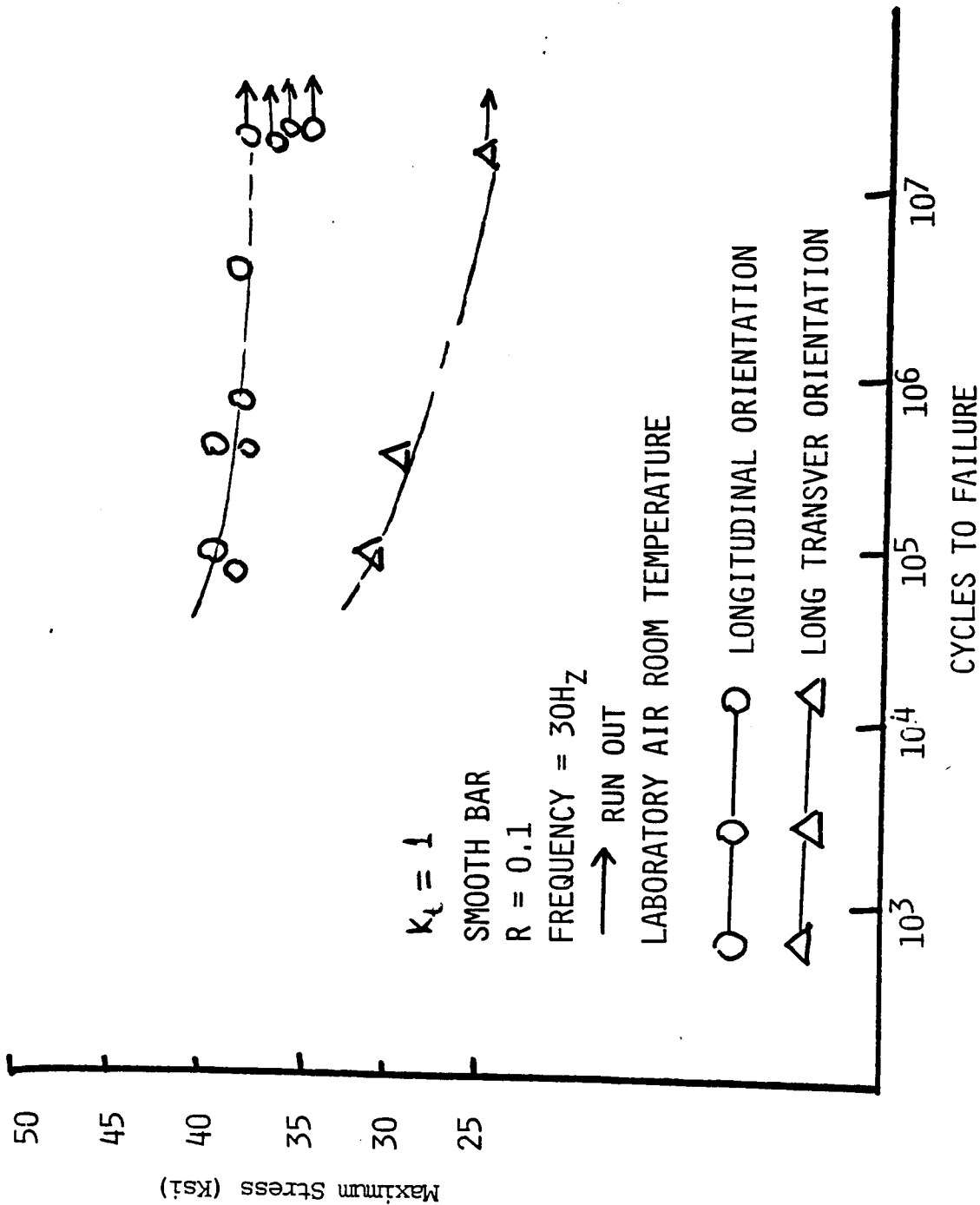
FIGURE 38 Constant Amplitude Fatigue Data of Class 2
Alloy (T4)

S. E. M. 25X

FIGURE 39 Scanning Electron Micrograph of the Fatigue
Fracture Surface of Class 2 Alloy in T4
Condition
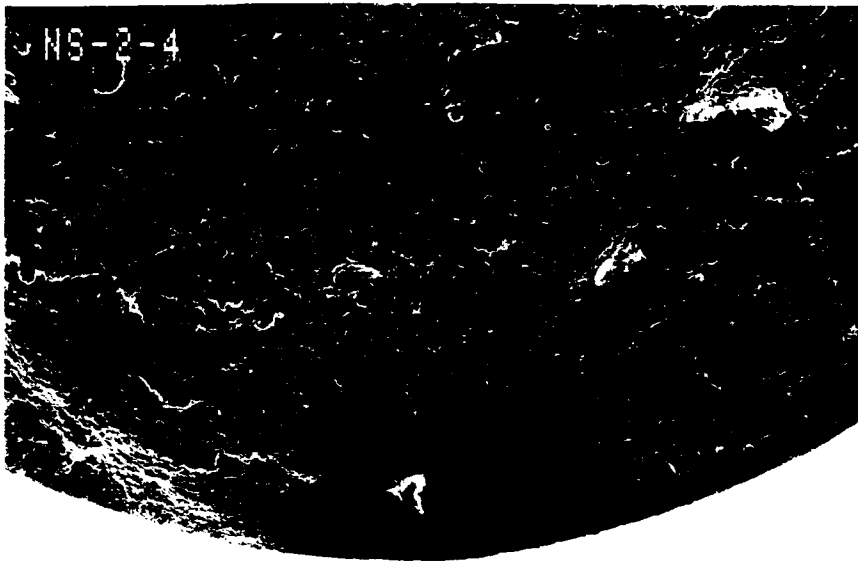
(A) S. E. M. 75X
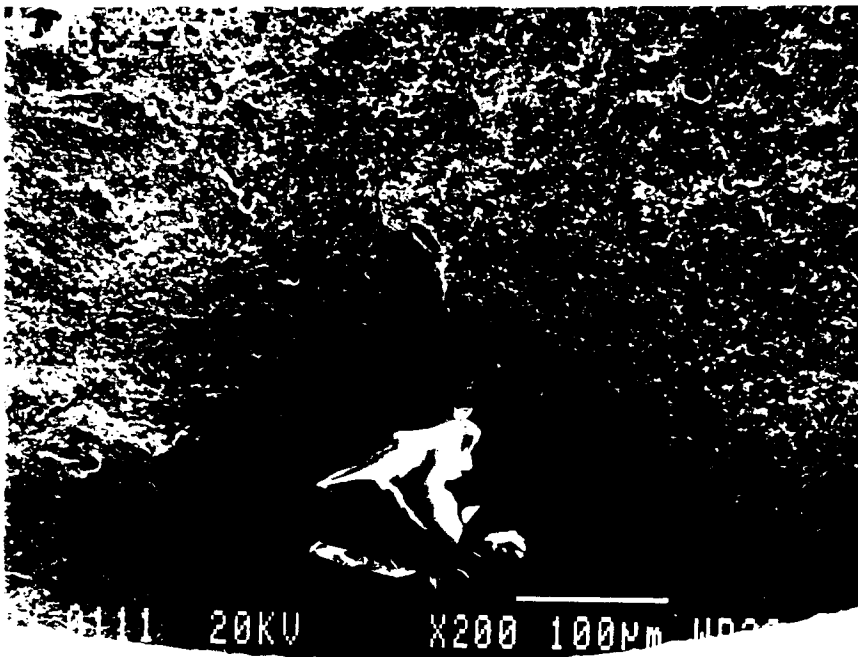
(B) S. E. M. 200X

FIGURE 40 Scanning Electron Micrograph of the Speci-
men in Figure 30 at Higher Magnification
Showing Fracture Initiation Site
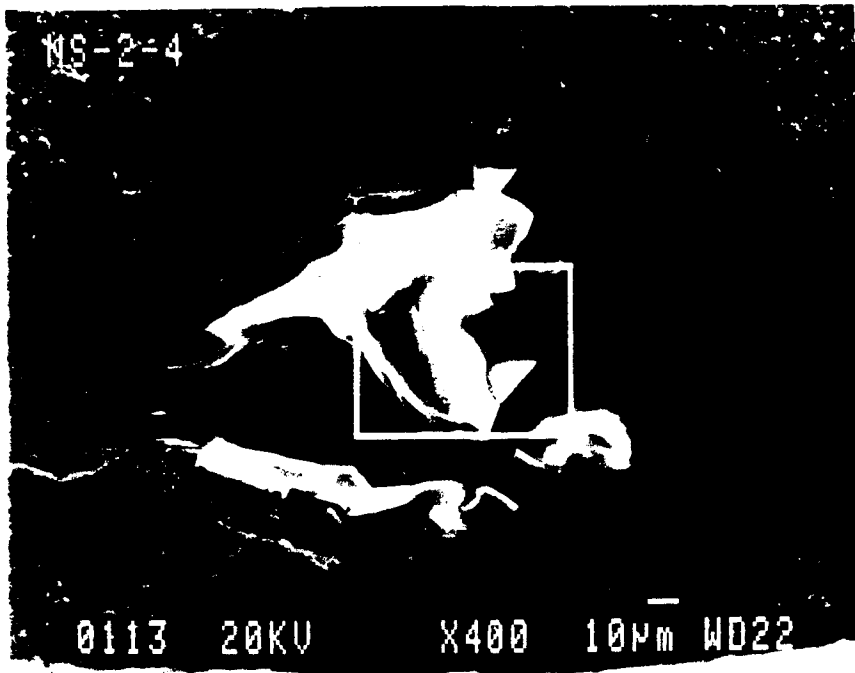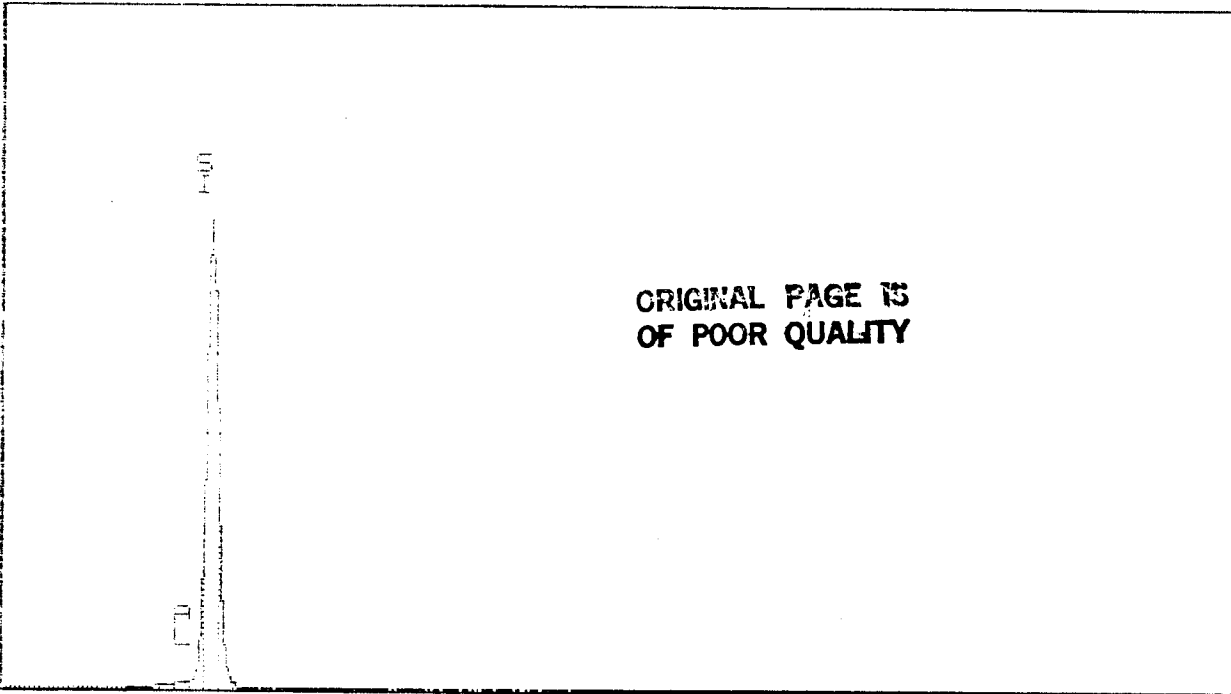
FIGURE 41 EDXA Spectrum of the Inclusion Causing
Fatigue Fracture Initiation in the Specimen
of Class 2 Alloy
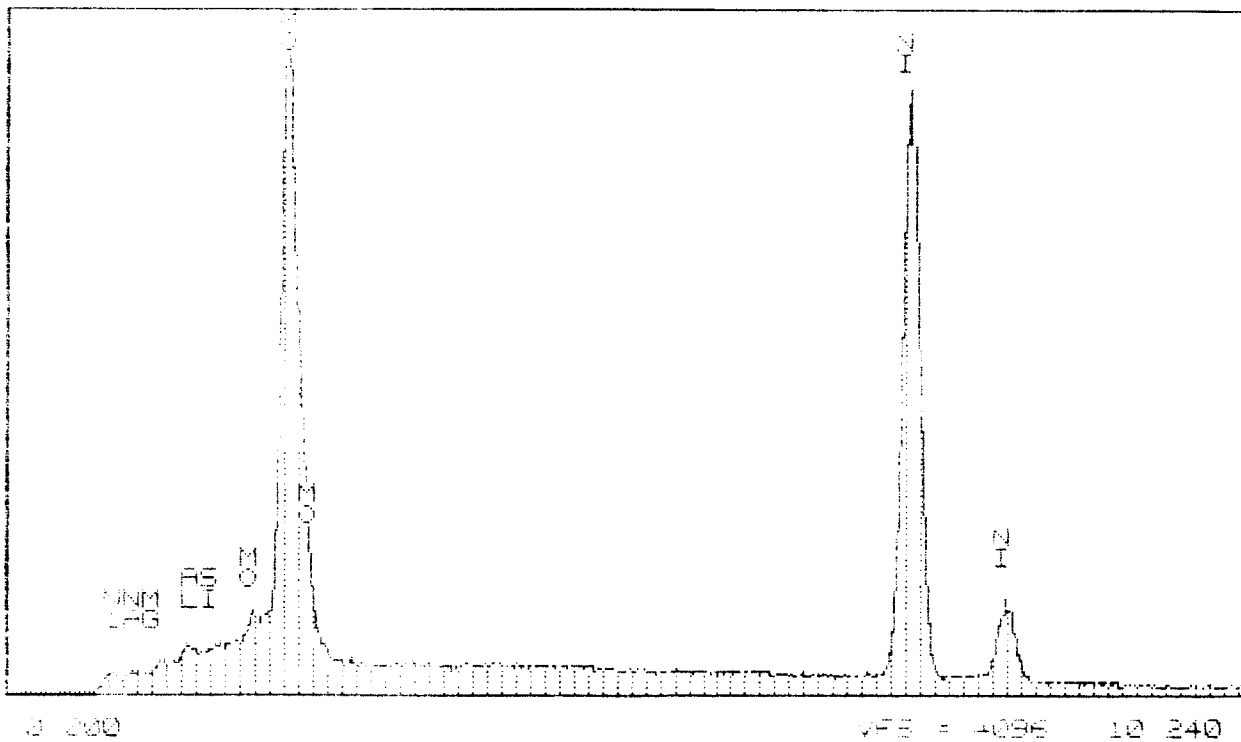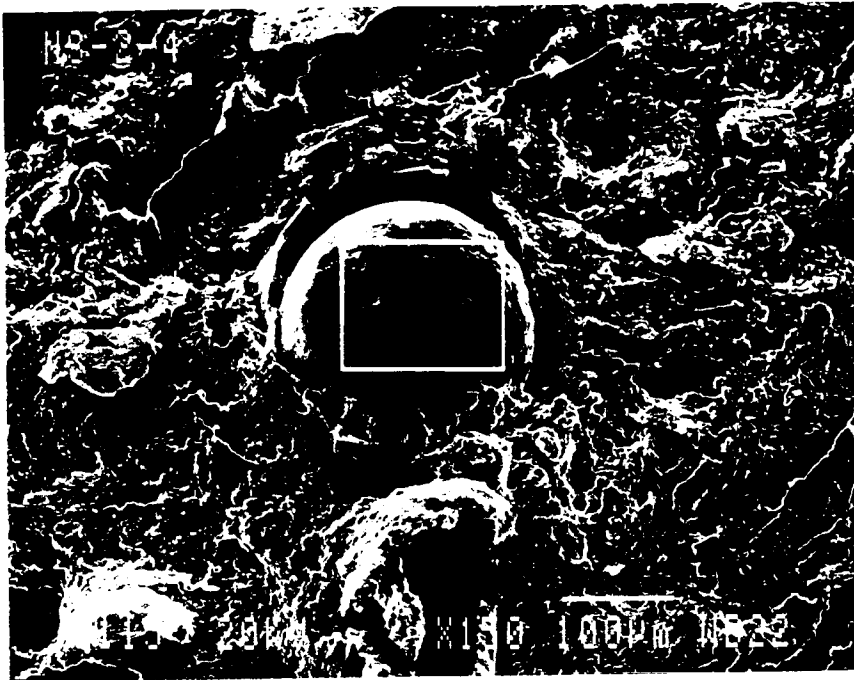
FIGURE 42 EDXA Spectrum Showing Composition of a
Round Inclusion in the Fatigue Specimen of
Class 2 Alloy
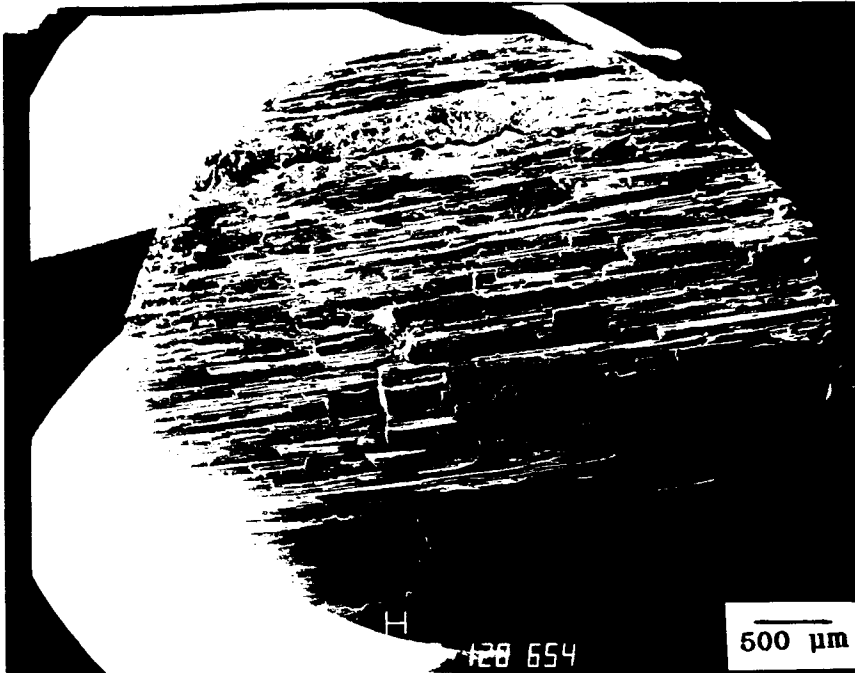
(A) S. E. M. 20X

(B) S. E. M. 70X

FIGURE 43 Scanning Electron Micrograph of the Fatigue
Fracture Surface of Class 2 Alloy (T4) in
L-T Orientation

FIGURE 44 Scanning Electron Micrograph of Fatigue
Fracture Surface of Class 2 (T4) Alloy
Showing an Inclusion (A)
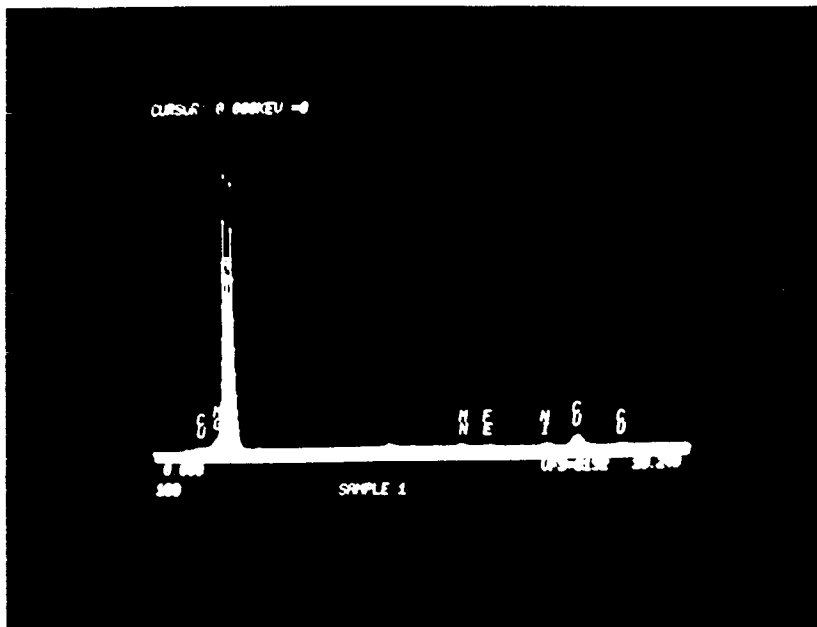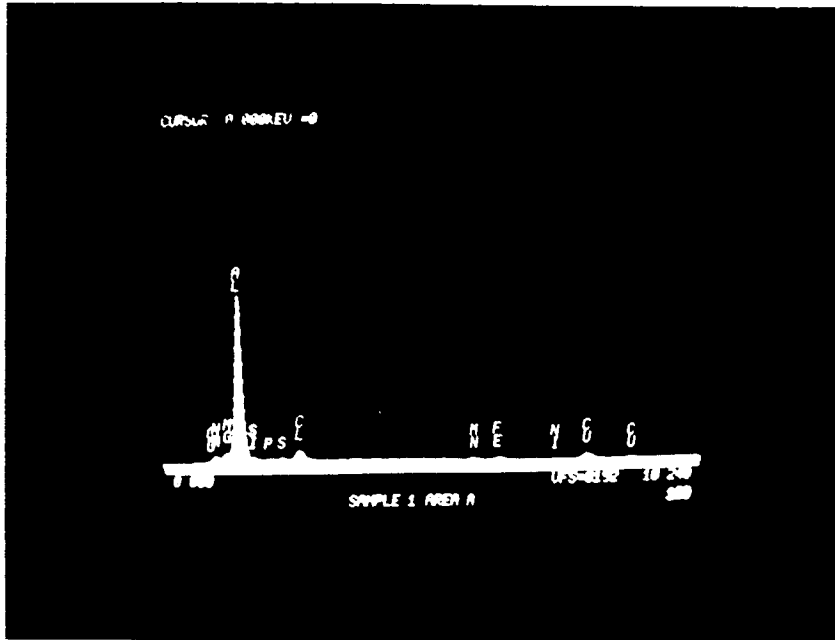
FIGURE 45: EDS SPECTRUM OBTAINED FROM THE INCLUSION AND THE FRACTURE
SURFACE OF THE FATIGUE FRACTURE SURFACE OF CLASS 2 (T4) ALLOY
SHOWN IN FIGURE 44.

2H = 1.201
A = 0.252
W = 0.999
L = 1.25
B = 0.252
N = .046
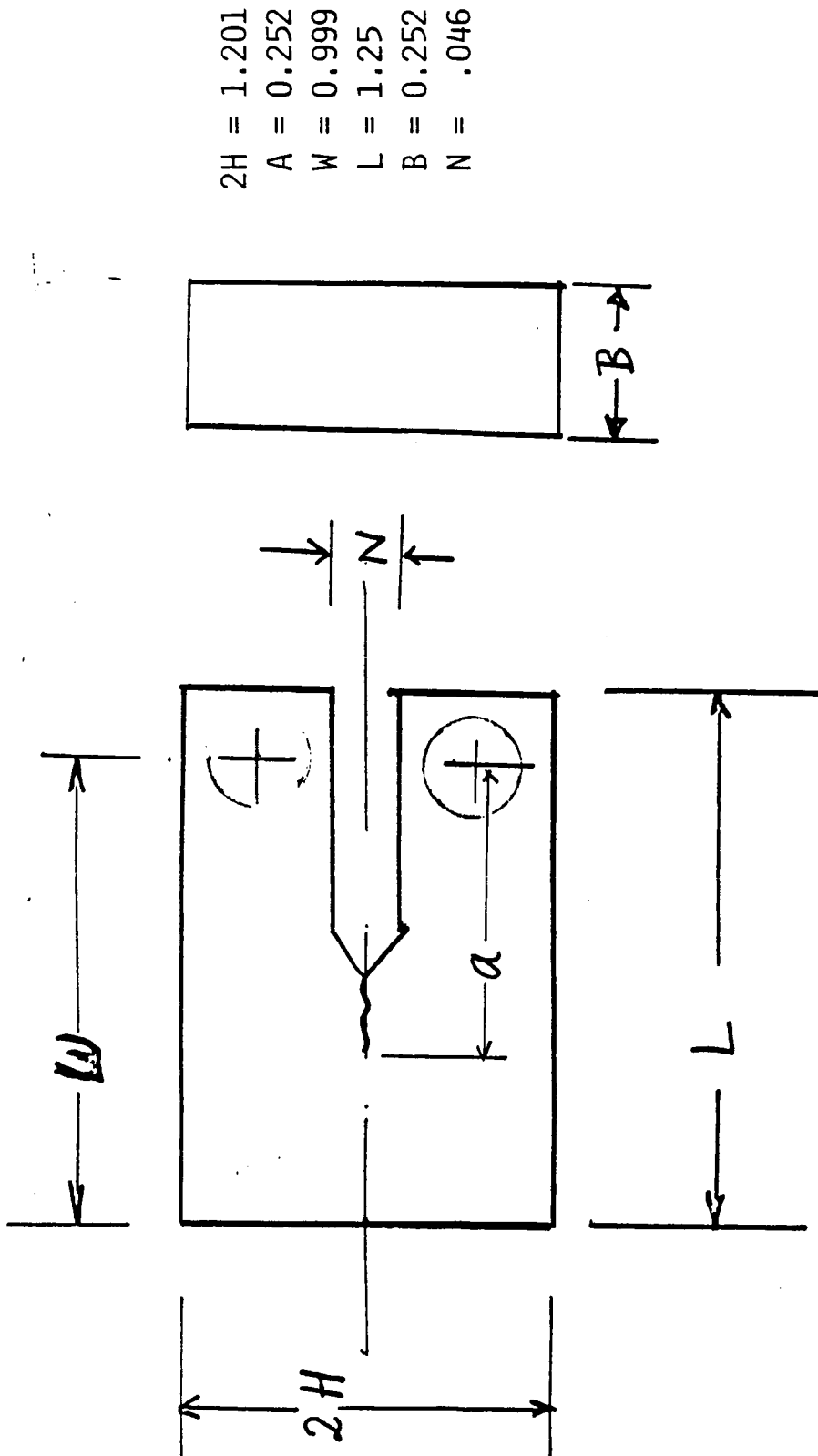
FIGURE 46 Compact Tension Specimen
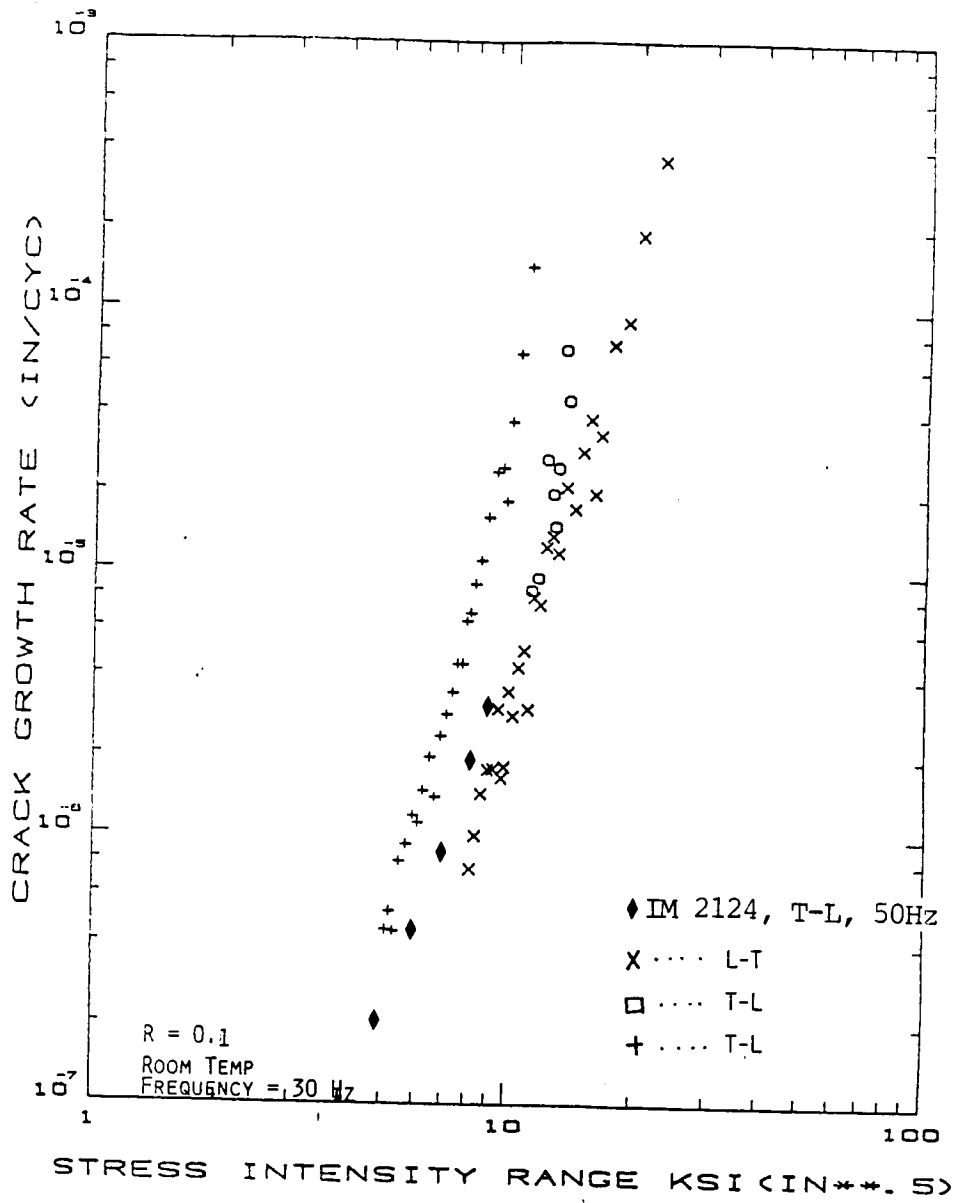
FIGURE 47 Fatigue Crack Growth Behavior of Class 2 Alloy (T-4)
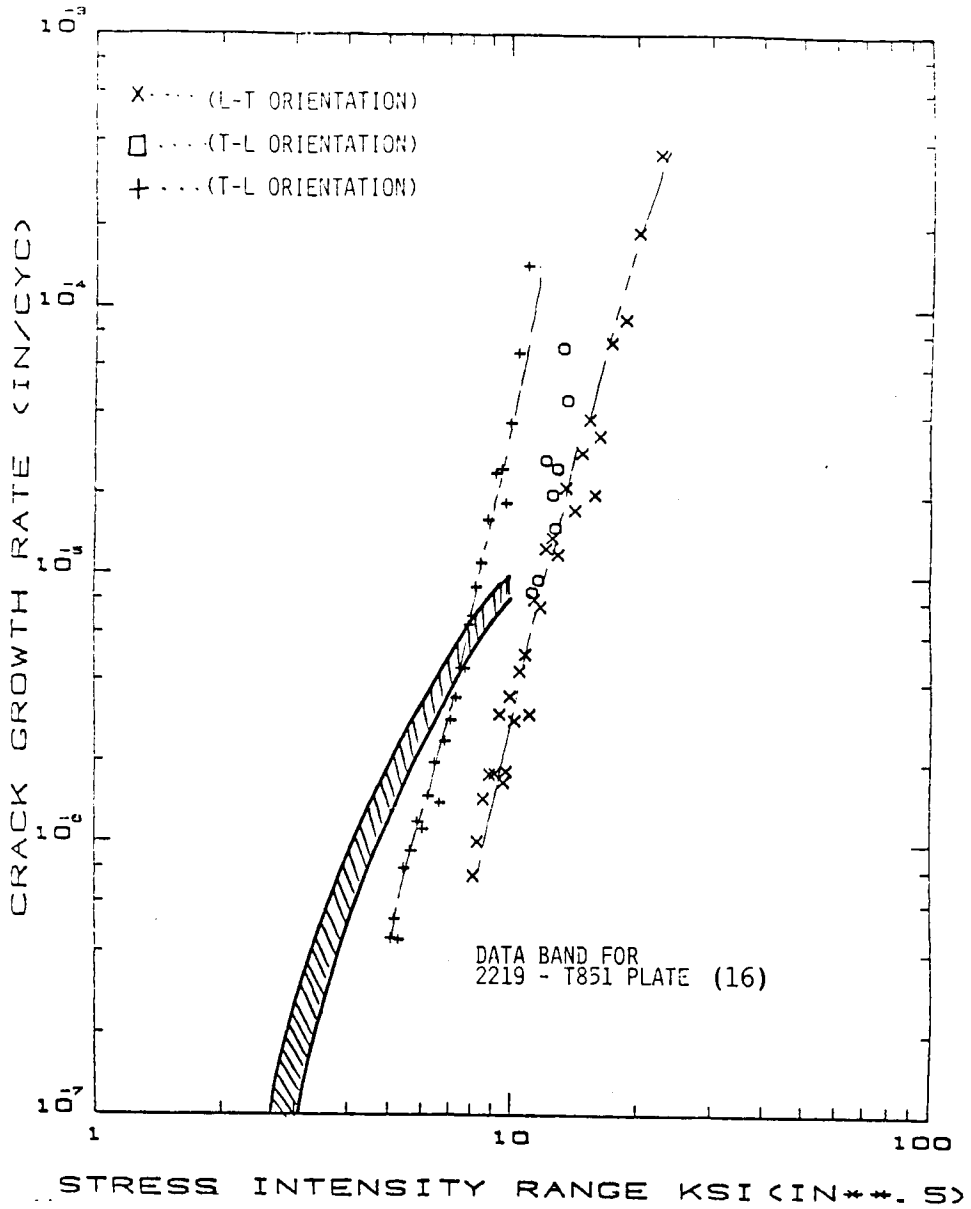
FIGURE 48 Fatigue Crack Growth Behavior of Class 2
Alloy and 2219-T851 Alloy

130
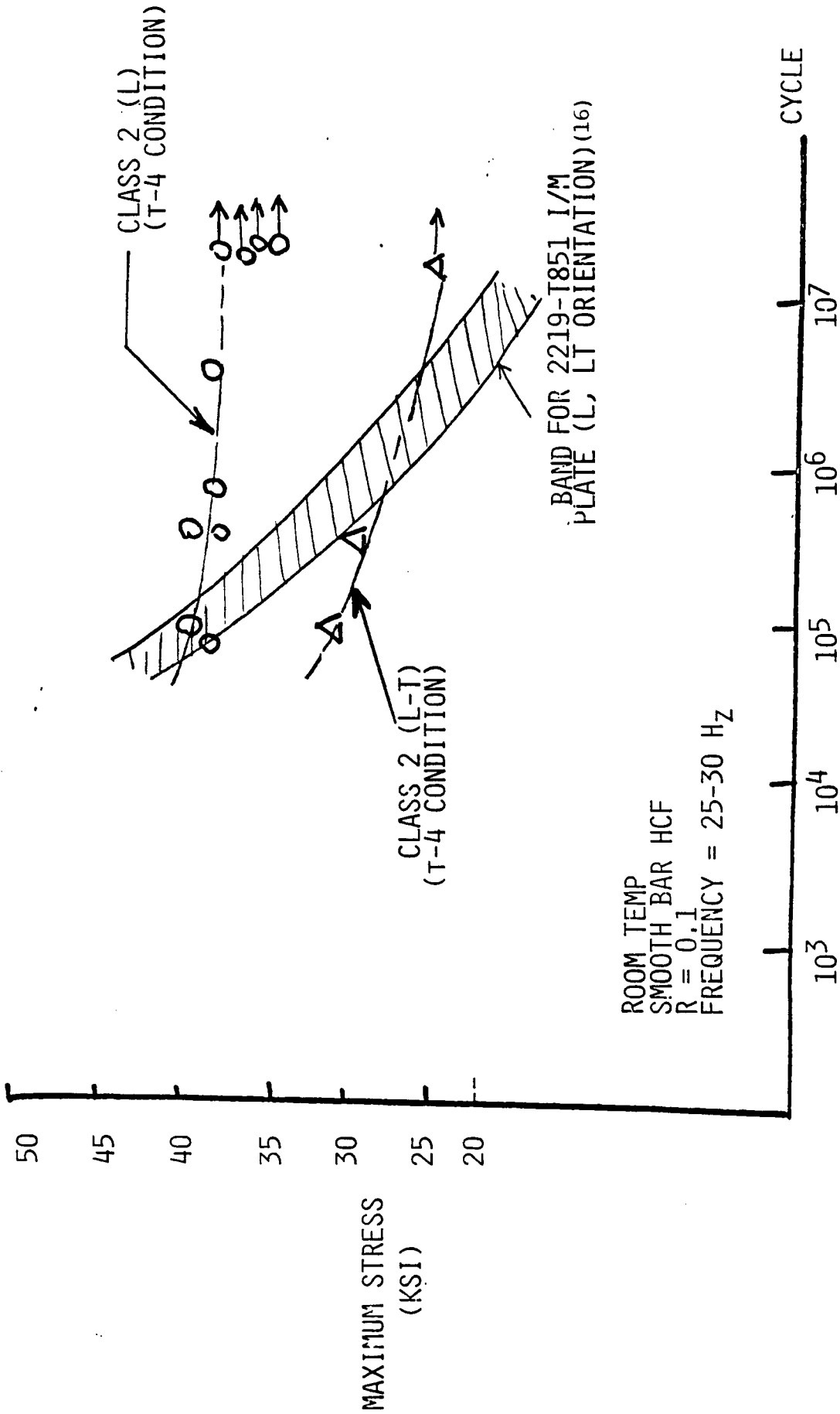
FIGURE 49 Constant Amplitude Fatigue Data for Class 2
Alloy in T4 Condition
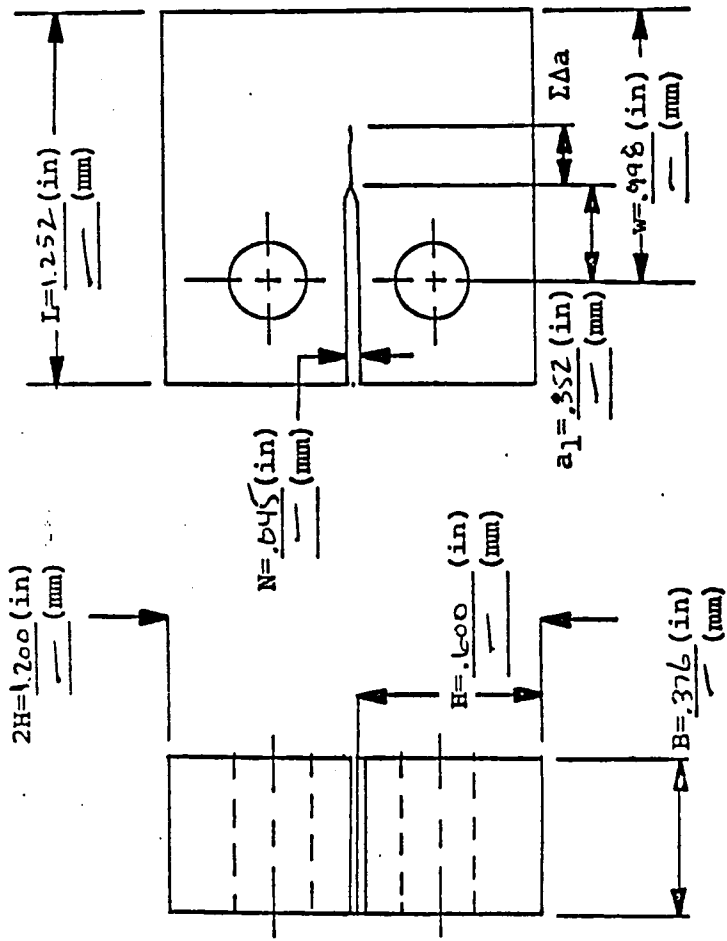
FIGURE 50 Compact Tension Specimen
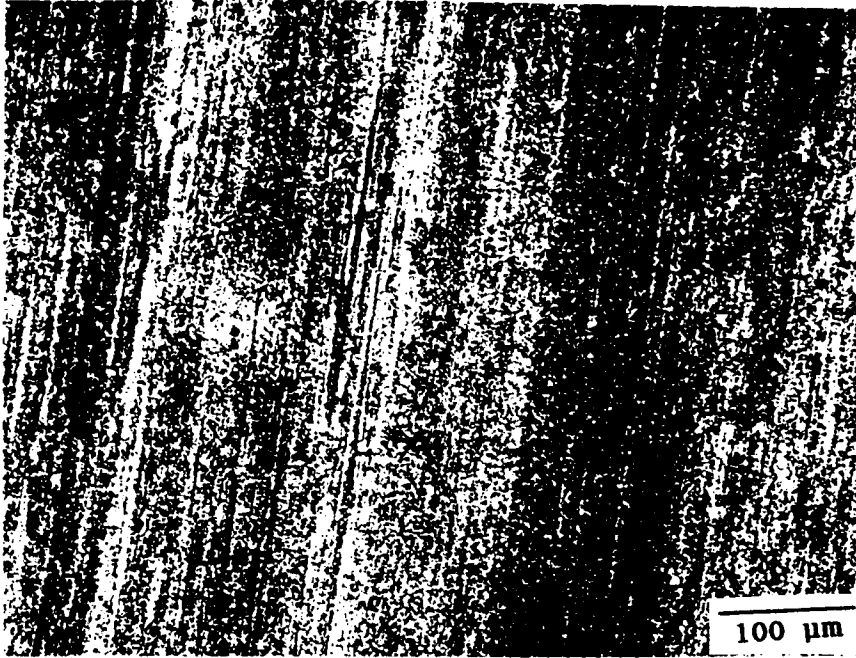
LONGITUDINAL

ORIGINAL PAGE IS
OF POOR QUALITY
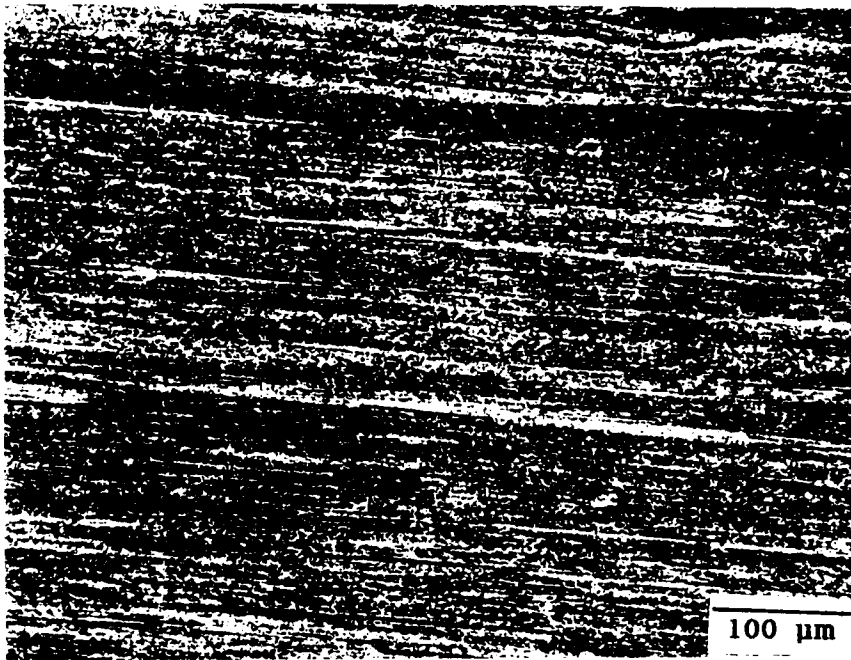
LONG TRANSVERSE

FIGURE 51 Photomicrograph of As-extruded Class 3
Alloy
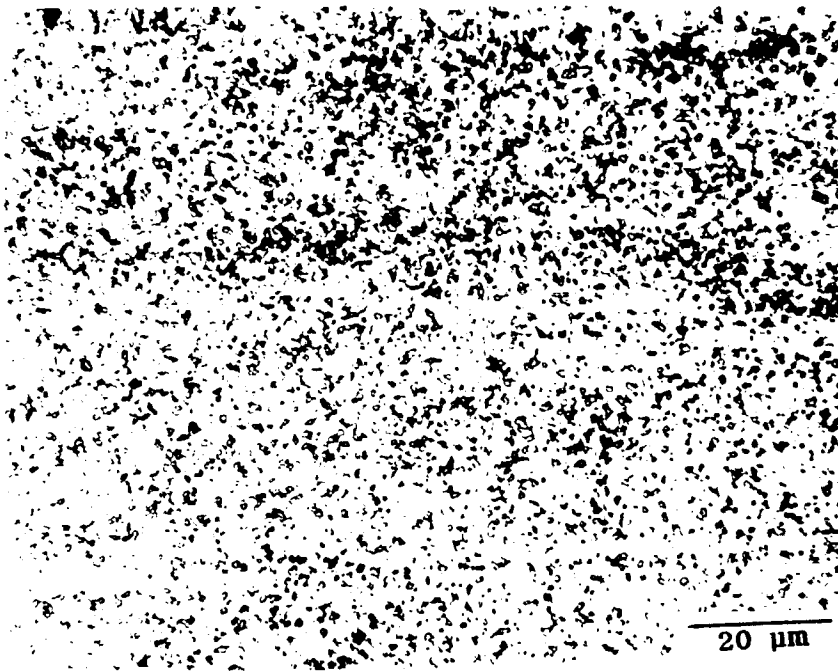
LONGITUDINAL

FIGURE 52 Photomicrograph of As-extruded Class 3
Alloy
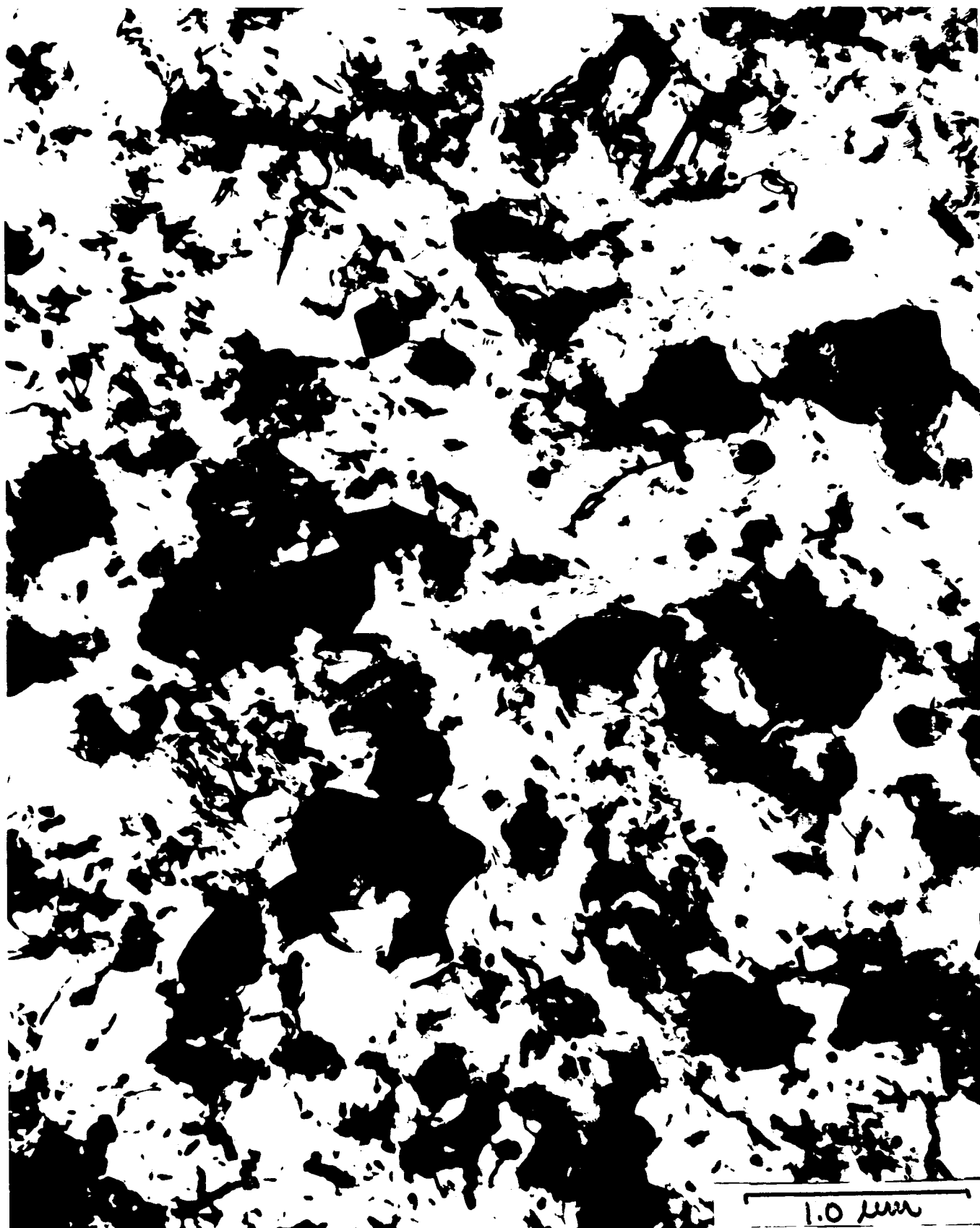
FIGURE 53 Transmission Electron Micrograph of a Typical Area of Class 3 Alloy

FIGURE 54 Transmission Electron Micrograph of Another
Typical Area of Class 3 Alloy
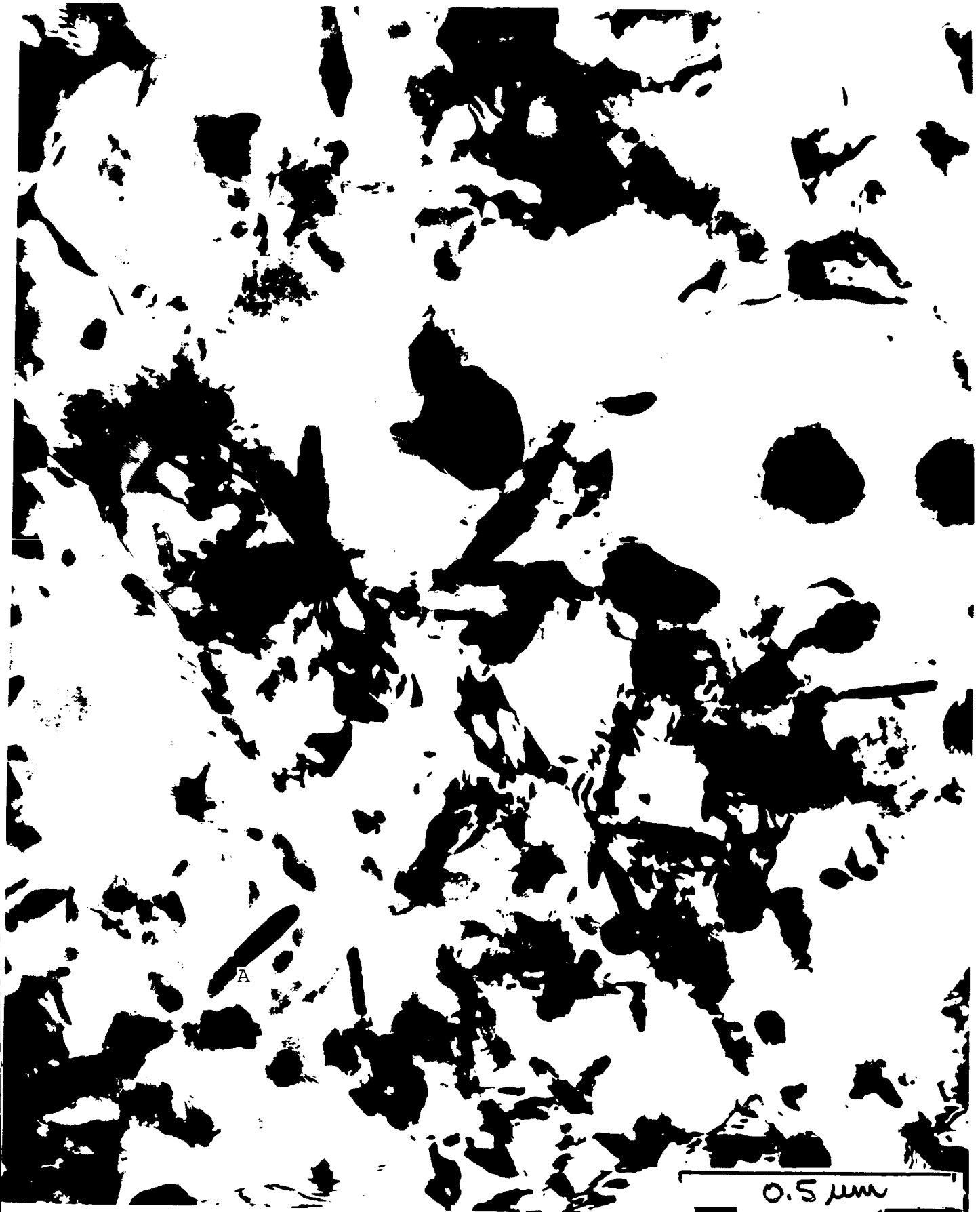
FIGURE 55 Transmission Electron Micrograph of a
Typical Area of Class 3 Alloy

0.5 μm

FIGURE 56 Transmission Electron Micrograph of a
Typical Area of Class 3 Alloy

FIGURE 57 TEM Photomicrograph of Class 3 Alloy

0.2 μm

FIGURE 58 TEM Photomicrograph of Class 3 Alloy
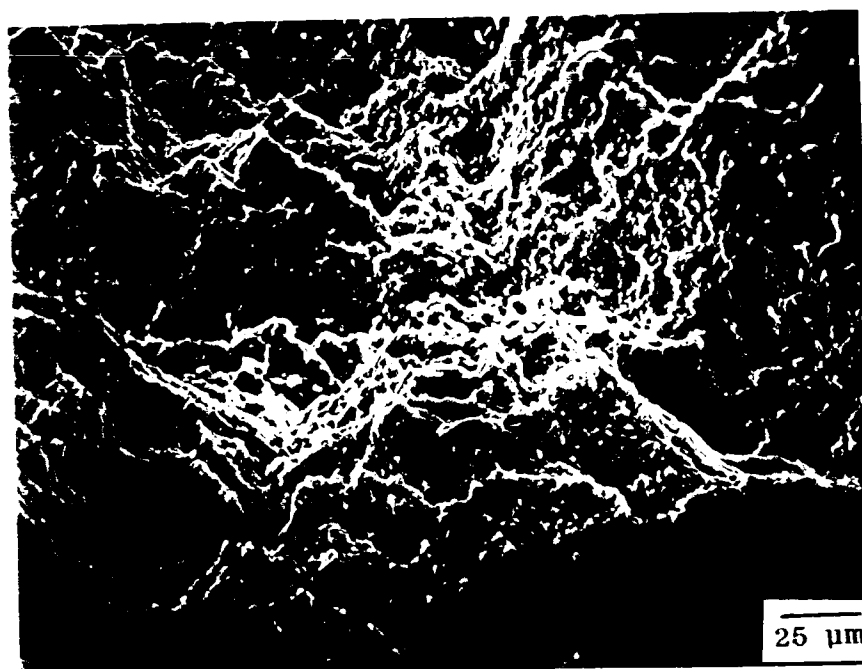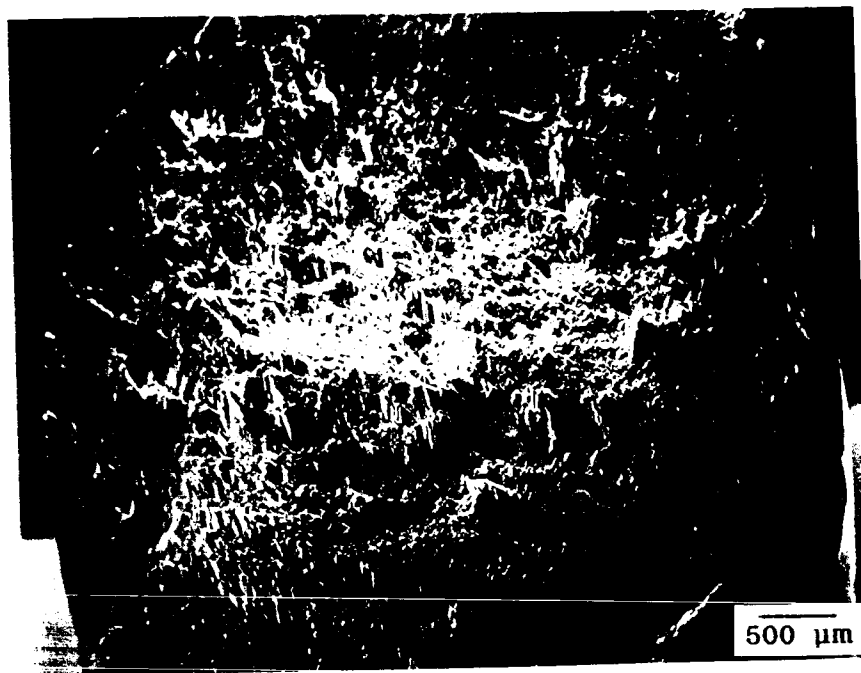
FIGURE 59 A,B: SCANNING ELECTRON MICROGRAPHS SHOWING TENSILE FRACTURE MODE IN CLASS 3 ALLOY.

141

5 μm

2000X

2 μm
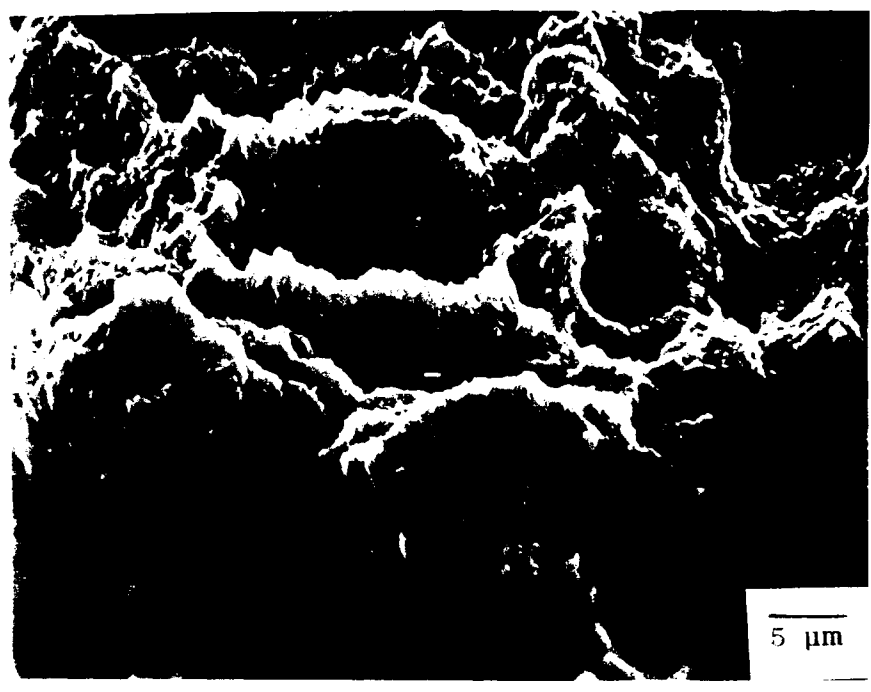
5000X

FIGURE 59 C,D: SCANNING ELECTRON MICROGRAPH SHOWING TENSILE FRACTURE MODE
                 IN CLASS 3 ALLOY.

142

100 μm

EXTRUDED + ANNEALED
AT 750°F/500 HRS.

100 μm
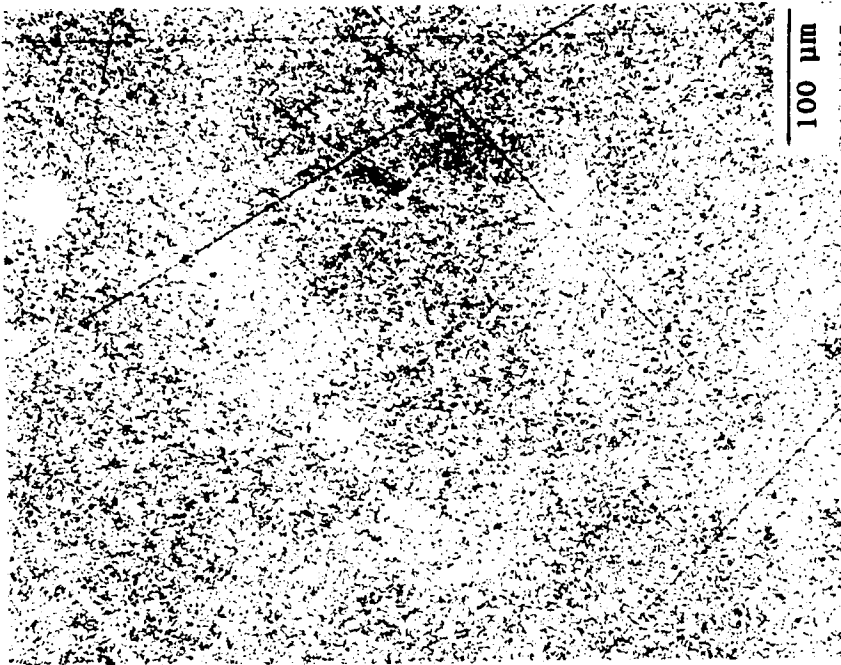
AS EXTRUDED

FIGURE 60 Photomicrograph of Extruded Class 3 Alloy
Annealed at 400 C for 500 hours
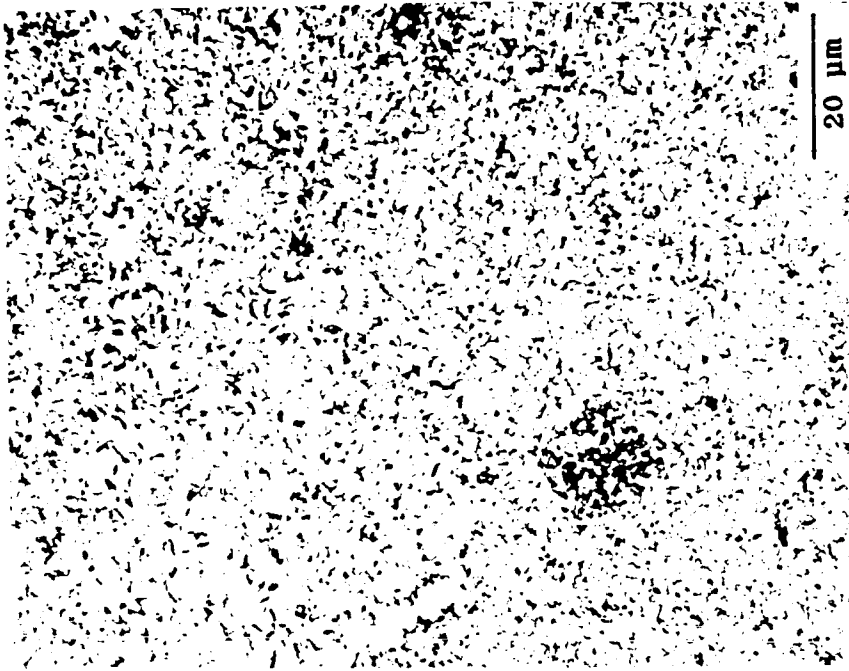
EXTRUEDE + ANNEALED
AT 750°F/500 HRS.

AS EXTRUDED

FIGURE 61 Photomicrograph of Extruded Class 3 Alloy
Annealed at 400 C for 500 hours
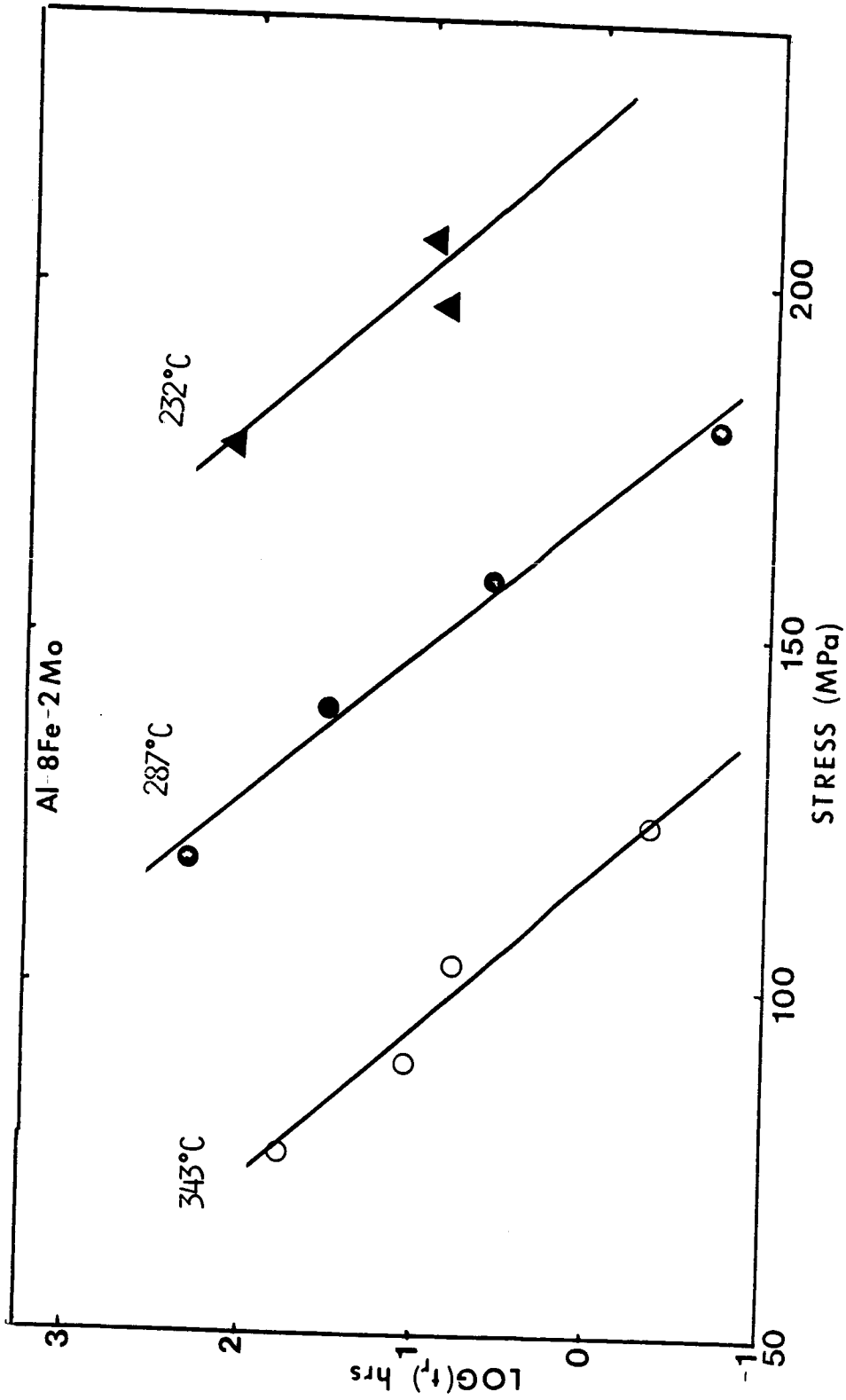
FIGURE 62 Stress Rupture Test Data at Different Temperatures for Class 3 Alloys Plotted on Semi-log Scale
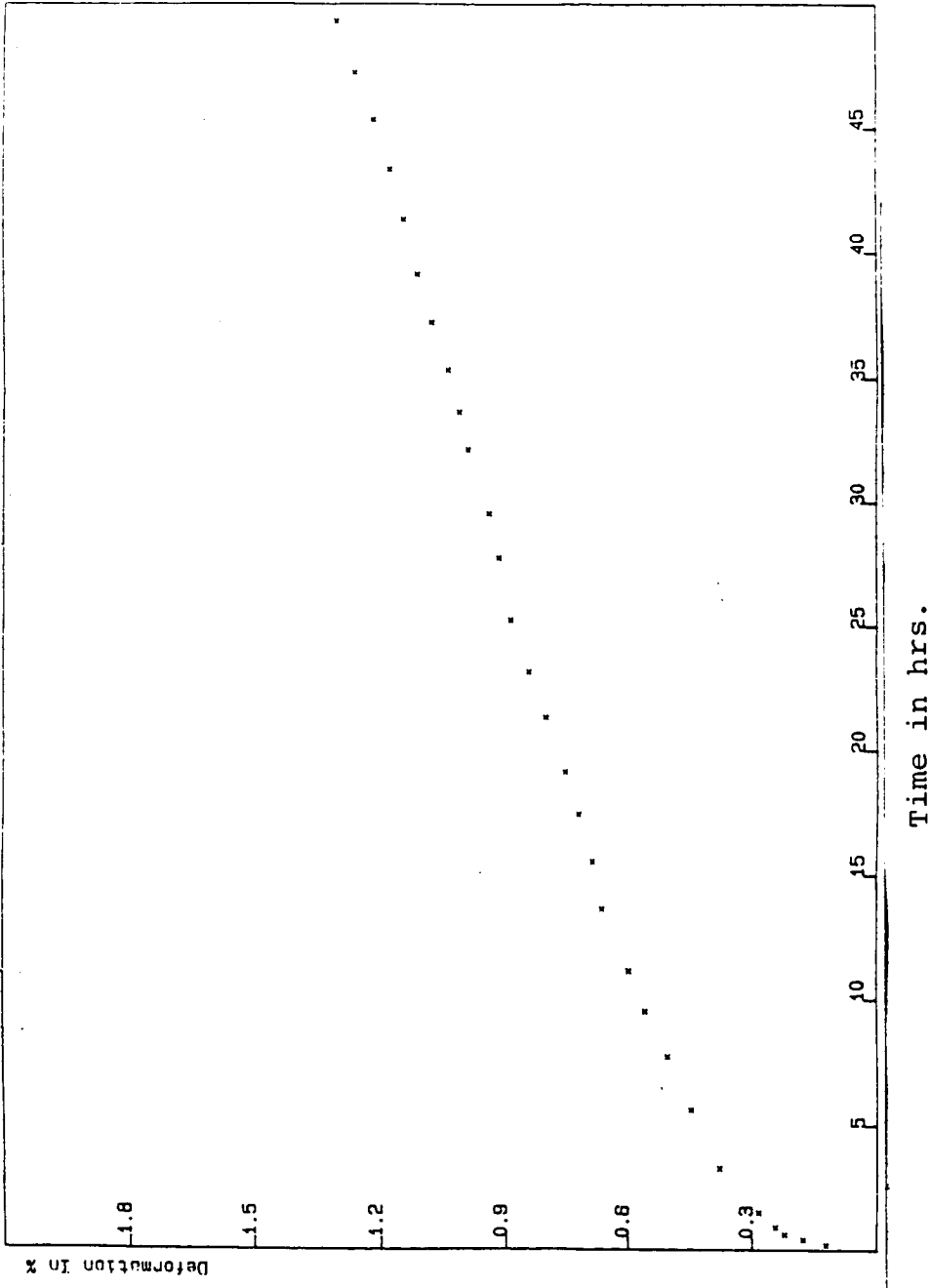
FIGURE 63 Creep Curve of Class 3 Alloy at 232 C and 26.5 KSI Stress
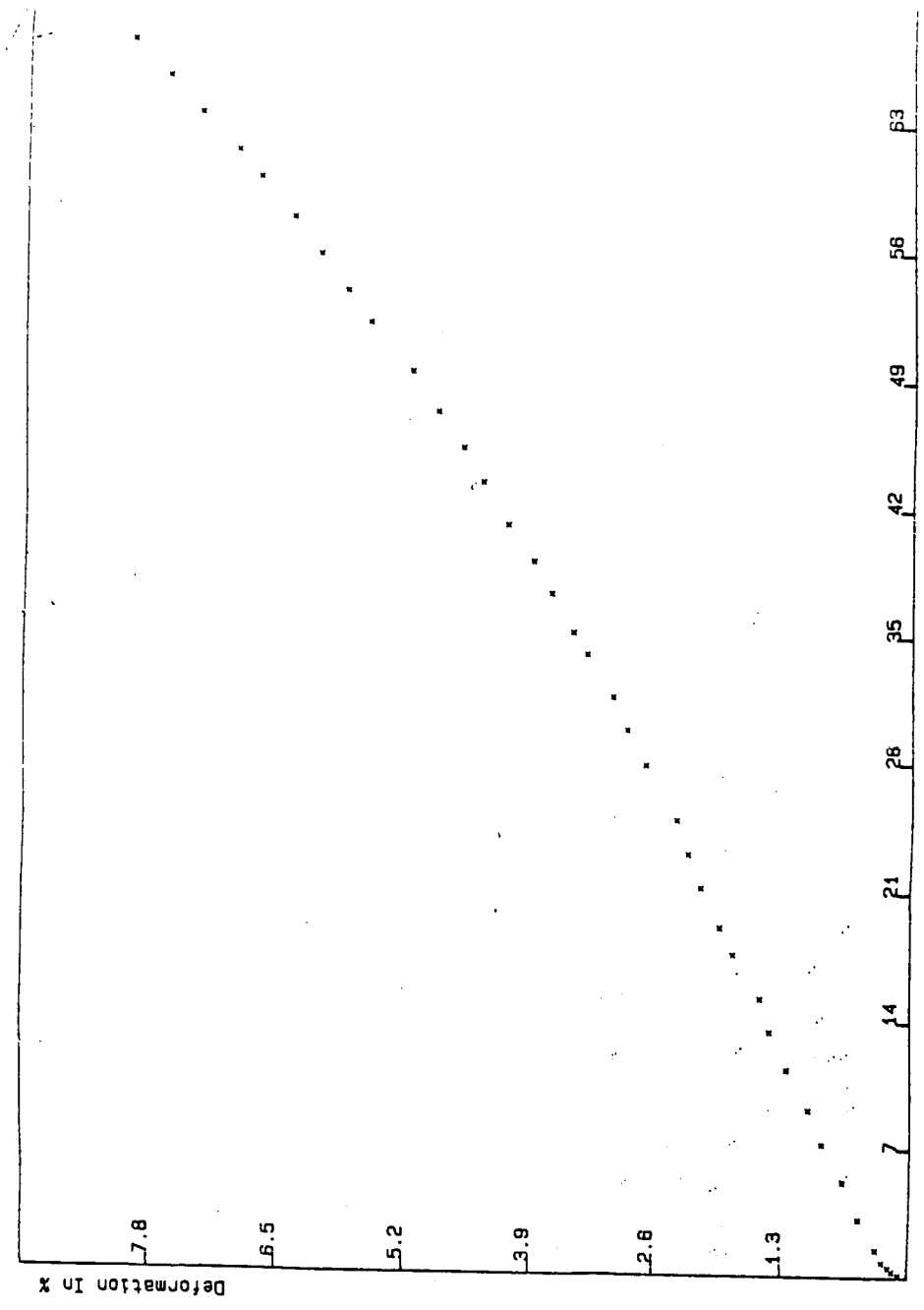
FIGURE 64 Creep Curve of Class 3 Alloy at 343 C and 11.0 Ksi Stress

180X
LONGITUDINAL
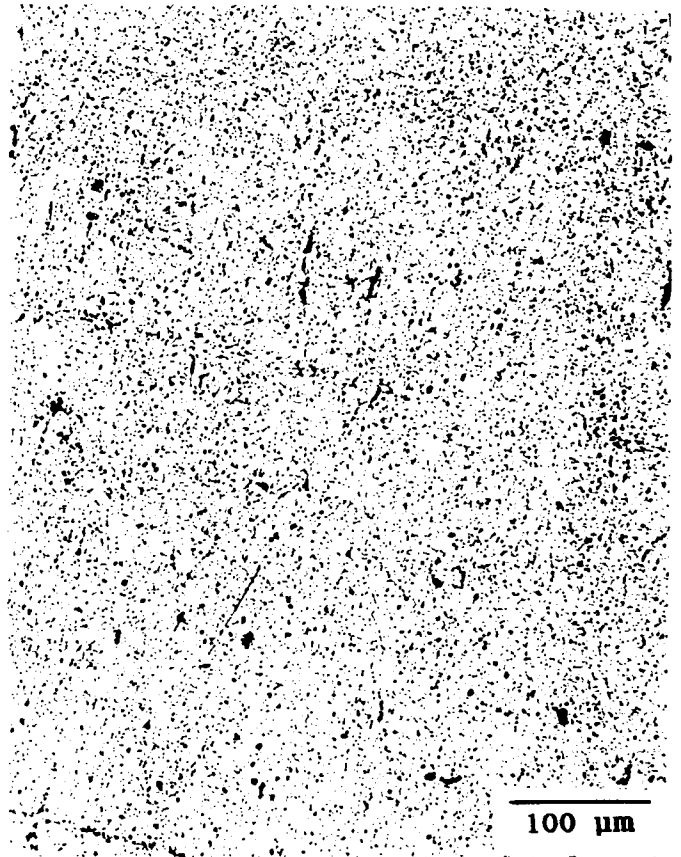
180X
LONG TRANSVERSE

FIGURE 65 Optical Photomicrographs of Class 4 Alloy
(RST X-7091) in As-extruded Condition
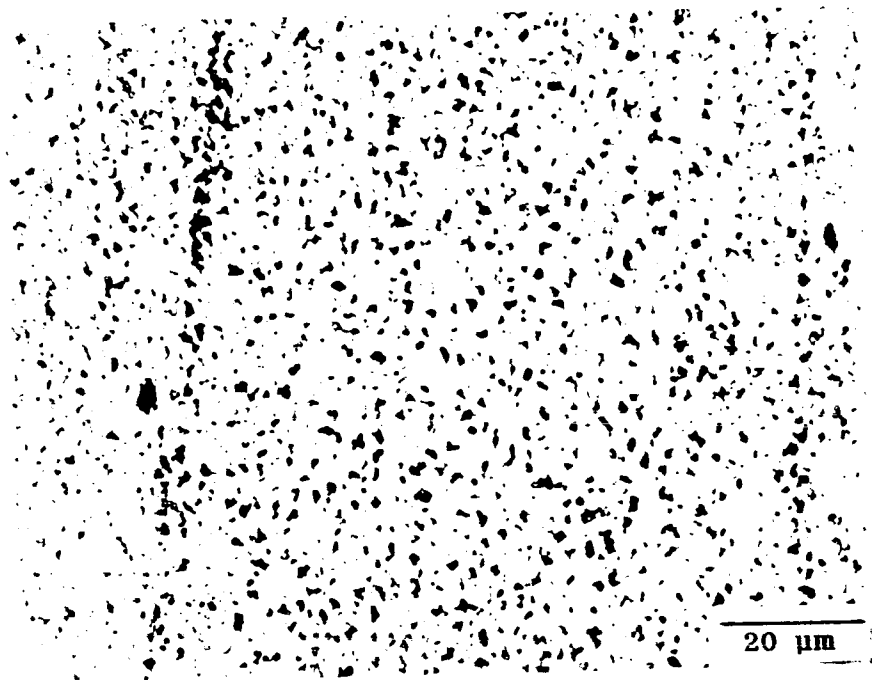
960X   (LONGITUDINAL)

FIGURE 66 Optical Photomicrograph at High Magnifica-
          tion of Class 4 Alloy (RST X-7091) in
          As-extruded Condition
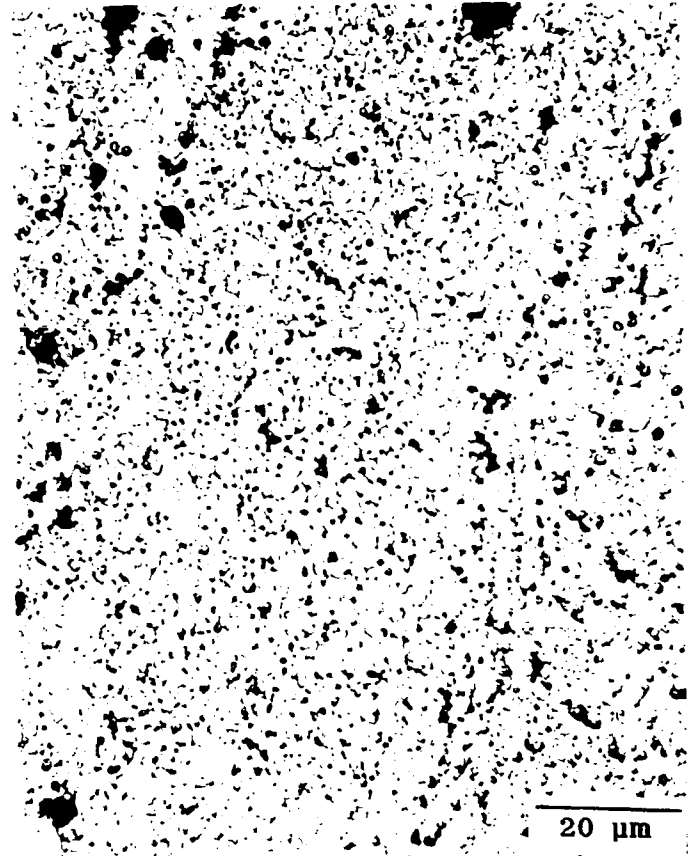
LONGITUDINAL   180X   LONGITUDINAL   960X

FIGURE 67 Optical Photomicrographs of Class 4 Alloy
           (RST X-7091) in Fully Heat Treated (Peak
           Aged) Condition
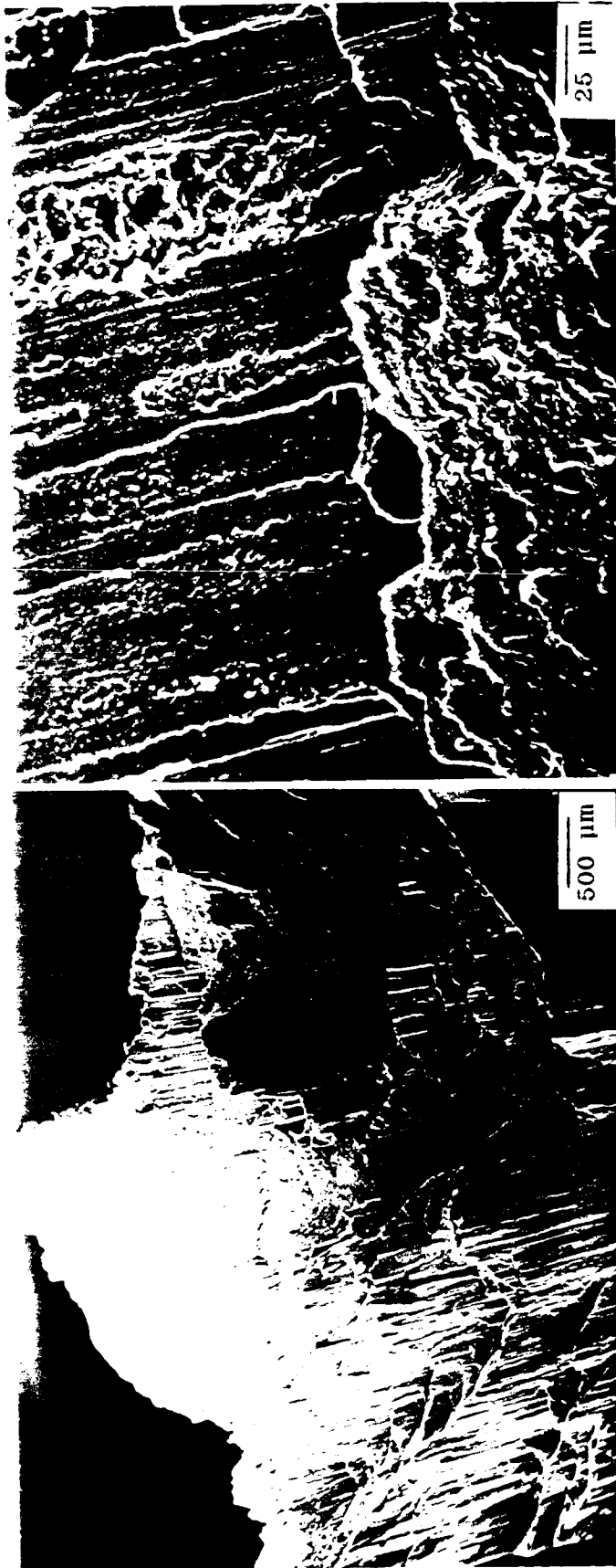
FIGURE 68   Scanning   Electron   Micrographs   Showing
Tension Fracture Mode for Class 4 Alloy in
Peak Aged Temper

2000X

(A)

5000X

(B)

FIGURE 69 Scanning Electron Micrographs of Tensile
Fracture Surfaces of Class 4 Alloy Showing
Dimples on Fracture Facets
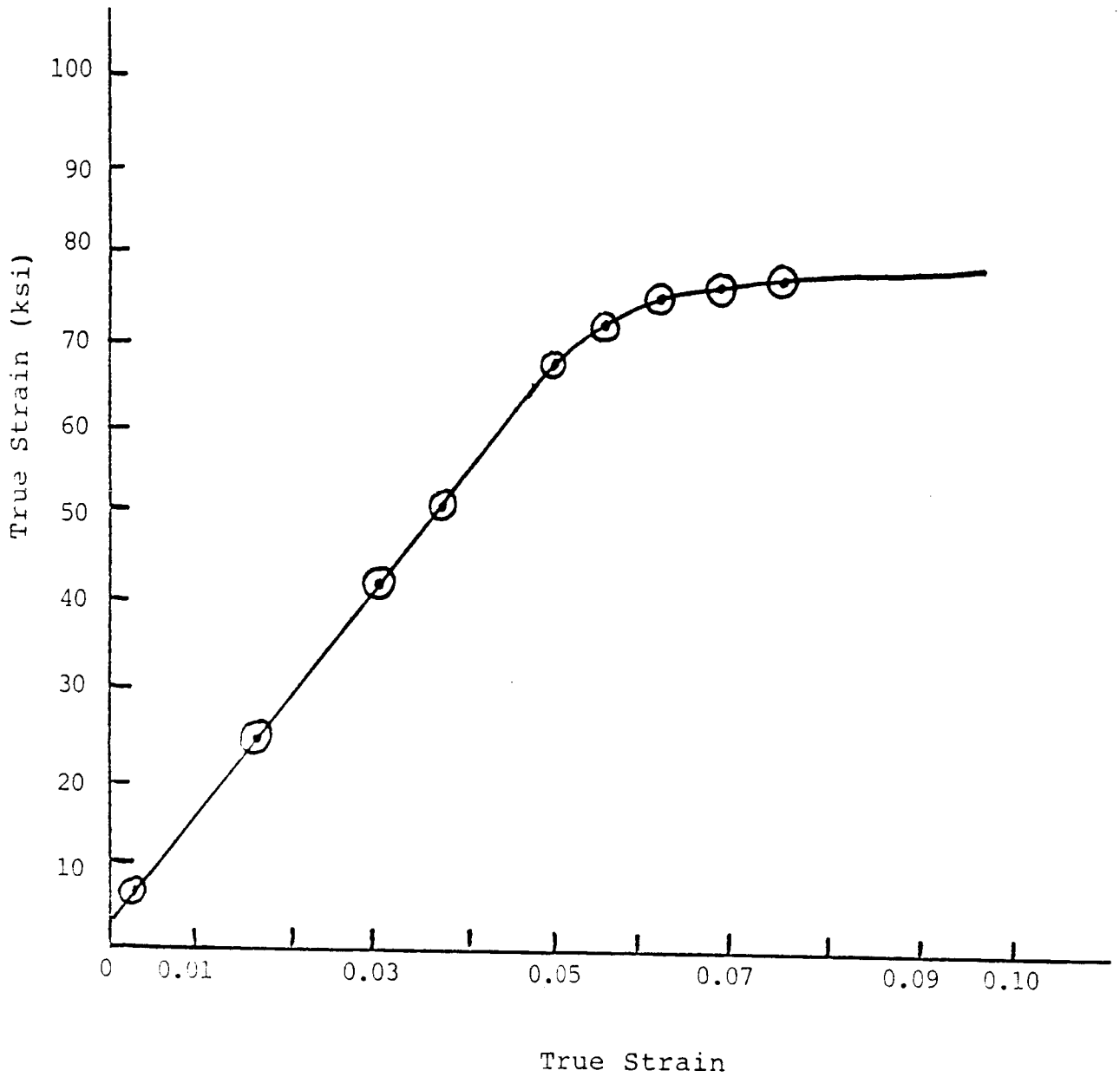
FIGURE 70 Stress-Strain Curve of Class 4 Alloy
(T7E69)
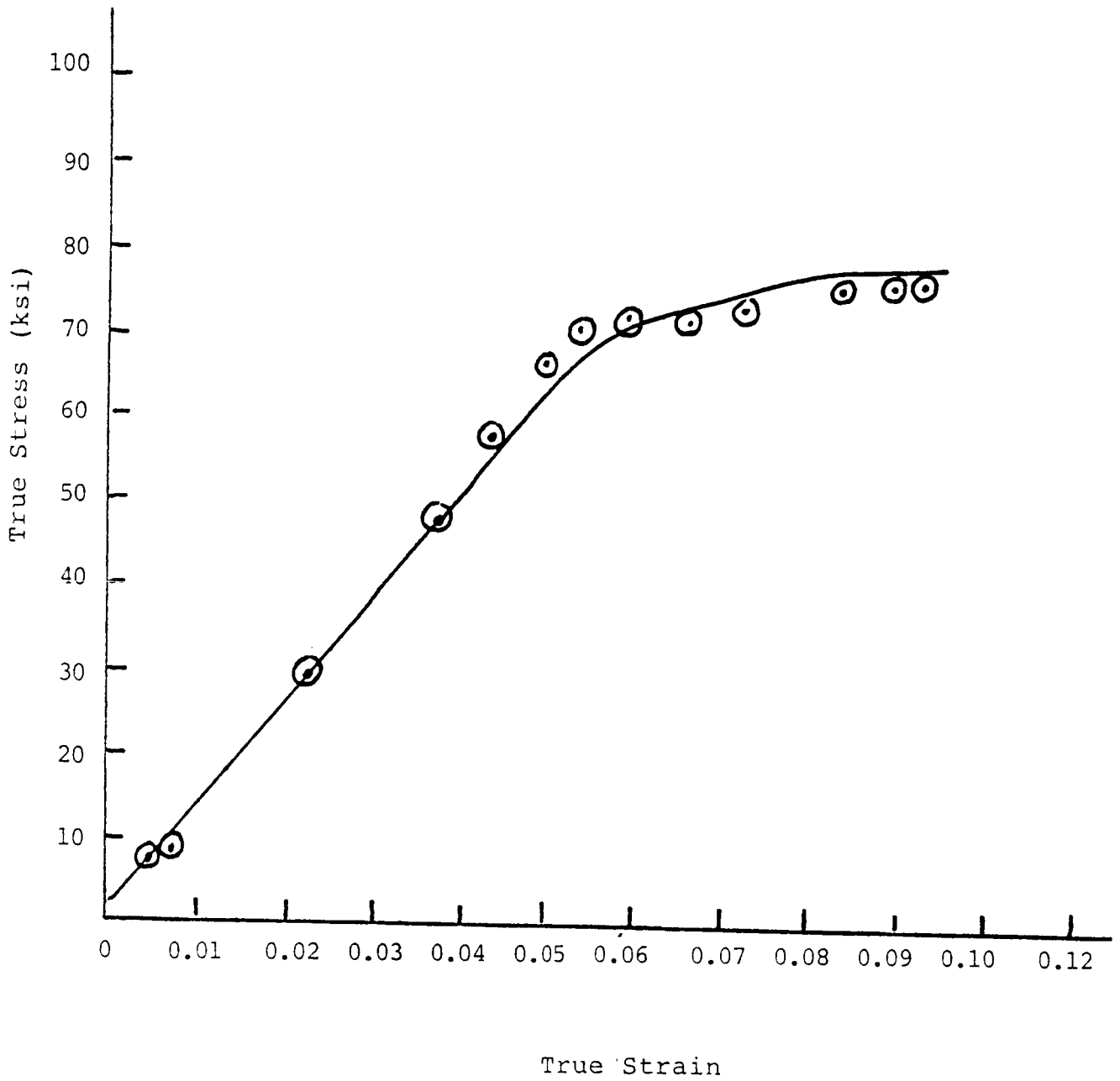
FIGURE 71 Stress-Strain Curve of Class 4 Alloy (T7E7⊘)
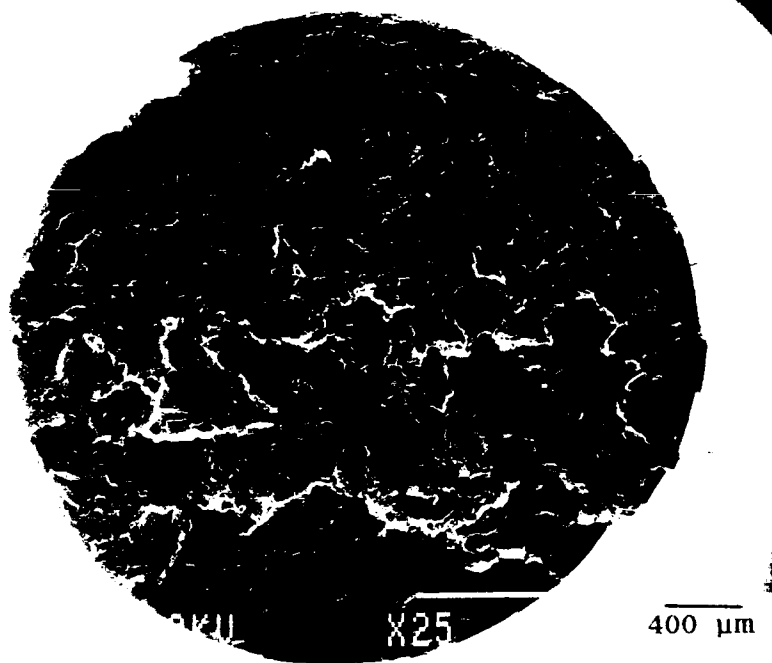
(A) S. E. M. 25X

FIGURE 72 Scanning Electron Micrograph Showing High
           Cycle Fatigue Fracture Surface of a
           Specimen of Class 4 Alloy
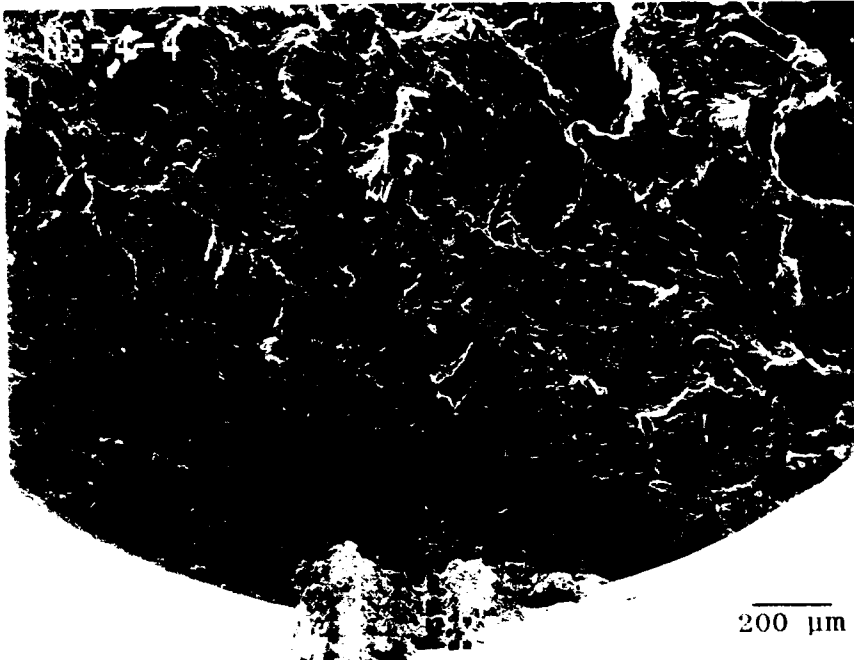
(A) S. E. M. 50X
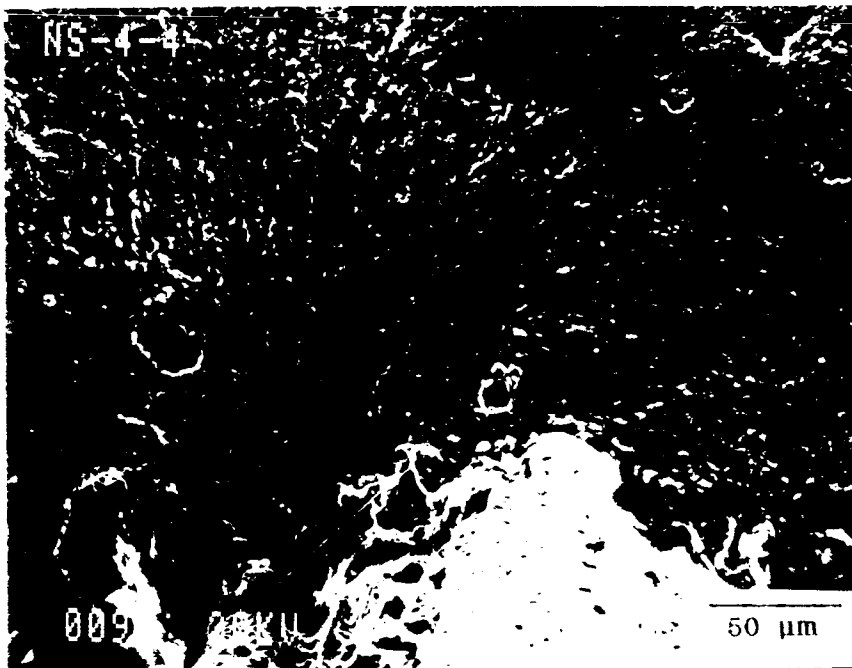
(B) S. E. M. 350X

FIGURE 73 Scanning Electron Micrographs at Higher
Magnification Showing Fatigue Fracture
Initiation Site in Specimen of Figure 72

(A) S. E. M. 40X

(B) S. E. M. 650X
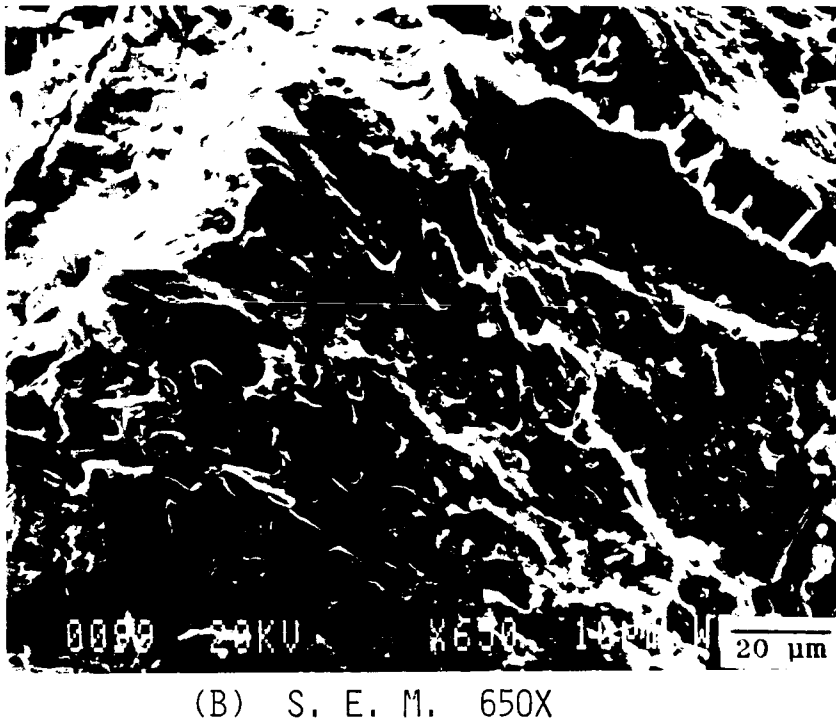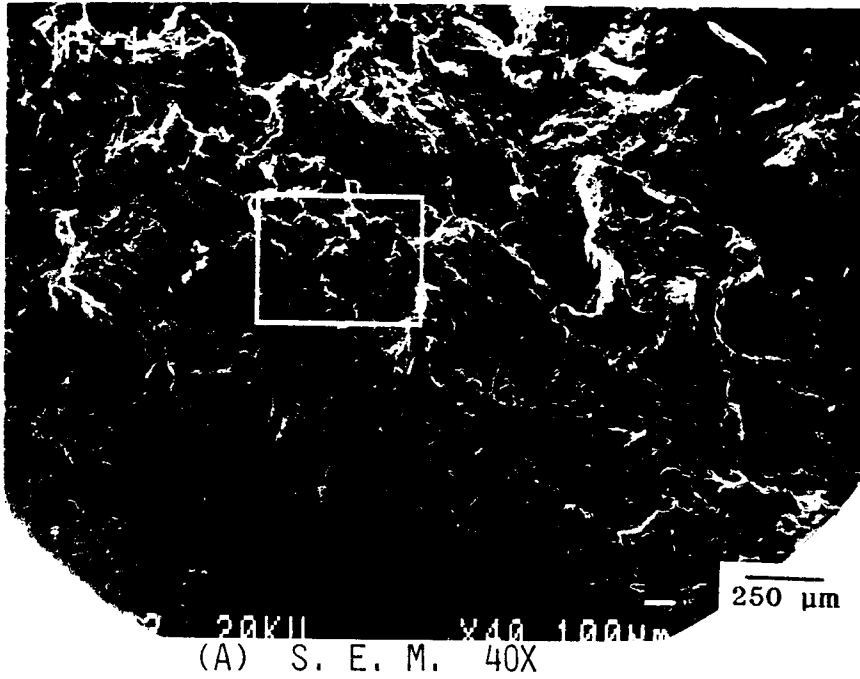
FIGURE 74 Scanning Electron Micrograph Showing Fracture Propagation Area in the Specimen of Figure 72
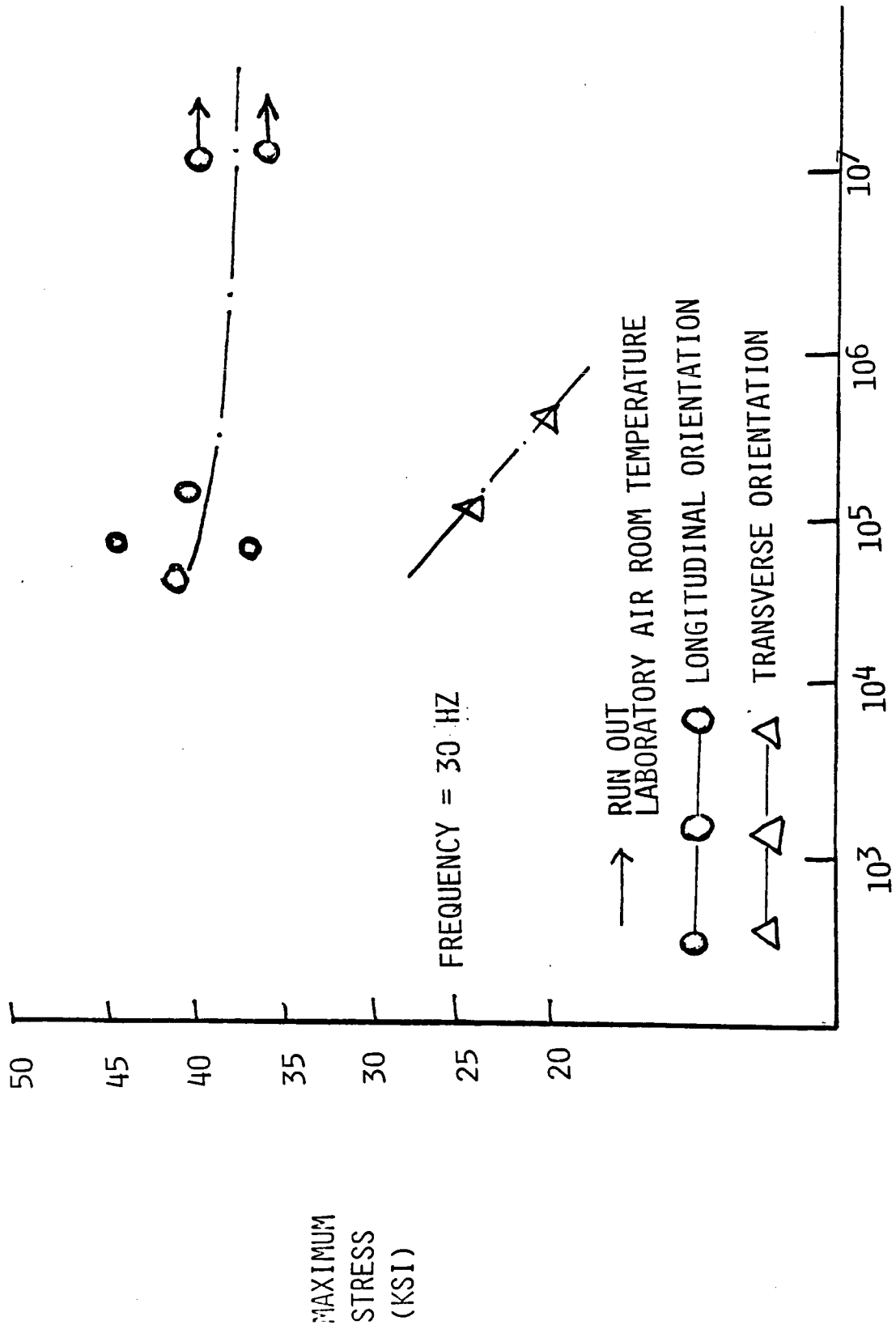
FIGURE 75 Constant Amplitude Fatigue Data of Class 4
Alloy (T7E70)

158
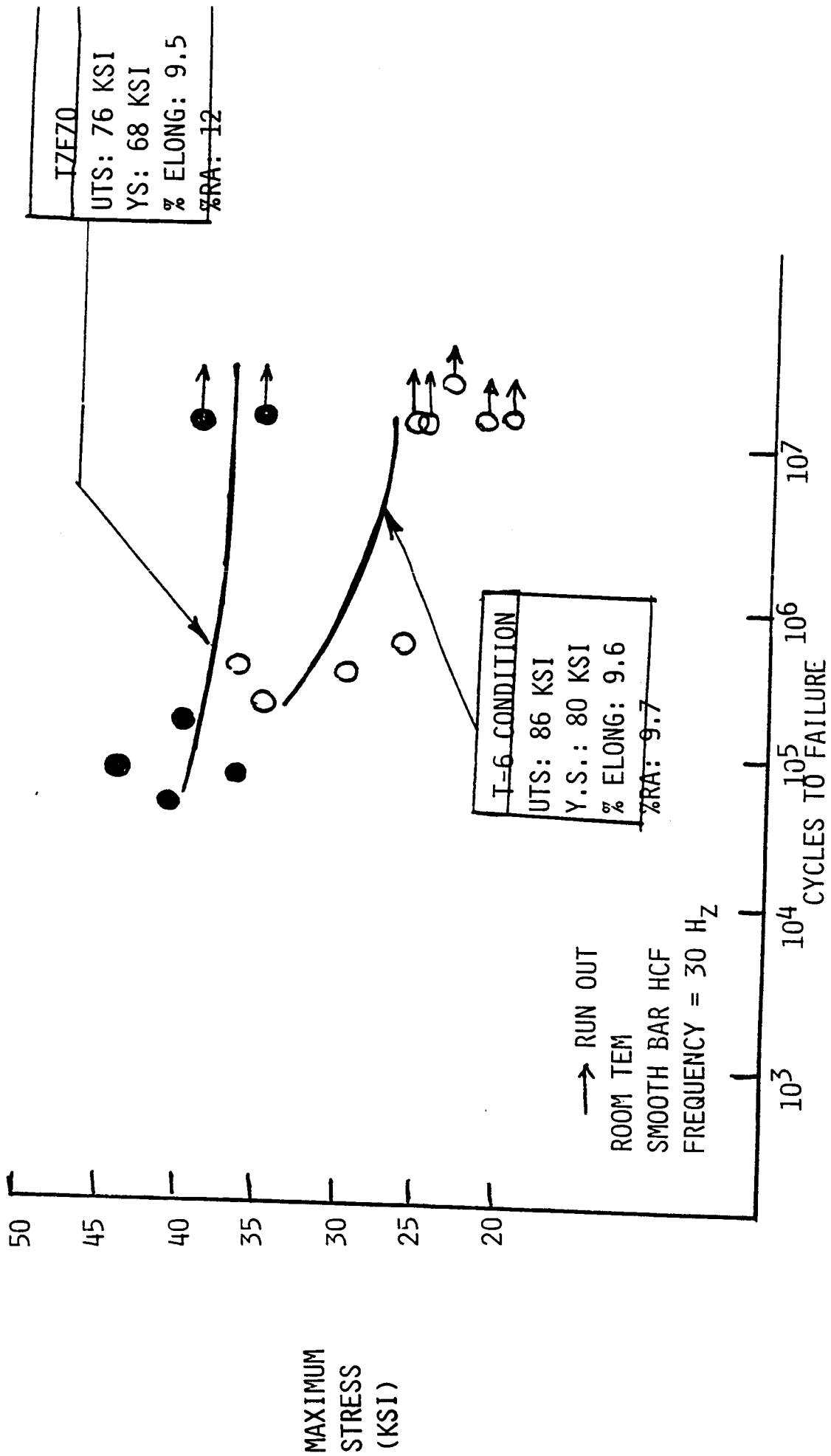
FIGURE 76 Constant Amplitude Fatigue Data of Class 4
Alloy in Longitudinal Direction
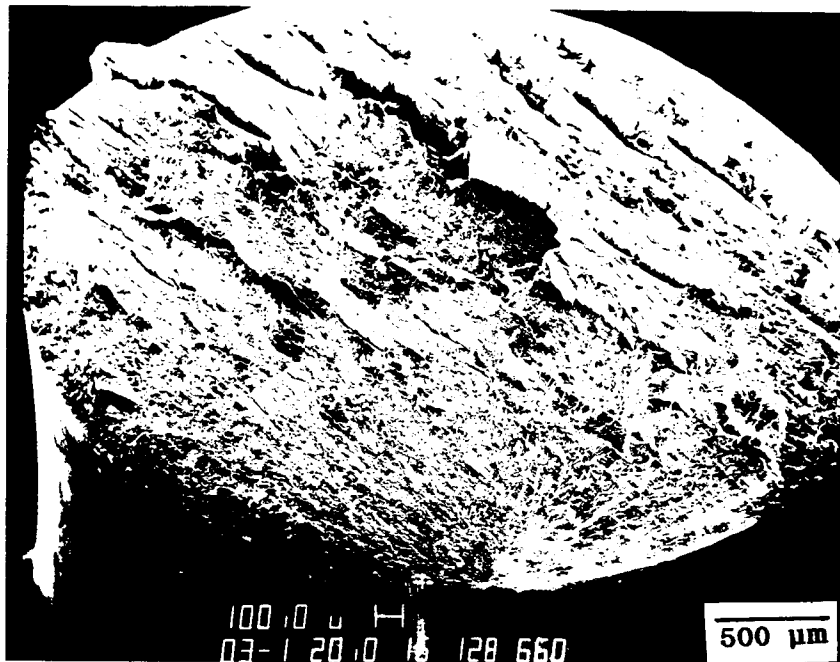
FRACTURE SURFACE

(A) S. E. M. 30X
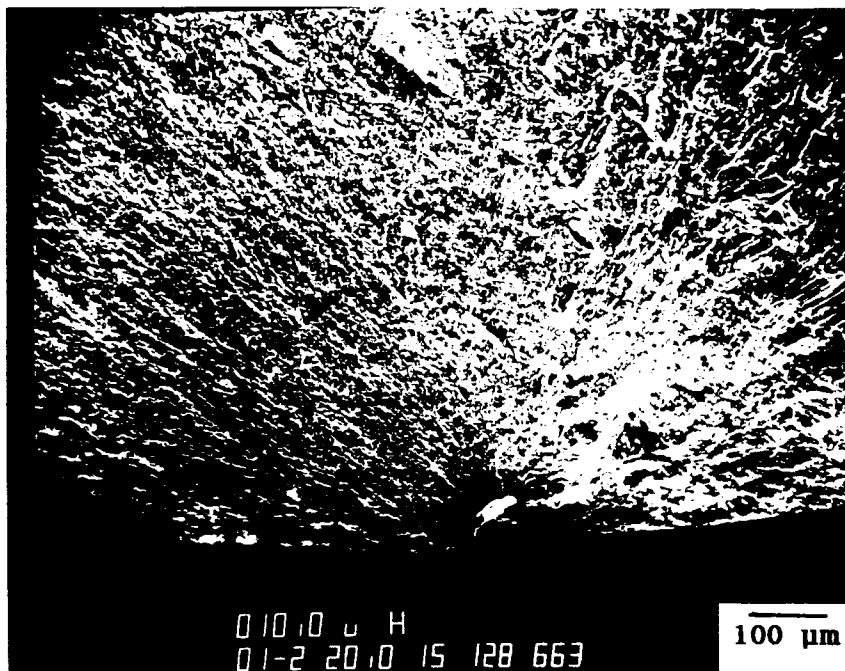
(B) S. E. M. 100X

ORIGIN SITE

FIGURE 77 Scanning Electron Micrographs of the
Fatigue Fracture Surface (38KSI/97,000
Cycle) of Class 4 (T7E70) Alloy
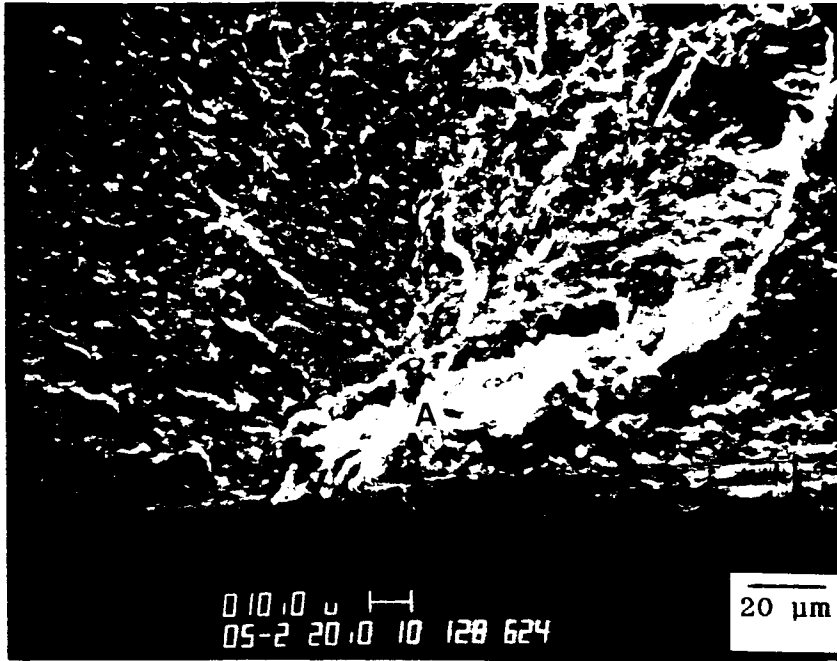
(A) S. E. M. 500X
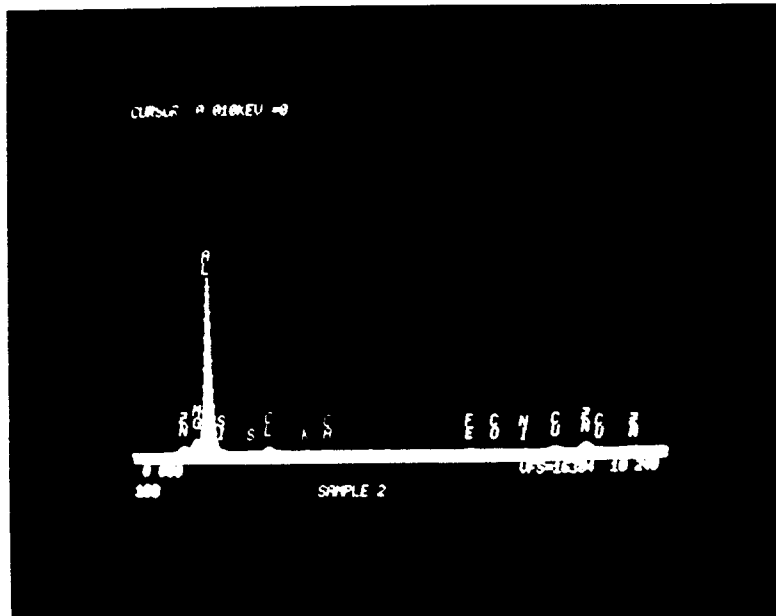
(B) E. D. S. 2000X

FIGURE 78 Scanning Electron Micrographs and EDXA of
Material in Void in the Fatigue Fracture
Surface of Specimen of Figure 77

(A) S. E. M. 700X
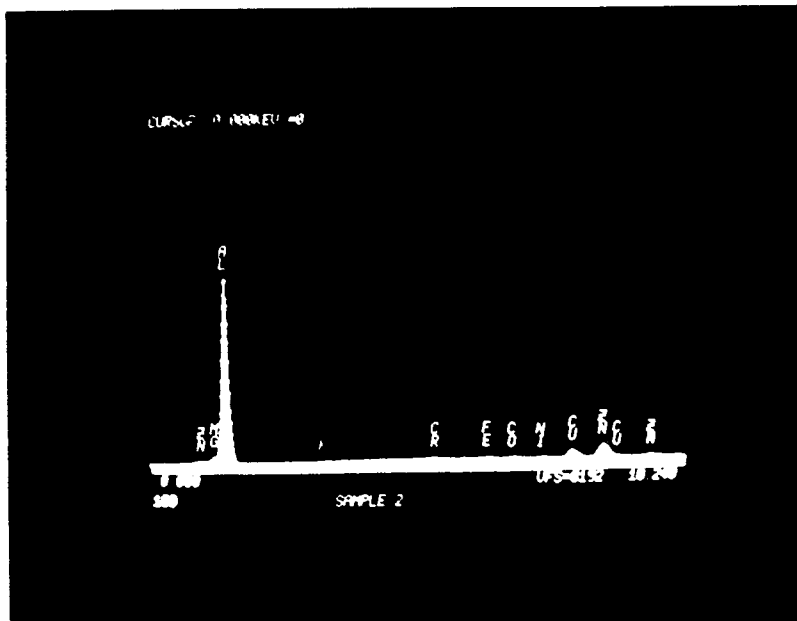
(B) E. D. S. 2000X

FIGURE 79 SEM and EDXA of the General Fracture
Surface in the Propagation Region Near
Fracture Origin of the Specimen in Figure
77
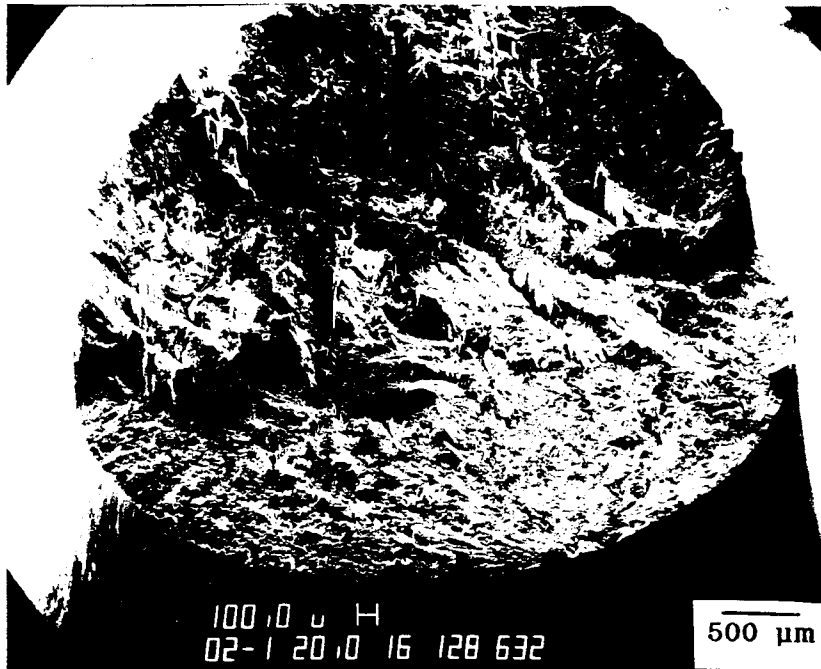
(A) S. E. M. 20X
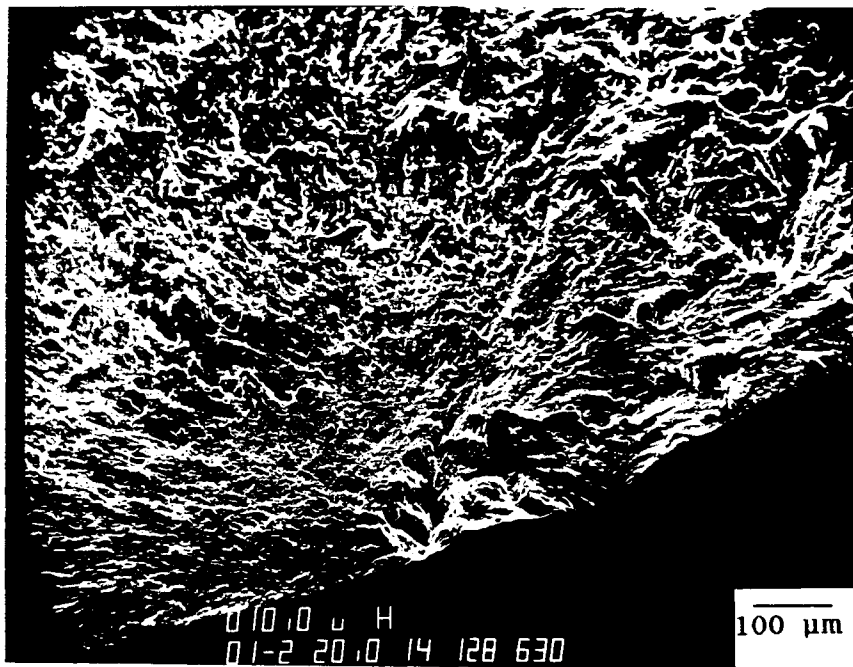
(B) S. E. M. 100X

FIGURE 80 SEM of Fatigue Fracture Surface of a Class
4 (T7E70) Specimen Which Failed at
45Ksi/92,000 Cycle
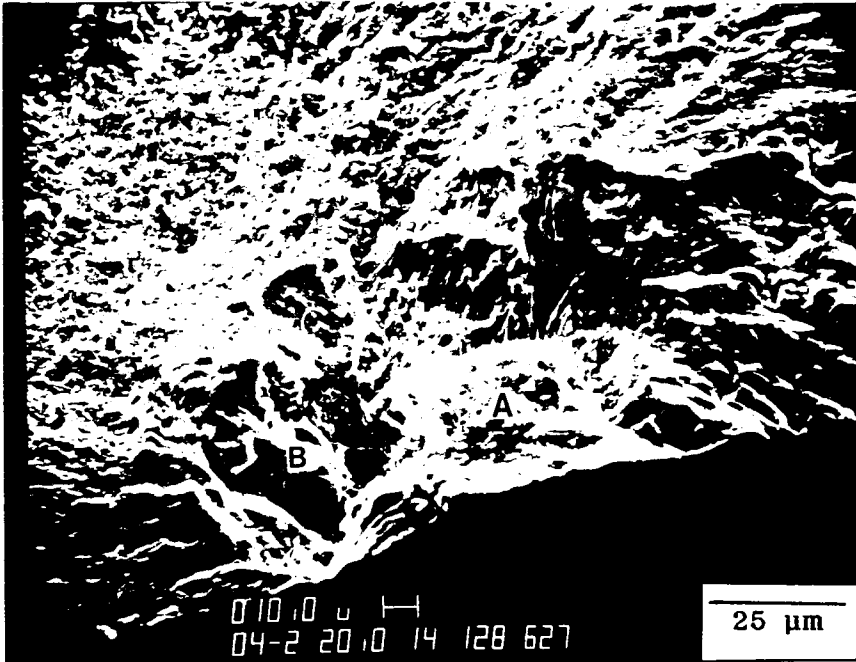
(A) S. E. M. 400X

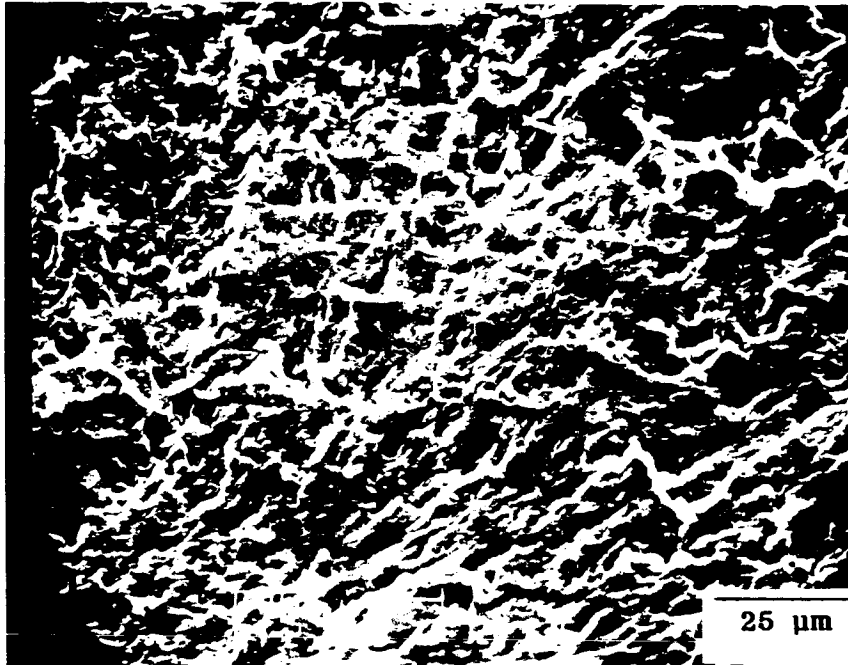A, B = MATERIAL AT ORIGIN
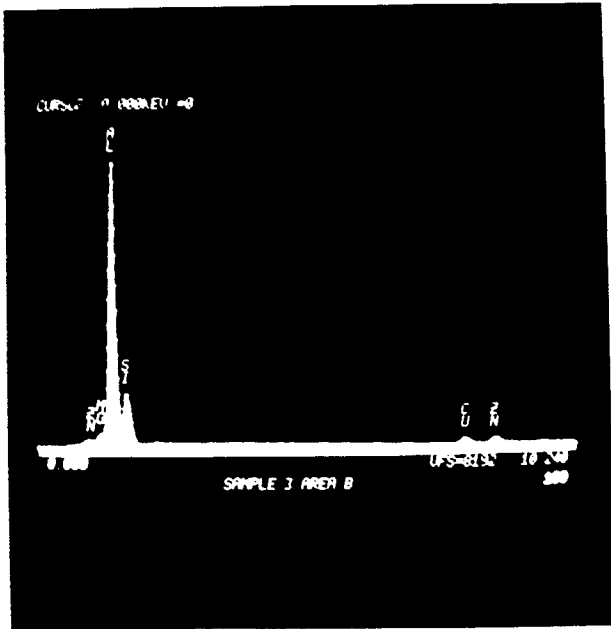
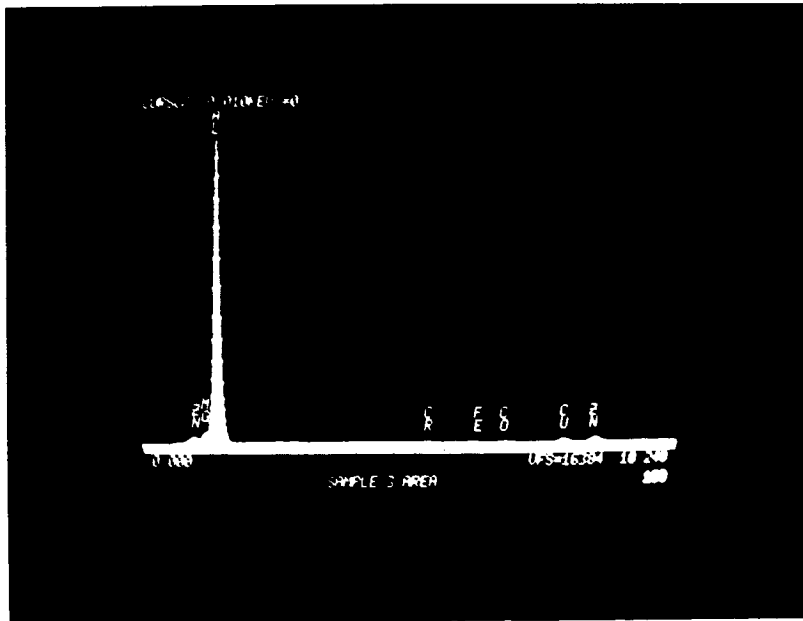(B) E. D. S. 2000X

LOCATION A
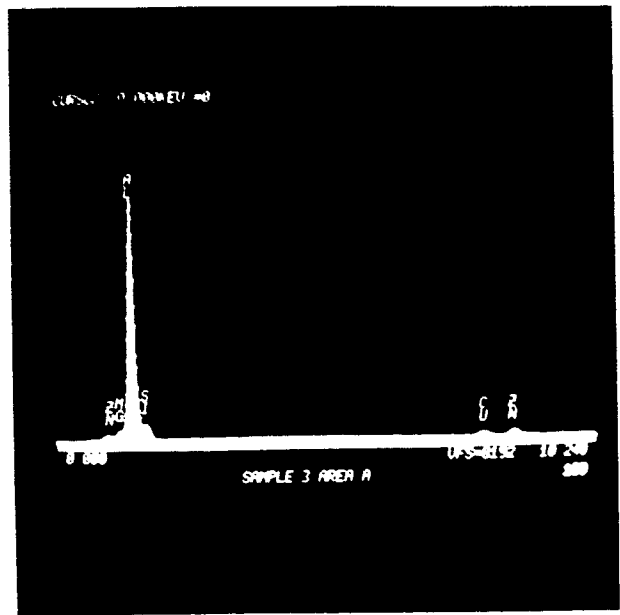
(C) E. D. S. 2000X

LOCATION B

FIGURE 81 SEM and EDXA of Surface at Fracture Origin
of the Specimen of Figure 80

FRACTURE SURFACE
PROGATION REGION NEAR ORIGIN

(A) S. E. M. 700X

(B) E. D. S. 1000X

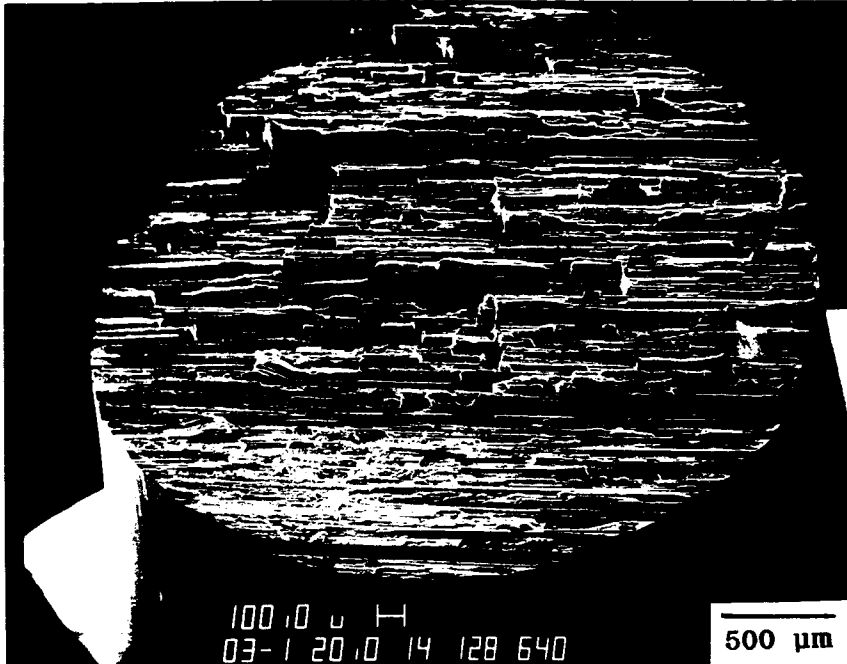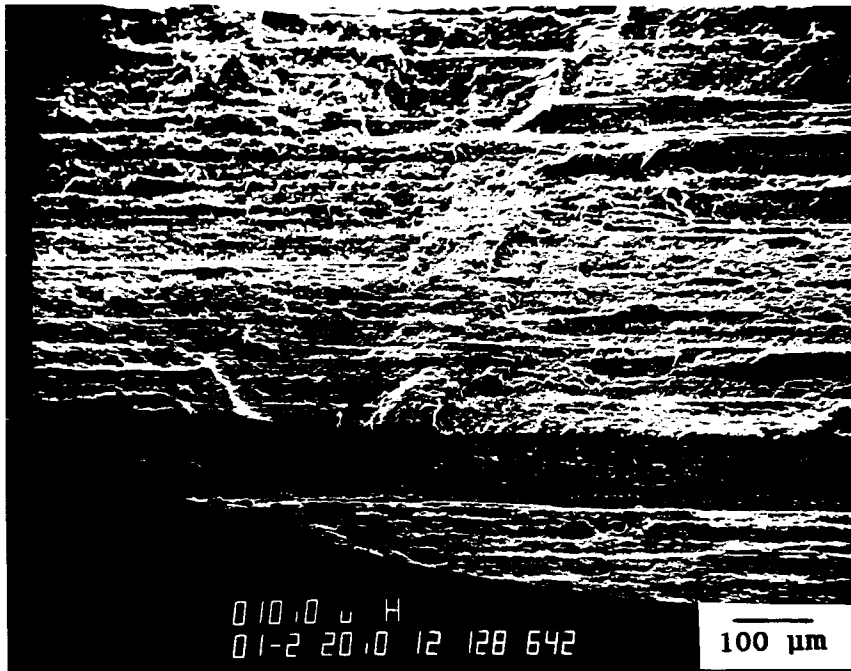FIGURE 82 SEM and EDXA of the General Fracture
Surface in the Propagation Region Near
Fracture Origin of the Specimen of Figure
80

FRACTURE SURFACE

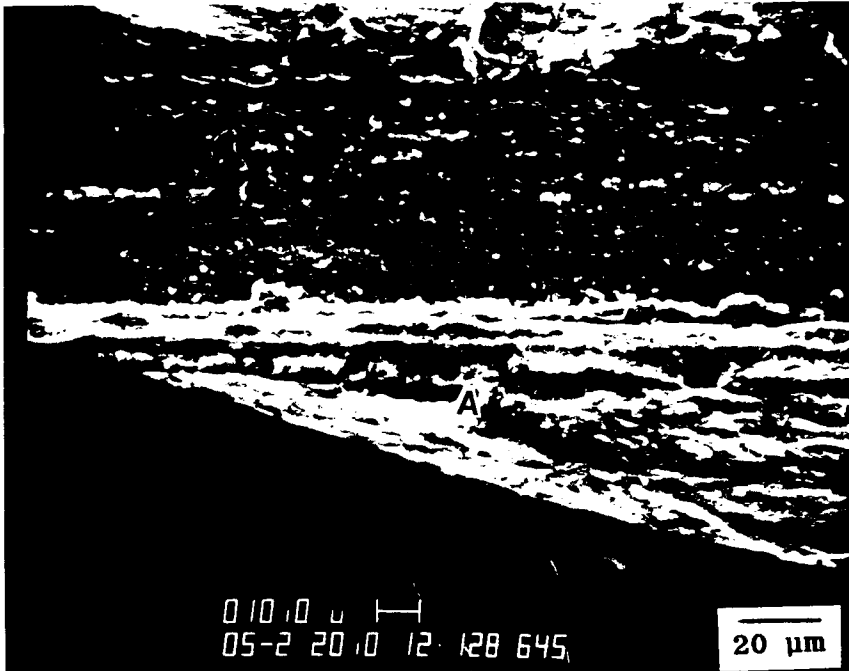(A) S. E. M. 30X

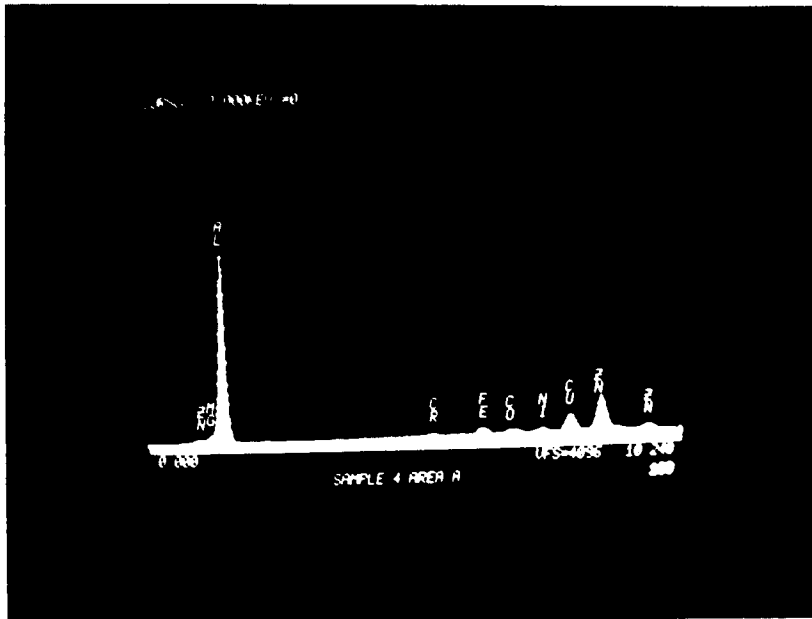(B) S. E. M. 100X

POSSIBLE ORIGIN SITE

FIGURE 83 SEM of the Fatigue Fracture Surface of
Class 4 Alloy (T7E70) in L-T Orientation
(20 Ksi/325,000 PSI)
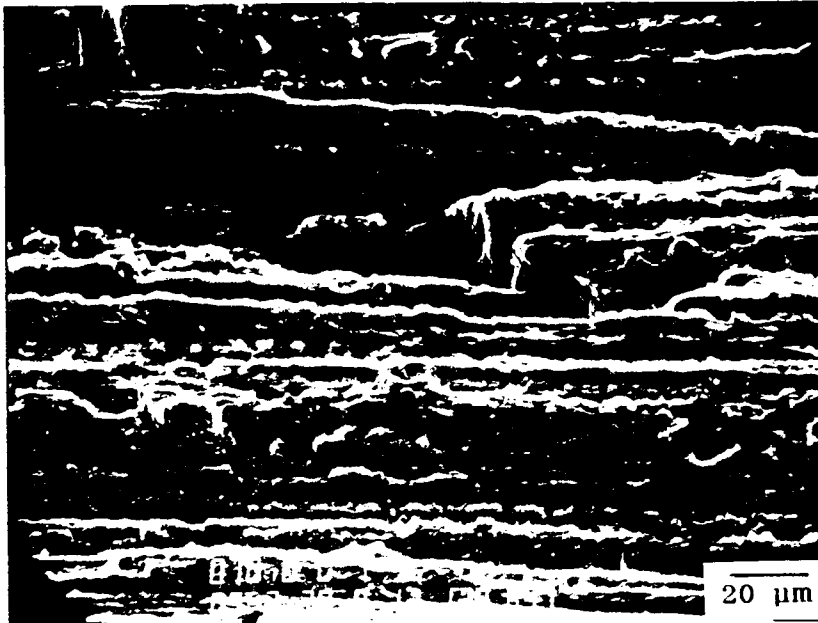
FRACTURE SURFACE
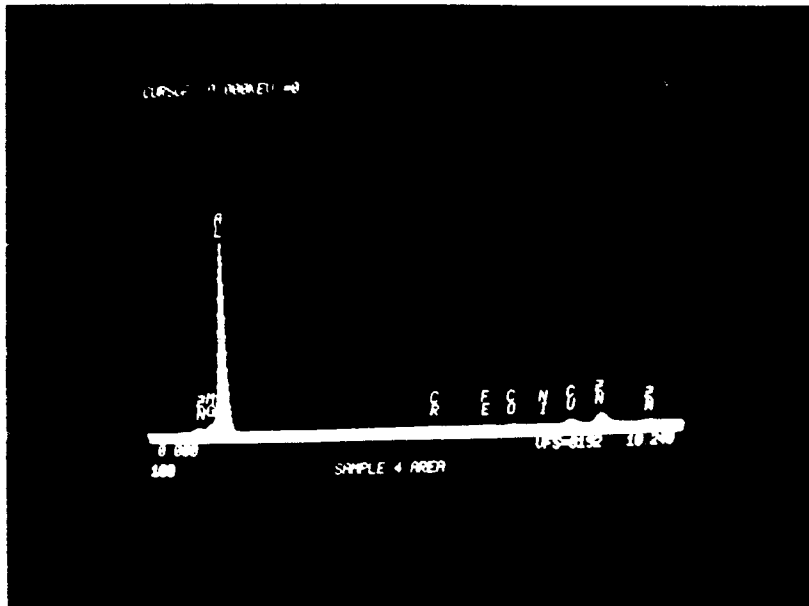POSSIBLE ORIGIN SITE

(A) S. E. M. 500X

(B) E. D. S. 5000X

LOCATION A

FIGURE 84 SEM and EDXA of Fracture at Possible Origin
Site of the Specimen in Figure 83

FRACTURE SURFACE
TYPICAL SURFACE FEATURES

(A) S. E. M. 500X

(B) E. D. S. 1000X

FIGURE 85 SEM and EDXA of General Fracture Surface of
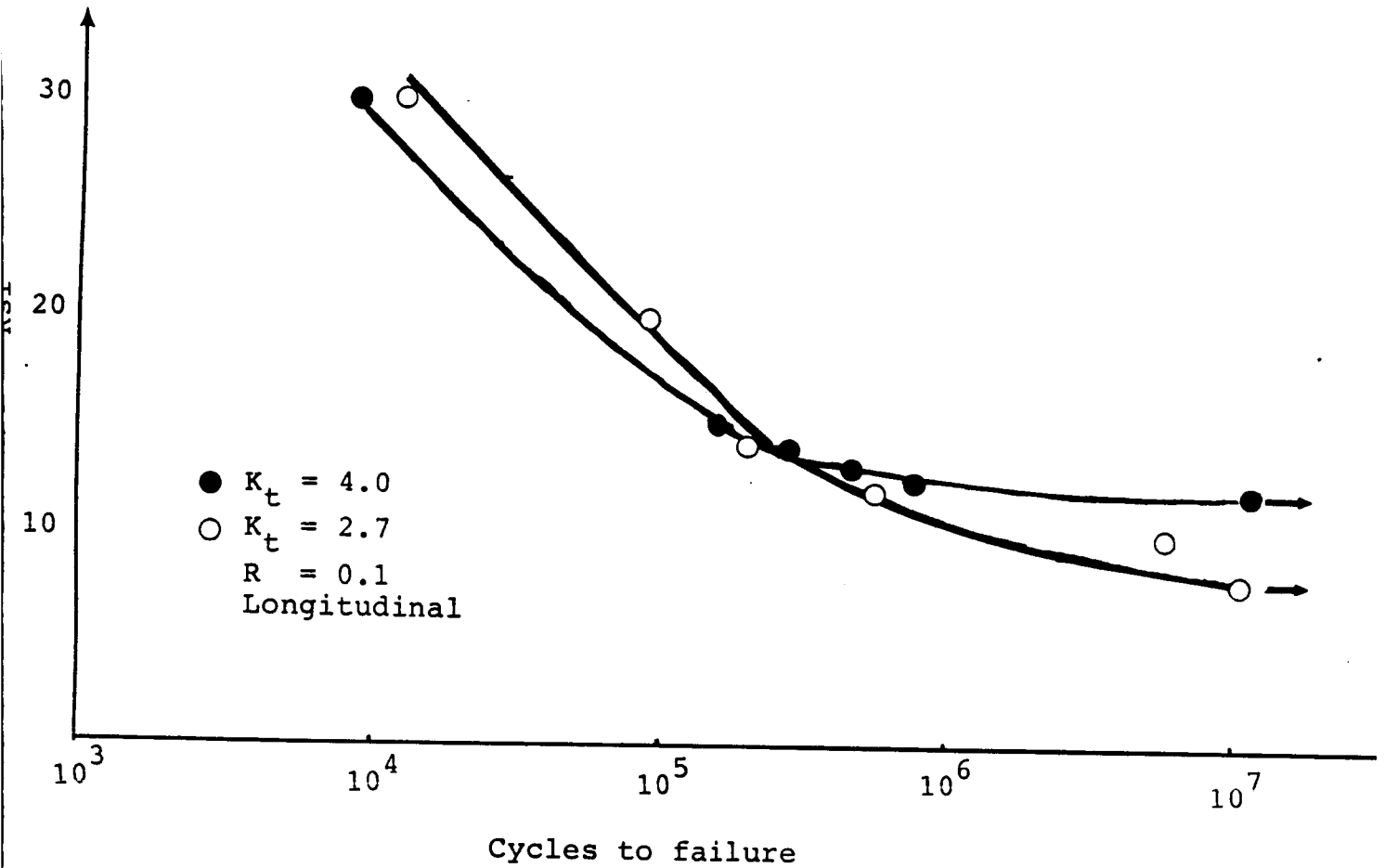the Specimen in Figure 83

FIGURE 86 Fatigue Data for Class 4 Alloy in T7E69
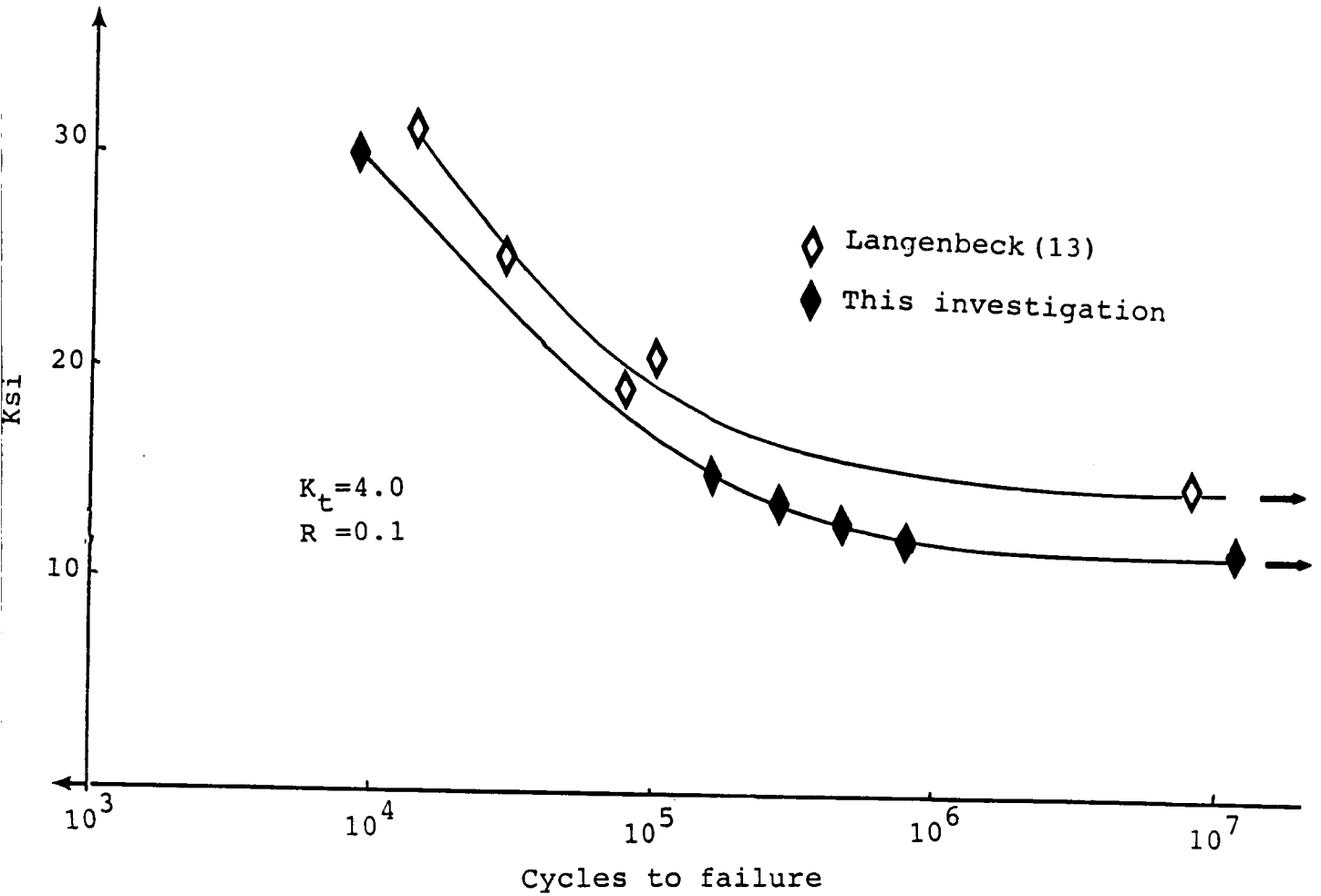Condition at Two Different Stress Concen-
tration Factors

FIGURE 87 Comparison of High Cycle Fatigue Data on Class 4 Alloy (T7E69) and on X7091-T7E69, Obtained Under Identical Test Conditions
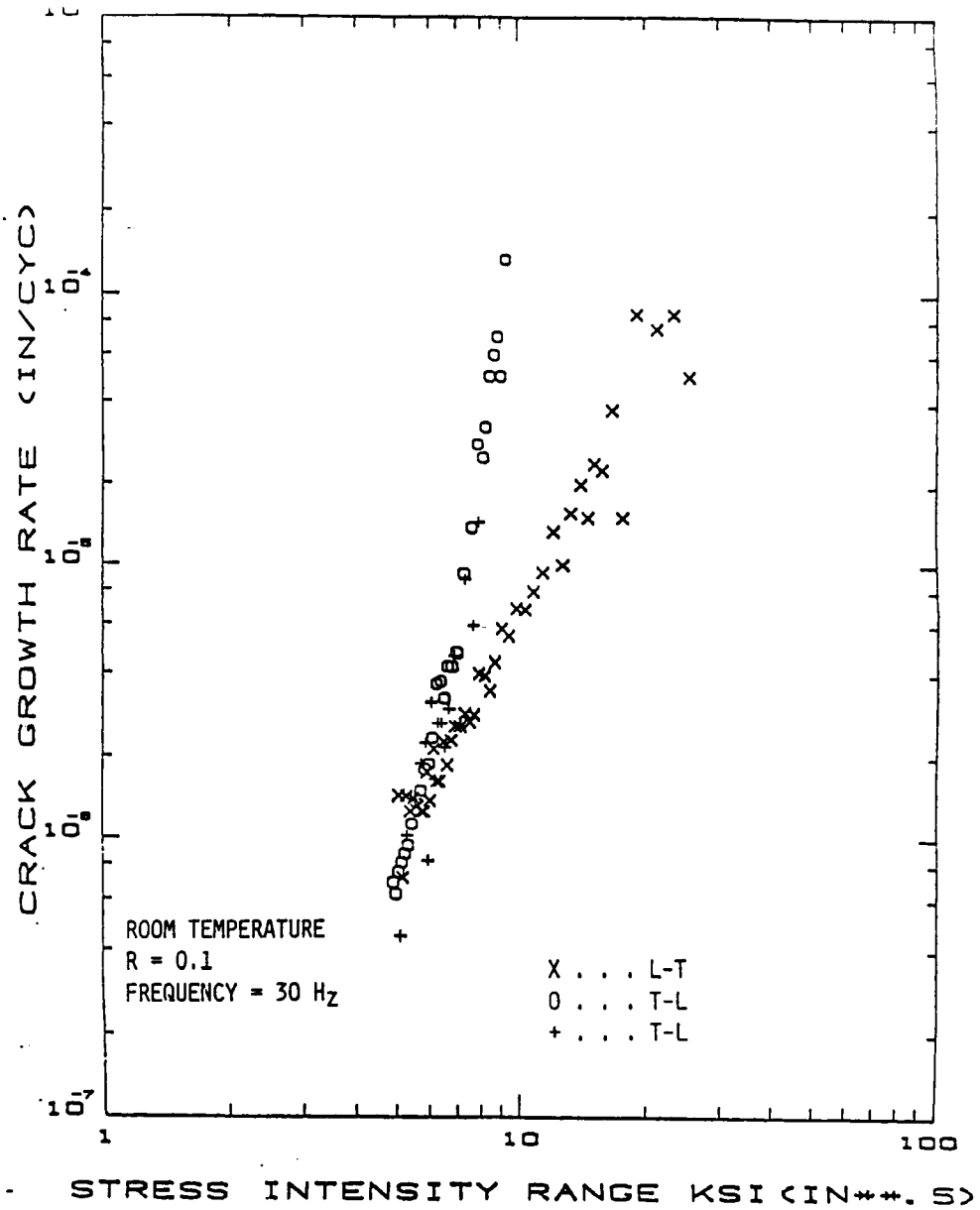
FIGURE 88 Fatigue Crack Growth Behavior of Class 4 Alloy (T7E70)

NASA
National Aeronautics and
Space Administration

Report Documentation Page

1. Report No. NASA CR-178356	2. Government Accession No.	3. Recipient's Catalog No.

4. Title and Subtitle	5. Report Date
Advanced Powder Metallargy Aluminum Alloys via Rapid Solidification Technology - Phase II	April 1987
	6. Performing Organization Code

7. Author(s)	8. Performing Organization Report No.
Ranjan Ray and Sunil C. Jha	
	10. Work Unit No.

9. Performing Organization Name and Address	11. Contract or Grant No.
Marko Materials Inc. 144 Rangeway Road North Billerica, Massachussets 01862	NAS1-18001
	13. Type of Report and Period Covered

12. Sponsoring Agency Name and Address	Contractor Report April 01,1985-March 31,1987
National Aeronautics and Space Administration Langley Research Center Hampton, VA 23665-5225	14. Sponsoring Agency Code

15. Supplementary Notes

Langley Technical Monitor: Mr. Dennis Dicus

Final Report

16. Abstract

The objective of this Phase II NASA-SBIR program was to apply Marko's rapid solidification technology to processing of new high strength aluminum alloys. Four classes of alloys, namely, Al-Li based (Class 1) alloy, 2124 type (Class 2) alloy, high temperature Al-Fe-Mo (Class 3) alloy, and PM X7091 type (Class 4) alloy, were produced as melt-spun ribbons. The ribbons were pulverized, cold compacted, hot-degassed and consolidated through single or double stage extrusion. The mechanical properties of all the four classes of alloys were measured at room and elevated temperatures and their microstructures were investigated optically and through electron microscopy. The microstructure of class 1 Al-Li-Mg alloy was predominantly unrecrystallized due to Zr addition. Yield strengths to the order of 50 Ksi were obtained, but tensile elongation in most cases remained below 2%. The class 2 alloys were modified composition of 2124 aluminum alloy, through the addition of 0.6w%Zr and 1w%Ni. Ni addition gave rise to a fine dispersion of intermetallic particles resisting coarsening during elevated temperature exposure. Class 2 alloy showed good combination of tensile strength and ductility and retained high strength (approx. 40 Ksi) after 1000 hour exposure at 177°C. The class 3 Al-Fe-Mo alloy showed high strength and good ductility both at room and high temperatures. The yield and tensile strength of class 4 alloy exceeded those of the commercial 7075 aluminum alloys.

17. Key Words (Suggested by Author(s))	18. Distribution Statement
Rapid Solidification, Powder Metallurgy, Elevated Temperature Aluminum Alloys, PM 2124, RST X-7091, Al-Fe-Mo, Al-Li-Mg Alloys, Fracture and Fatigue Properties	Unclassified-Unlimited

19. Security Classif. (of this report)	20. Security Classif. (of this page)	21. No. of pages	22. Price
Unclassified	Unclassified	183	

NASA FORM 1626 OCT 86